Development of a Polyamide12/Carbon nanotube Nanocomposite for Laser Sintering

By

Jiaming Bai

A thesis submitted in fulfilment of the requirements for the degree of

Doctor of Philosophy

Wolfson School of Mechanical and Manufacturing Engineering

Loughborough University

Abstract

This thesis presents a comprehensive study on the preparation, processing and characterisation of a polymer nanocomposite for laser sintering. Well-dispersed nanocomposite powder with near-spherical morphology and suitable particle size for processing by laser sintering was successfully produced by a novel method of coating individual polyamide 12 (PA12) powder particles with carbon nanotubes (CNTs). Mechanical specimens produced by laser sintering the PA12-CNT powder showed good definition and no distortion. Compared to the laser sintered PA12 parts, PA12-CNT nanocomposite parts showed enhanced flexural, impact and tensile properties without sacrificing elongation at break. This enhancement may be attributed to the well-dispersed CNTs in the PA12 matrix and corresponding denser laser sintered parts. By adding the CNTs into the PA12 powder, the thermal conductivity was increased. This could increase the fusion of the powder and flow of melted PA12, resulting in denser and stronger parts. Parallel oscillatory rheology tests were completed in co-operation with Toyota Technological Institute (TTI), Japan. Results demonstrated that CNTs have a significant effect on the melt rheological properties of the PA12-CNT nanocomposites, as the storage modulus G', loss modulus G'' and viscosity η of the PA12-CNT nanocomposites increased compared to neat PA12. To evaluate the dispersion of CNTs in the laser sintered PA12-CNT nanocomposite parts, three dimensional transmission electron microscopy (3D-TEM) was carried out at National Institute for Materials Science (NIMS), Japan. Results revealed that the CNTs were dispersed well in the laser sintered PA12-CNT parts without agglomerates, which is very important for the mechanical enhancement by nanofillers. The method used in this work

appears to be a cost-efficient and effective way to produce polymer nanocomposite powders for laser sintering, while maintaining the optimum powder morphology for the laser sintering process and enhancing the mechanical properties of the laser sintered parts.

Acknowledgement

I wish to acknowledge and express my sincere thanks and gratitude to my supervisors, Dr Ruth Goodridge, Prof Richard Hague and Prof Mo Song, for their invaluable supervision, encouragement, continued help and support throughout this endurance research study.

My thanks also go to all other staff, colleagues and friends that I have worked with and who have helped me reach this stage, especially Prof Phill Dickens, Dr Chris Tuck, Prof Ricky Wildman, Prof Ian Ashcroft, Mr Mark East and Mr Mark Hardy.

I would like to thank the Royal Society and the Great Britain Sasakawa Foundation (GBSF) for providing a travel grant to allow me to carry out research at Toyota Technological Institute (TTI) and National Institute of Materials Science (NIMS), Japan. I greatly appreciate the advice provided by Prof Masami Okamoto at TTI and Dr Hideyuki Murakami in NIMS.

Finally, I would like to acknowledge my family, particularly my mother Jinfeng Lu, for endless support, encouragement and love which enabled me to stay focussed.

Table of Contents

List of Tables

List of Figures

Chapter 1

Introduction

1.1. Scope of research

Additive Manufacturing (AM), which is an outgrowth of rapid prototyping, aims to offer greater flexibility in respect to design freedom and manufacture than traditional technologies. This description, additive manufacturing, relates to the way a series of processes fabricate 3D end-use parts by adding material in layers. By using AM, complex parts can be built without tools, which provides great design freedom. Also, the design-manufacturing cycle can be shortened, therefore reducing the production cost and increasing competitiveness. Furthermore, AM will enable a push towards affordable customised products, which can meet exactly the needs of each individual customer.

Laser Sintering (LS), is one of the most established and widely used additive manufacturing techniques. In this process, an object is created layer-by-layer from heat-fusible powdered materials with heat generated from a scanning laser beam. In principle, all materials that can be melted or fused can be used in the laser sintering process. However in practice, this is far from reality. The term 'laser sintering' is generally applied to the processing of polymers, which is the focus of this project.

Thermoplastic materials are well-suited for laser sintering because of their relatively low melting temperature and low melting viscosity. Polymers such as Polyamide (PA), polypropylene (PP), polystyrene (PS), polycarbonate (PC), poly(ether-ether-ketone) (PEEK) have been developed and used for laser sintering. However, limitations exist with current laser sintering materials. Firstly, there is a very limited variety of polymers that can currently be processed. Polyamides 11 and 12 (PA11/PA12) are by far the most commonly used laser sintering materials at present. Polymers that are able to be processed are only available in a handful of grades compared with the hundreds to thousands of grades available for conventional manufacturing techniques, such as injection moulding. Secondly, due to unsatisfactory mechanical, thermal or electrical properties, the polymers that are available at the moment cannot completely meet the needs of all applications. For these two reasons, it is necessary to increase the number of laser sintering polymers which can meet the various requirements for end-use parts. It is envisaged that the ability to process polymer nanocomposites by laser sintering could provide a way to address some of these problems.

Nanocomposites are growing in importance in materials and manufacturing research. In traditional manufacturing, nanofiller-reinforced polymers have been seen to improve the base material's properties while remaining processible with extruders and moulding machines[1]. Polymer nanocomposites use nanoscale fillers to improve the base materials' mechanical, thermal, and electrical properties without reducing impact strength. For these reasons, polymer nanocomposite materials have great potential for processing by laser sintering. This research investigates the processing of polymer nanocomposites by laser sintering.

1.2. Thesis structure

There are four parts to this thesis, as shown in Table 1-1. Part 1, which includes Chapters 1, 2 and 3, introduces the background, literature, novelty and objectives of this study. Part 2, which is Chapter 4, provides information about the preparation of the polymer nanocomposite powder, laser sintering of the powder and the technologies used to characterise the powder and laser sintered parts in this work. Part 3, which includes Chapter 5 and 6, is the results and discussion section. Chapters 5 provide details about the characterisation of PA12 and PA12-CNT nanocomposite powders and optimisation of the laser sintering process. In Chapter 6, the laser sintered PA12-CNT parts, along with neat PA12 laser sintered parts, were characterised by mechanical, thermal and microscopy experiments. The influence of CNTs on the polymer matrix is analysed. Chapter 7 makes up the last part of this thesis (Part 4), which includes conclusions from this study and recommendations for future work.

Part 1	• Chapter 1 - Introduction • Chapter 2 - Literature review • Chapter 3 - Novelty and objectives
Part 2	• Chapter 4 - Methodology
Part 3	• Chapter 5 - Characterisation and laser sintering of PA12-CNT nanocomposites powders • Chapter 6 - Characterisation of laser sintered PA12-CNT nanocomposites
Part 4	• Chapter 7 - Conclusions and future work

Table 1-1: Thesis structure

Chapter 2

Literature review

2.1. Additive manufacturing

Additive manufacturing (AM) is a collection of advanced manufacturing processes which produce physical 3D objects directly from 3D model data. Often referred to as 3D printing nowadays, these processes build a finished part layer-by-layer in an additive way, as opposed to the conventional subtractive processes that cut away material, or moulding manufacturing processes[2-5].

AM, which aims to offer greater flexibility in respect to product design and manufacture compared to traditional manufacturing routes, is an outgrowth from the early days of rapid prototyping in the late 1980s and early 1990s. From then on, there have been many related terminologies used to describe AM and common synonyms include: additive fabrication, additive layer manufacturing, direct digital manufacturing, and freeform fabrication. In recent years, the ASTM International F42 committee on Additive Manufacturing Technologies was formed to standardise AM terminology and industry standards. AM is defined in their first standard as[6]:

"The process of joining materials to make objects from 3D model data, usually layer upon layer, as opposed to subtractive manufacturing technologies."

2.1.1. Classification of additive manufacturing processes

After more than 20 years of development, there are dozens of recognised layered manufacturing technologies, but not all of them can be considered suitable for additive manufacturing as some have material properties that render them useless for anything beyond visualisation. In 2012, the ASTM International Committee F42 on Additive Manufacturing Technologies published AM processes categories, which are listed in Table 2-1.

Category	Brief description
Powder bed fusion	An additive manufacturing process in which thermal energy, from a laser in most cases, selectively fuses regions of a powder bed. In the case of polymer powders, the powder surrounding the part being built makes possible the creation of complex three-dimensional objects without supports.
Material extrusion	Material extrusion machines work by forcing material through a heated nozzle or orifice in a controlled manner to build up a structure.
Material jetting	Material jetting is the use of inkjet printers or other similar techniques to deposit droplets of build material which are selectively dispensed through a nozzle or orifice to build up a three-dimensional structure.
Binder jetting	An additive manufacturing process in which a liquid bonding agent is selectively deposited to join powder materials. The only commercially available full-colour 3D printing machines are binder jetting machines.
Sheet lamination	An additive manufacturing process in which sheets of

	material are bonded to form an object.
Vat photopolymerisation	Vat photopolymerisation processes involve selective curing of pre-deposited photopolymers using some type of light source (such as UV, laser).
Directed energy deposition	Directed-energy-deposition machines melt material with a laser or other energy source as material is being deposited.

Table 2-1: Main categories of additive manufacturing[6,7]

The seven processes listed in Table 2-1 are the current approaches to AM. As the development of AM continues, new processes will inevitably be invented. These categories will be revised as necessary to accommodate possible new technologies.

2.1.2. The benefits and limitations of additive manufacturing

Many people have described AM as revolutionising product development and having the potential to change the paradigm for manufacturing[2,4]. Compared to traditional manufacturing processes, the layer-upon-layer nature of AM enables the manufacture of highly complex components with very few geometric limitations. With this improved design freedom, AM has been used to manufacture topologically optimised shapes for various applications. For example, in the aerospace and automotive industries, AM is used to improve strength-to-weight ratios, which is an important consideration during design to reduce vehicle weight and fuel consumption[4].

The capabilities of additive manufacturing have resulted in numerous changes to the traditional product design process. One of the main problems encountered in the traditional product design process is that designers create designs that are difficult to manufacture and therefore have to be corrected, resulting in high inefficiency during production. Many new designs are never realised because they are risky to manufacture due to the high cost of mould tooling. With additive manufacturing not using mould tooling and being cost-effective for low volume parts, it is feasible to introduce new products in low quantities to see whether a market demand exists for them. In addition, when highly complex components are produced without any need for tools, the lead-time and ultimately the overall manufacturing costs for items will be reduced. Moreover, additive manufacturing can also reduce the need for assembly processes by building a multi-component unit as singular unit, without any fastening mechanism[8,9].

Another design benefit for AM is customer input and customisation. If a product is specifically designed to suit the needs of a unique individual then it can truly be said to be customised. Hague *et al.*[10,11] discussed true mass customisation. True mass customisation is the production of goods and services for a large market, which meet exactly the needs of each individual customer with regards to certain product characteristics, at costs roughly corresponding to those of standard mass-produced goods[12]. With the benefits of tool-less manufacturing and freedom-of-design, AM enables the manufacturing of customised products economically, from medical implants to consumer goods such as shoes and jewellery. The newly introduced home-based 3D printing equipment enables consumers to engage in the design and manufacture process directly[13].

It has been predicted that AM will be able to compete with current mass production techniques, such as injection moulding, blow moulding or metal casting, when the quantities required are up to a certain amount[14-16]. The study developed by Hopkinson and Dickens[15] calculated an approximation break-even analysis for additive manufacturing against injection moulding in order to find when AM was economically advantageous. Figure 2-1 shows an example result of the break-even analysis. Before the break-even point, which is 14000 parts in this case, injection moulding was more expensive due to the cost of tooling. Their work indicated that AM is economically suitable for low and medium production volumes. However, the possibility of recycling supporting materials was not considered in their model. It is believed that as the cost of the AM machines and materials goes down, and the improvement of the recycle rates for supporting material, AM will be a stronger competitor in the future[23].

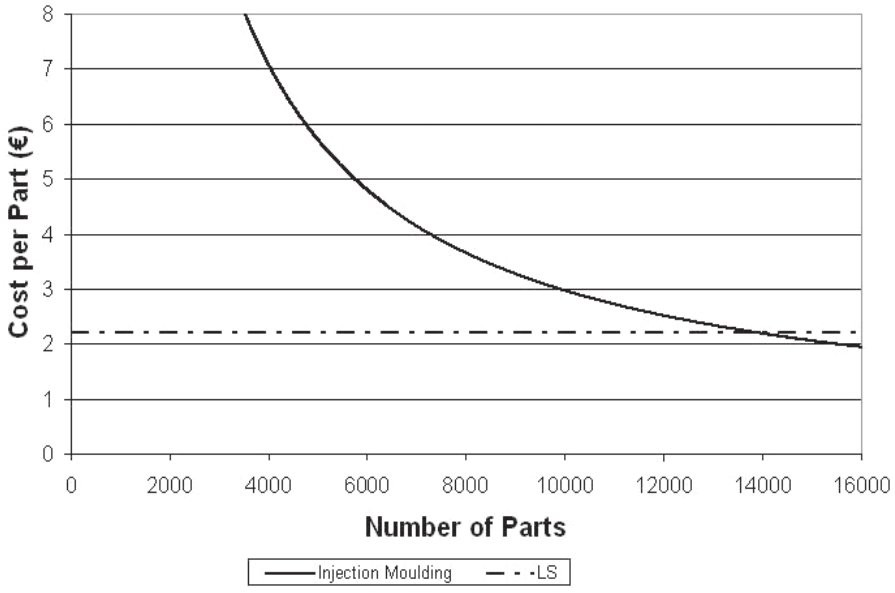

Figure 2-1: Graph of break-even analysis comparing laser sintering with injection moulding [15,16]

In addition to cost advantages for low and medium volumes production, the supply chain can be greatly compressed by AM, which allows manufacture at

multiple locations closer to the point of consumption at the same time. This has obvious benefits to the consumer, environment and local economy.

However, it must be acknowledged that AM also has limitations. Many of the processes used still have inferior dimensional accuracy, generous tolerances, poor surface finish, machine size constraints, limited material types, high material cost and high machine cost[17]. In comparison to conventional manufacturing systems, the build time of large components is often slow. Research is being carried out to develop AM techniques and thus minimise or eliminate these limitations.

2.1.3. Applications of additive manufacturing

Over the past few decades, a lot of work has been carried out to apply AM to a number of applications. At the moment, laser sintering/melting systems are the most generic AM technologies, with applications spanning the aerospace, automotive, medical, energy, creative industries, defence and electronics sectors[18,19]. Table 2-2 shows current and emerging applications of laser sintering/melting technologies, as reported by the UK Technology Strategy Board in 2012.

Applications	Powder bed fusion technologies		
	Polymer	Metal	Ceramic
Aerospace (airframe)	N	Y	N
Aerospace (power)	N	Y	Y
Aerospace (Cabin)	Y	Y	N
Auto (road)	Y	Y	N
Auto (sport)	Y	Y	N
Medical (orthopaedic)	Y	Y	Y
Medical (prosthetic/orthotic)	Y	N	N
Medical (Dental implants)	N	Y	Y
Medical (surgical guides)	Y	N	N
Medical (hearing aids)	Y	N	N
Energy (generation)	N	Y	N
Energy (storage)	Y	Y	Y
Creative industries (artefacts)	Y	Y	Y
Consumer goods (Jewellery)	Y	Y	N
Consumer goods (Toys & games)	Y	N	N
Consumer goods (Home / fashion)	Y	N	N
Defence (Weapons)	N	Y	N
Defence (PPE & armour)	Y	Y	Y
Defence (logistics & support)	Y	Y	N
Electronics (packaging)	Y	N	N
Electronics (sensing)	Y	Y	Y
Prototyping	Y	Y	Y
Tooling & Casting	Y	Y	Y

Table 2-2: Current commercial or near to market application of powder bed fusion AM technology. Y = applied; N = not applied [13]

With research and development into the areas of machine, design and materials further unlocking the potential of AM, the number of applications is increasing widely across a great number of disciplines, such as the aerospace industry, medical, creative and sports. Some recent applications are shown below:

- AM has shown great potential applications in the medical world. It has been applied to provide patient specific implants to reconstruct parts of the human's skeleton for individuals[20]. Figure 2-2 shows a demonstration of a fully customised implant constructed by laser sintering PEEK (polyaryletherketone) from a patient's computer tomography (CT) data. This provides a fast and safe way to produce customised reconstruction implants for an individual patient.

Figure 2-2: An example of patient-specific implant made by laser sintering[20,21]

- With the benefits of tool-less manufacturing and freedom-of-design, AM has big advantages for small volume manufacturing, such as aerospace and sports automobiles. AM has been used by various teams in Formula 1 racing. One of the pioneers of this type of application was the Renault F1 race car,

shown in Figure 2-3 (a), which includes a number of parts built by AM. Figure 2-3 (b) shows the cooling duct used in this car. This duct was designed to improve the cooling of the electrical system. The nature of the geometry makes it impossible to manufacture in one piece using traditional manufacturing techniques. Therefore, laser sintering technology was used to produce this duct[2].

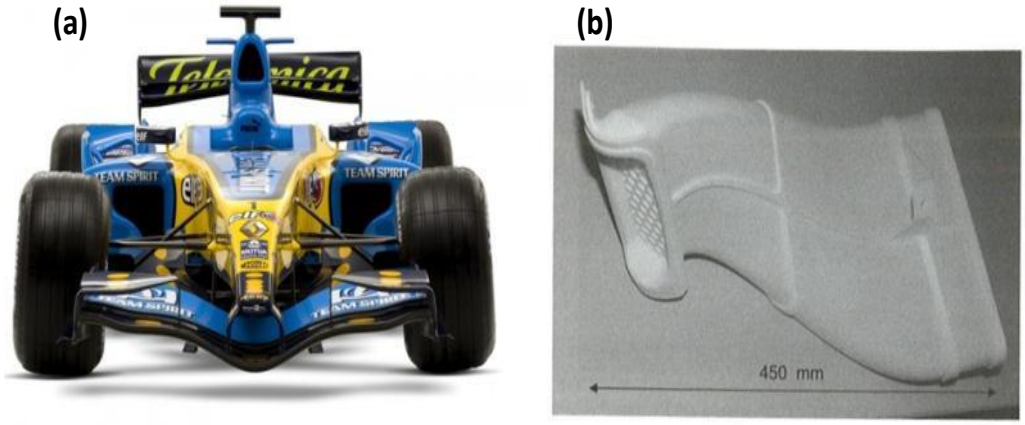

Figure 2-3: (a) Renault Formula 1 race car, (b) Cooling duct used in the Formula 1 race car, which was produced by laser sintering[2]

2.2. Polymer laser sintering

2.2.1. General principle

One of the most widely used additive manufacturing techniques for processing of polymers, laser sintering (LS), also referred to as Selective laser sintering (SLS™), is a powder-based additive layer manufacturing process. A schematic diagram of the laser sintering process is shown in Figure 2-4. In the laser sintering process, a laser either in continuous or pulse mode is used as a heat

source for scanning and joining powder particles into predetermined shapes. The geometry of the scanned layers corresponds to the various cross sections of a CAD (computer aided design) model of the object.

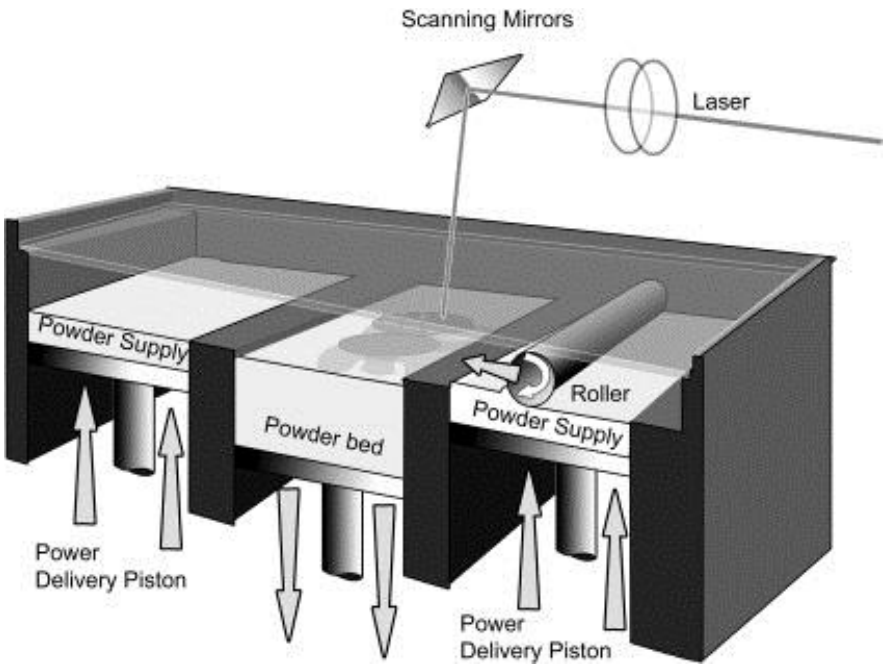

Figure 2-4: Schematic diagram of the laser sintering process[2]

On commercial machines, the part building process takes place inside an enclosed chamber filled with nitrogen gas to minimise oxidation and degradation of the powder material. Several layers of powder are deposited on the building area before the actual parts start to build. The powder deposited in the build area is collectively referred to as the 'powder bed'. The powder bed is first heated to bring the temperature of the powder up to typically a few degrees centigrade below the material's melting point. This pre-heating of powder and maintenance of an elevated, uniform temperature is necessary to minimise the laser power required and to prevent warping of the part during the build due to non-uniform thermal expansion and curling. (Details about thermal expansion and curling are reported in section 2.2.3.)

After the first layer is scanned, the build platform is lowered and a second layer of loose powder is deposited over it. The process is then repeated from bottom to top until the part is complete[22]. The sintered material forms the part while the un-sintered powder remains in place to support the structure. Finally, the parts are removed from the powder, loose powder is brushed away from the parts, and further finishing operations, if necessary, are performed.

The laser sintering process has a number of advantages. Firstly, compared to other additive techniques, such as Stereolithography and fused deposition moulding (FDM) which require support structures, in the laser sintering process support structures are not required as the surrounding un-fused powder provides support, which avoids some post-processing and increases design freedom. The unused powder can often be recycled and reused with a mix of fresh powder (see section 2.3.3.). Secondly, unlike Stereolithography which is limited to photopolymers, there are in theory large numbers of materials that can be processed using laser sintering[23], even though the current available laser sintering materials are limited (see section 2.4).

2.2.2. Consolidation mechanisms in laser sintering

In the polymer laser sintering process, there are two main consolidation mechanisms: partial melting and full melting. Partial melting happens when the heat supplied to a powder particle is insufficient to melt the whole particle, only a shell at the grain border is melted, and the core of the grain remains solid. Full melting means the polymer powders are melted entirely during laser sintering, which could lead to the increased density of the laser sintered parts[24,25]. Full melting actually is laser melting, but this terminology is rarely used for laser processing of polymer powders.

Partial melting and full melting could both exist in laser sintering, which was indicated in the study carried out by Zarringhalam et al[26]. Figure 2-5 shows the cross section of a laser sintered PA12 part. Partially melted particles, which had an unmolten central core, remained in the laser sintered parts. On the other hand, spherulites without cores also existed in the laser sintered parts, which were from fully melted particles. It is believed that the unmolten cores remaining in the laser sintered parts have a significant effect on the mechanical properties of the parts. For instance, elongation at break for laser sintered PA12 parts is much lower than parts produced by traditional processes such as injection moulding. This is believed to be partly due to the porosity of laser sintered parts. However, another possible reason is the presence of these unmolten particles in the laser sintered parts, which introduce a composite-like inter-crystal form structure[26]. If the inter-crystal form interface is weak, crack formation and propagation under stress will be accelerated and will lead to inferior mechanical properties such as elongation at break.

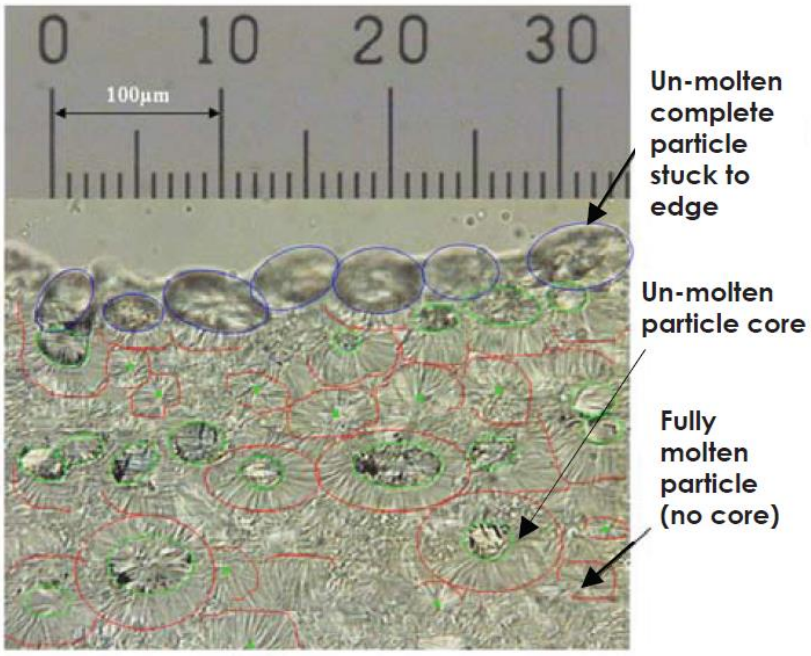

Figure 2-5: Micrograph of the cross-section of a laser sintered PA12 part showing fully melted and partially melted particles[26].

For semi-crystalline polymers, full melting and partial melting mechanisms both exist. Laser consolidation results from heating the polymer above its melting temperature T_m. Above T_m, the molten polymer flows in between the powder particles, forming sintering necks. With enough heat, the complete layer is fully molten and overlaps to the previous layer. When the temperature is cooled below T_m, polymer crystals nucleate and grow, recreating crystallites regions and amorphous regions[27].

For amorphous polymers, a partial melting consolidation mechanism is more common[25]. The consolidation happens by laser heating above the glass transition temperature, when the polymer becomes soft and less viscous. However, compared to semi-crystalline materials at a similar temperature, the sintering rate for amorphous polymers is lower due to inferior polymer flow, which leads to a lower degree of consolidation, higher porosity and lower strength[27]. As a result, amorphous polymer parts are not suitable for applications which require strength and durability. Therefore, most laser sintering polymer materials are semi-crystalline polymers at present.

2.2.3. Fabrication parameters in laser sintering

Use of optimum process parameters in the laser sintering process is extremely important for producing satisfactory parts. The important parameters are listed below. An appropriate combination of these parameters is needed to achieve laser sintered parts with good geometric definition, structure, density and mechanical properties[28-30].

- **Powder bed temperature (Tb)**

In the laser sintering process, the powder bed temperature is controlled in order to achieve repeatable results. 'Curling' and 'caking' can happen if the powder bed temperature is not set correctly. Curling occurs when the powder bed temperature is too low, which causes a high thermal gradient between the sintered and un-sintered material. This will cause distorted or warped final parts, or even worse the curling will block the powder recoater which can lead to the termination of the building process[23,28]. When the powder bed temperature is too high, the powder particle surface starts to melt, which leads to powder agglomeration and caking, resulting in poor part definition and accuracy[31,32].

Selecting the precise powder bed temperature for laser sintering is highly dependent on the choice of polymer due to the complex thermal properties of different materials[28]. The powder bed temperature should be kept as high as possible but below the melting temperature (T_m) for semi-crystalline polymers, or below the glass translation temperature (T_g) for amorphous materials, to achieve optimum mechanical properties for laser sintered parts with relatively low laser input[23,33].

- **Laser power (P)**

Laser power is the power available from the laser as it scans the area of each layer at the powder bed surface. Increased laser power naturally results in increased energy input.

A polymer will become a viscous liquid when heated above T_m or T_g. When it is in its liquid state it can flow, which leads to liquid phase sintering and a

reduction in the porosity of laser sintered parts and a subsequent increase in certain mechanical properties, such as tensile strength and Young's modulus. After the laser scans over the powder bed, the viscosity increases and the diffusion rate decreases. Then, the chains have the chance to rearrange themselves and hence to form the whole part layer-by-layer. The minimum required laser power can be calculated by Equation 1[28]:

$$P = \frac{SS \times \rho \times D_b \times h\,[\,C \times (T_m - T_b) + l_f\,]}{(1-R)} \qquad \text{Equation 1}$$

where SS is the laser scan speed, ρ is powder density, C is specific heat, l_f is latent melting heat, D_b is the diameter of laser beam on powder bed, R is reflectivity (fraction of laser light reflected by the powder)[28].

Laser power has a combination effect with powder bed temperature. Generally, high laser power/high powder bed temperature combinations produce dense parts, but can result in part growth, poor powder recyclability (powder recycling will be discussed in Section 2.3.3.) and difficulty cleaning parts. On the other hand, low laser power/low powder bed temperature combinations can produce improved dimensional accuracy, but result in lower density parts and a higher tendency for layer delamination. High laser power/low powder bed temperature results in an increased tendency for non-uniform shrinkage and the build-up of residual stresses[34]. Therefore, to get satisfactory parts, finding the suitable laser power/powder bed temperature combination for a given material is vital.

- **Scan Speed (SS)**

Laser scan speed is a parameter describing how fast the laser moves when scanning over the powder bed. This parameter influences building time and energy density, as lower scan speed can lead to higher energy input (see 'Energy density' later).

- **Scan spacing (SCSP)**

Scan spacing is the distance between two neighbouring parallel scan vectors. If scan spacing is too great, the cross-section may not be completely sintered. If scan spacing is too small, the laser energy input can be excessive and the part will take a long time to build. Scan spacing is related to the laser beam size and energy input. Scan spacing should not exceed the diameter of the laser beam on the powder bed. Figure 2-6 shows the scan spacing and beam overlap - as the scan spacing decreases, the energy input increases.

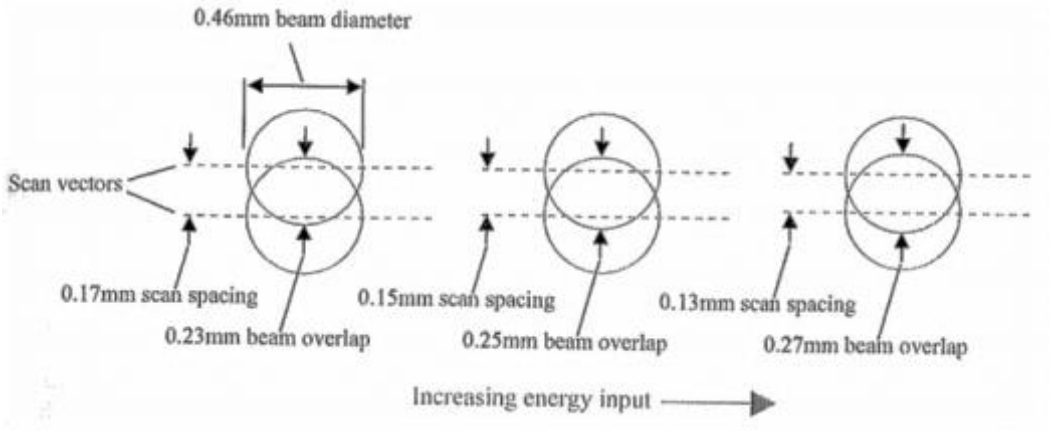

Figure 2-6: The effect of scan spacing and beam overlap on energy input[35]

- **Layer thickness**

Layer thickness is the thickness of each new layer of powder that is deposited, which specifies the depth that the part piston needs to lower for each layer. The layer thickness can affect building time and surface roughness. Parts with rough surfaces and inaccurate dimensions may be built if the layer is too thick. A small layer thickness can decrease surface roughness; however, it takes more time to build the part. Normally, the range of layer thickness is from 0.07mm to 0.5mm. Mostly, on commercial laser sintering systems, the default setting is 0.1mm for polymer laser sintering[4,23]. It must be mentioned that due to penetration of laser energy, the actual layer thickness is normally larger than the set layer thickness in the laser sintering process.

- **Energy density**

Energy density, which is an important factor for laser sintering, defines the intensity of the energy input of the laser. The most common calculation of energy density used by the laser sintering community is a function of laser power (P), fill scan spacing (SCSP) and laser scan speed (SS), shown in Equation 2[36].

$$Energy\ density = \frac{P}{SCSP \times SS}\ J/MM^2 \qquad \text{Equation 2}$$

This equation does not take into account other processing parameters such as layer thickness, powder bed temperature or processing delay. However it has been used widely in the literature. In the research carried out in the current thesis, the same laser sintering parameters were used for both neat

and composite powders for comparison of results. Therefore for simplification purposes and to compare more easily to past research, Equation 2 was used despite these limitations to calculate energy density in this work.

It has been found that there is an optimum energy density for each material, and increased energy density can lead to improved mechanical properties (up to a point), see details in Section 2.2.4.

2.2.4. Factors influencing mechanical properties of laser sintered polymer parts

In the case of mechanical properties, polymer laser sintered parts usually fall short of their injection moulded counterparts[4]. This is due to issues such as porosity and the absence of high pressures and consolidation during manufacturing[50]. Table 2-3 compares the tensile properties of commercial laser sintered PA12 with the range of tensile properties found in typical cast and moulded PA12. The comparison shows that laser sintered PA12 has comparable tensile modulus and ultimate tensile strength (UTS) to traditionally processed PA12. However, elongation at break is significantly lower for laser sintered parts.

Material/process	UTS (MPa)	Tensile modulus (GPa)	Elongation at break (%)
PA12/cast/injection	55 – 83	1.4 - 2.8	60 – 200
PA12/LS	45 ± 3	1.700 ± 0.15	20 ± 5

Table 2-3: Tensile properties of conventionally processed and laser sintered PA12[37-39]

The mechanical properties of other commercial laser sintering polymer materials were compared to some injection polymer materials[25], shown in Figure 2-7. Tensile strength, tensile modulus and elongation at break were compared for laser sintered and injection moulded samples. It can be seen that most laser sintering materials had lower properties than injection moulded materials. Even though some laser sintering samples showed comparable properties to injection moulded parts, none of them were close to the highest values of tensile strength, modulus and elongation at break of injection moulded parts. Elongation at break was lower for laser sintered parts, which can be explained by the possible presence of porosity and short binding/high stiffness necks with little elongation[25].

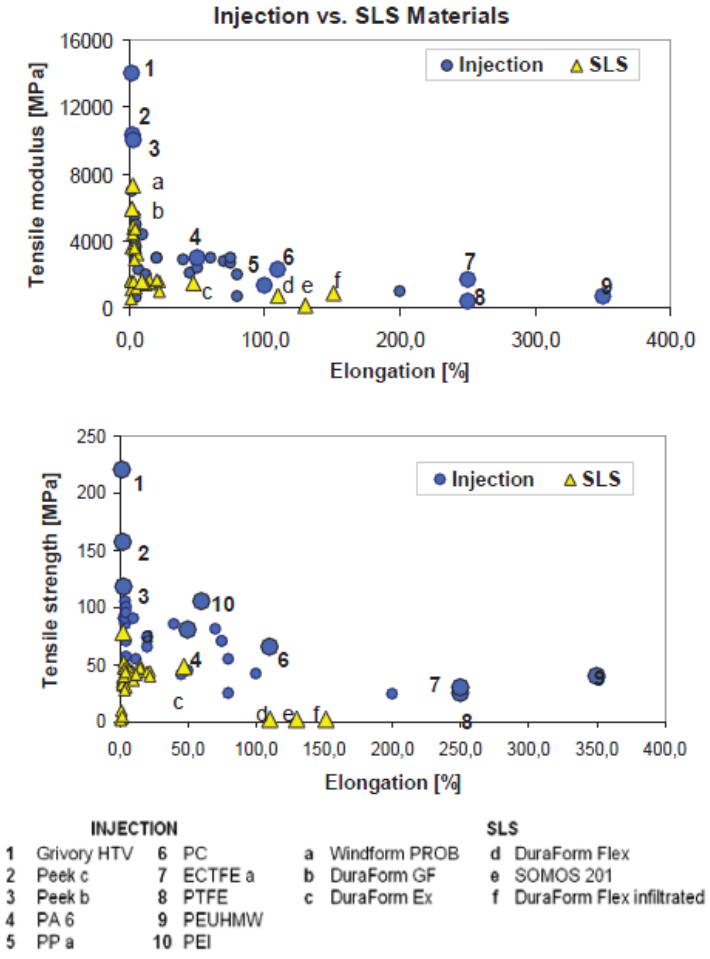

Figure 2-7: Mechanical properties of commercially available laser sintering materials (yellow) and some injection moulded polymer materials (in blue)[25]

For many engineering applications, mechanical properties are the most important aspect. The main aspects which have an influence on the mechanical properties of laser sintered parts are discussed below.

- **Energy density**

Energy density has been shown to have a significant influence on the mechanical properties of laser sintered parts[40]. Ho *et al.*[41,42] carried out some research looking at the effect of energy density on the consolidation of polycarbonate powder. By increasing the energy density levels, the part density and strength of the polymer material increased until a maximum was achieved, which was due to improved particle fusion and melting. When the energy density was raised further, a reduction in material properties occurred. This was due to polymer degradation as a result of the high energy density levels.

Caulfield *et al.*[43] reported the effects of energy density on physical and mechanical properties of PA12 processed by LS. In their research, specimens were produced with laser powers ranging from 6 to 21W. Figure 2-8 shows the effect of energy density on part density. It can be seen that the part density increased with increasing energy density level up until 0.023 J/mm^2. This indicated that higher energy density levels lead to better fusion of the powder particles, resulting in a more solid part being formed.

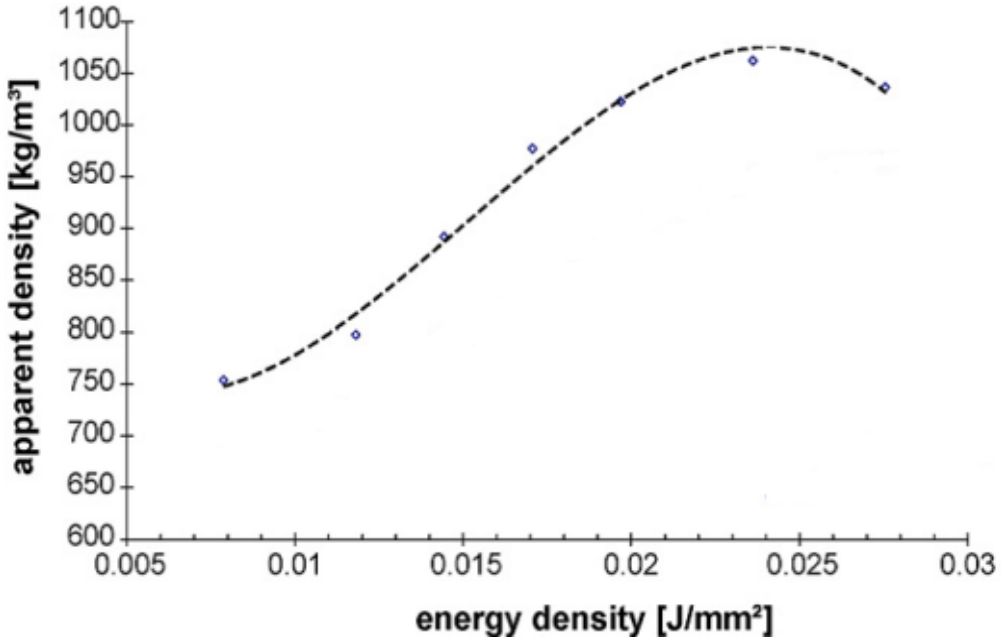

Figure 2-8: Effect of energy density on part density of PA12, modified from reference[43]

The effect of energy density on Young's modulus is shown in Figure 2-9. It can be seen that the energy density level used to produce the parts had a strong influence on the resultant Young's modulus value. Increased energy density caused higher Young's modulus up to a certain point, which can be related back to the density of the parts. Furthermore, the Young's modulus began to fall at an energy density of 0.023 J/mm^2, which was possibly due to particle degradation as a result of excessive exposure of the laser; these results supported the theory put forward by Ho *et al.*[41,42].

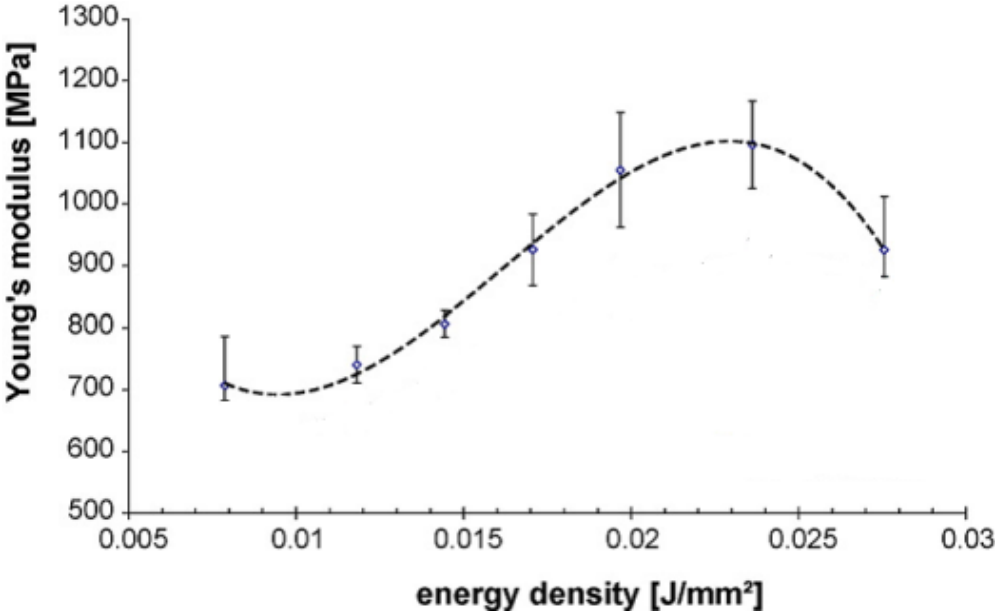

Figure 2-9: Effect of energy density on Young's modulus, modified from Reference[43]

- **Part location**

Beside energy density, the location of a part on the powder bed of a LS machine has been shown to affect the mechanical properties obtained[40,44]. In the research carried out by Childs and Tontowi[44], rectangular blocks were built at nine locations and the densities of the resulting parts were measured. The results obtained highlighted differences in densities which were attributed to the locations of the parts within the bed. Another study carried out by Saleh[45] showed variations across 30 different areas on the powder bed. The parts with the lowest mechanical properties were from the edges and corners of the powder bed, and the parts with the highest mechanical properties were from the centre of the powder bed. The authors in both studies thought that the uneven mechanical properties were due to the inhomogeneous temperature distribution across the powder bed.

Inhomogeneous temperature distribution in the build chamber is one of the major problems found in the laser sintering process[23,40,44,45]. Figure 2-10 shows the temperature distribution on a commercial laser sintering machine EOS P390, recorded in 2011. The inhomogeneous temperature distribution can be seen clearly, which could lead to uneven mechanical properties of parts laser sintered at different locations in the powder bed[23,40,46]. An example is shown in Figure 2-11, where the PA11 parts built in the centre were significantly different (standard deviation of $\pm$ 583MPa) to the parts built in the corners[23]. Therefore, it is suggested that to achieve even and comparable results, parts should be built in the centre area of laser sintering machine where temperature distribution is relatively homogeneous.

The detailed temperature distributions for other laser sintering machines were rarely reported in the literature. To achieve repeatable laser sintered parts, it is believed that the laser sintering machine vendors are improving design and manufacture of their machines in order to achieve more homogeneous temperature distribution.

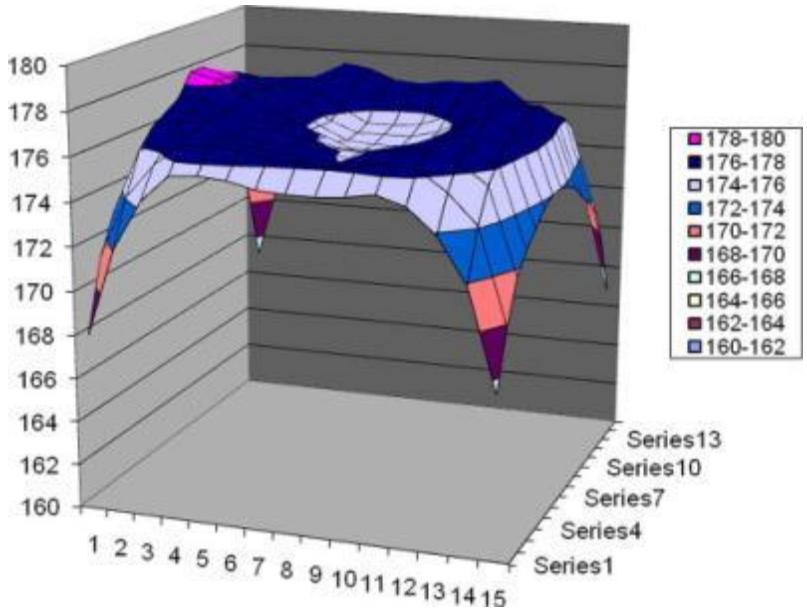

Figure 2-10: Temperature distribution on an EOS P390 laser sintering machine[23]

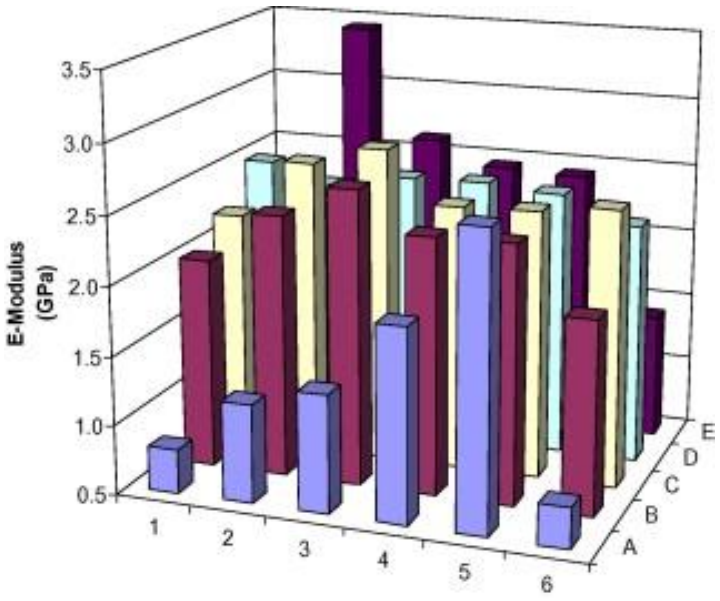

Figure 2-11: Distribution of modulus values on the LS Build Platform for a commercially available LS PA11[23]

- **Part orientation**

Determined by the nature of the layer-by-layer laser sintering process, build orientation also has an influence on the mechanical properties of laser sintered parts[11,28,47]. There are three main build orientations in the laser sintering process, which are X-axis, Y-axis and Z-axis orientations (see Figure 2-12).

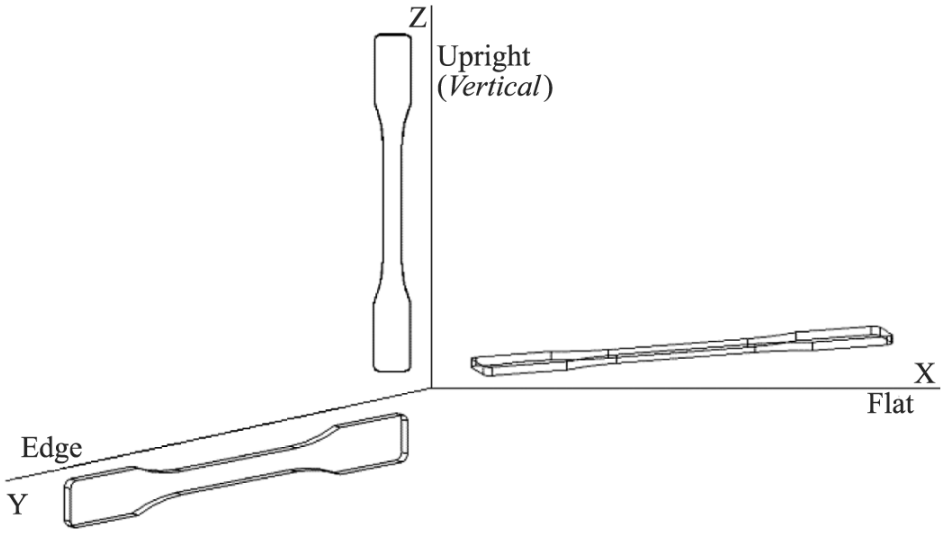

Figure 2-12: Three main build orientations in laser sintering[11]

Gibson and Shi[28] carried out some research into the influence of orientation on mechanical properties. From Figure 2-13, it can be seen that Z-axis orientation had the lowest tensile strength because the applied force was in the direction of the layers. Parts built at X-axis and Y-axis had similar tensile strengths, but X-axis had a larger deviation. This might be due to the cross-section area of X being larger than Y, and a larger area can cause more curling and distortion.

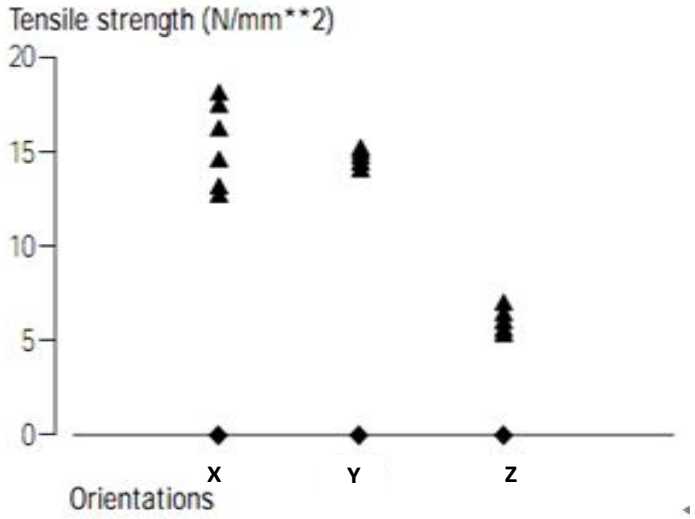

Figure 2-13: Variation in tensile strength of laser sintered PA12 with different orientations[28]

Moeskops *et al*[47] also investigated part orientations for laser sintered PA12. The test parts were produced in a total of six orientations in the XY, XZ, YX, YZ, ZX and ZY orientations, which is shown in Figure 2-14. From the results, there was little variation between the XY, XZ, YZ and YZ orientation test parts. The ZX and ZY orientation parts showed 25% lower tensile strength, which indicated that the tensile strength of z-axis orientation test parts was inferior to those orientated in the x and y axes.

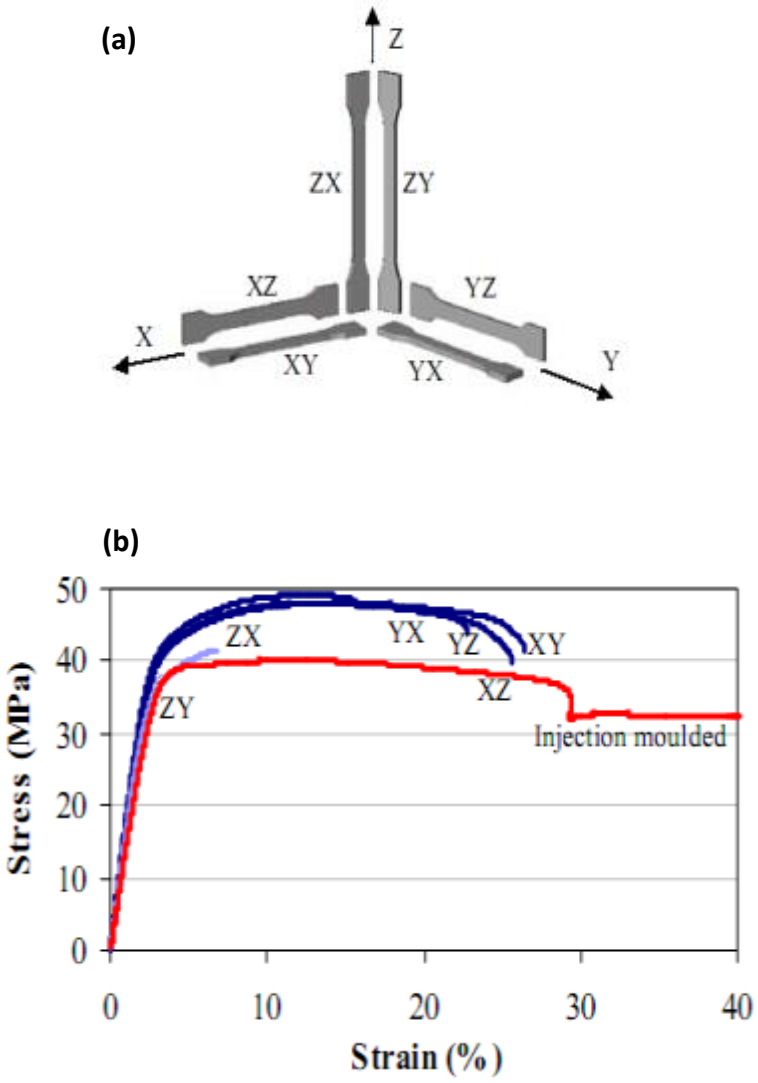

Figure 2-14: Different orientations of fabrication of laser sintered PA12 and their tensile behaviour, which shows the tensile properties variations of parts made from different orientations[47]

There was no a standard to define the different part orientations systematically prior to 2011. To cover this gap, a new standard terminology for Additive Manufacturing—Coordinate Systems and Test Methodologies was therefore published in 2011[48]. According to the definitions from it: "**X axis** shall run perpendicular to the *Z* axis and parallel to the front of the machine; **Y axis** shall

run perpendicular to the *Z* and *X* axes and parallel with one of the edges of the build platform; **Z axis**, for processes employing planar layer-wise addition of material, shall run normal to the layers"[48]. Figure 2-15 shows the six primary build orientations and their notations described in the standard, which are encouraged to be used in the laser sintering work.

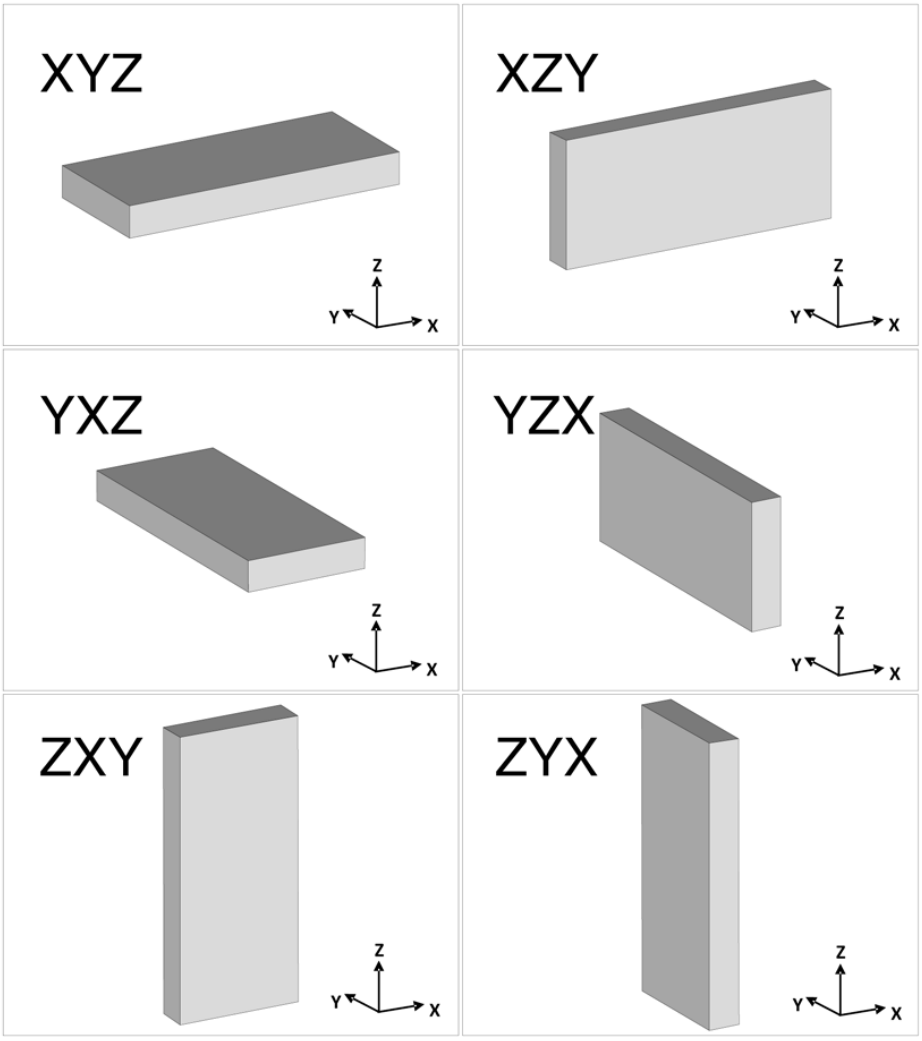

Figure 2-15: Six build orientations and their notation in laser sintering[48]

The feature of the anisotropic properties of laser sintered parts needs to be considered carefully in the product design and manufacturing process. This is particularly important for the building of engineering parts where uniform mechanical properties are normally desired.

- **Part porosity**

Porosity, which is a measure of the total volume of pores, can be described as a percentage of the total non-solid volume to the total volume of a unit quantity of material, shown below:

$$\varepsilon = \left(1 - \frac{\rho}{\rho_s}\right) \times 100\% \qquad \text{Equation 3}$$

where ε is the porosity, ρ is the sintered density and ρ_s is the theoretical density of solid phase[2].

The occurrence of pores is an inherent property of LS parts, and is determined by several factors, such as particle morphology, particle size, powder bed temperature or energy density[42,43,49,]. Porosity, corresponding to density, has been found to have a major influence on the mechanical properties of laser sintered parts, in order of decreasing severity: fracture, fatigue, strength, ductility, and modulus[3,40].

The porosity of laser sintered polyamide has been investigated in many studies[50,71]. In the work carried out by Kruth *et al*[71], the densities of laser sintered PA12 parts (~0.95 g/cm^3) were just slightly below those of compression moulded PA12 parts (~1.04 g/cm^3). Both parts yielded very similar mechanical properties under compression, but somewhat lower tensile strength and

notched Izod impact values that are sensitive to small voids. Besides single PA materials, porosity was also noticed in laser sintered PA composite materials[50], shown in Figure 2-16. Porosity could reduce the reinforcement effect of the filler material. To achieve better mechanical properties, porosity must be minimised during and after the laser sintering process.

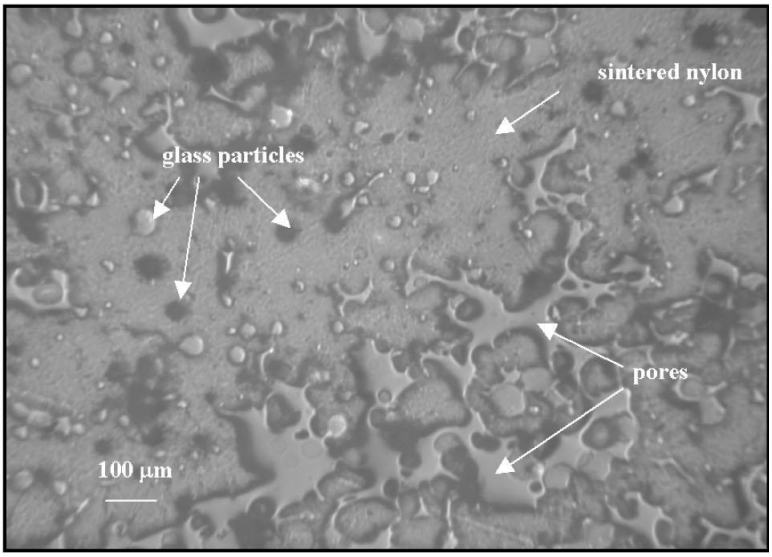

Figure 2-16: Cross section of a glass filled PA part made by laser sintering; some zones of remaining porosity (filled with the sample's embedding material)[50].

In sections 2.2.1. – 2.2.4, the general principle and consolidation mechanism of laser sintering were introduced. The majority of work reviewed here is based on polyamide, which is currently the most commonly used laser sintering material (see section 2.4. for details of polymers for laser sintering). The fabrication parameters in laser sintering, and the influence of these parameters on the properties of laser sintered parts were also discussed. In the next section, the materials properties in laser sintering are reviewed.

2.3. Materials Properties in laser sintering

2.3.1. Particle properties

Due to the nature of the laser sintering process, suitable polymer materials should be in powder form. To date, there are two main methods to produce polymer powders for laser sintering: precipitation and cryogenic milling. Both of them are very costly, which limits the availability of polymer powders[25]. By cryogenic milling, polymer pellets are milled in a pinned disc mill at a defined cryogenic temperature (normally about -35^{o}C for polyamide) to powder particles. Particles produced by this method have random morphology and wide particle size distribution. Monsheimer et al patented[51] a precipitation method to prepare powder particles for laser sintering. Polyamide 12 pellets were dissolved in ethanol (denatured with 2-butanone) in a stirred vessel at 152^{o}C. After a period of 40 minutes stirring with a rotation rate of 160 rpm, the suspension temperature was cooled to 110^{o}C, when the precipitation began. After 25 minutes, the temperature decreased, indicating the end of the precipitation process. Then the suspension was transferred to a paddle drier and dried at 80^{o}C. This method produced near-spherical PA12 powder particles with an average particles size of 55 μm.

Powder morphology, size and size distribution have been found to play a key role in both the ability to process powders by laser sintering (e.g. ease of deposition and spreading over the powder bed) and the quality of laser sintered parts (e.g. surface roughness, density/porosity)[23,54]. Therefore, understanding the properties of the laser sintering powder particles is very important for the process.

- **Particle size**

For optimum spreading over the powder bed, there are limitations on the powder particle size. Powders should flow freely, even at elevated temperature, since good powder flow and spreading are required to form each new layer evenly in laser sintering processing[52]. Powder particles with too small diameter exhibit poor bulk flow at high temperatures, presumably due to the higher interparticle friction found in extremely fine powders. Fine powder particles could produce coagulations clustering, which will have a negative influence on the homogeneous deposition of layers and layer consolidation[27]. On the other hand, particles that are too large have a negative influence on surface finish and part density[53]. For a standard commercial laser sintering machine, which typically has a layer thickness of 100 μm, the optimum particle size in terms of processing ability is generally around 45 – 90 μm[53,54]. Normally, commercial powder has a mean particle size of around 50 μm[23].

- **Particle size distribution**

A typical particle size distribution for laser sintering PA12 (Duraform PA12) is shown in Figure 2-17[25]. Particle size distribution has an effect on the part properties (e.g. density)[55,56]. A previous study by Karapatis *et al.* [55] demonstrated that with a suitable size ratio between coarse and fine particles (over 1: 10) and adequate composition (about 30 %) of fines, a density increase of about 15 % can be expected. McGeary[56] found that a size ratio of approximately 1:7, where the smaller particles constituted 30 % of the volume, gave optimum density when using spherical powders.

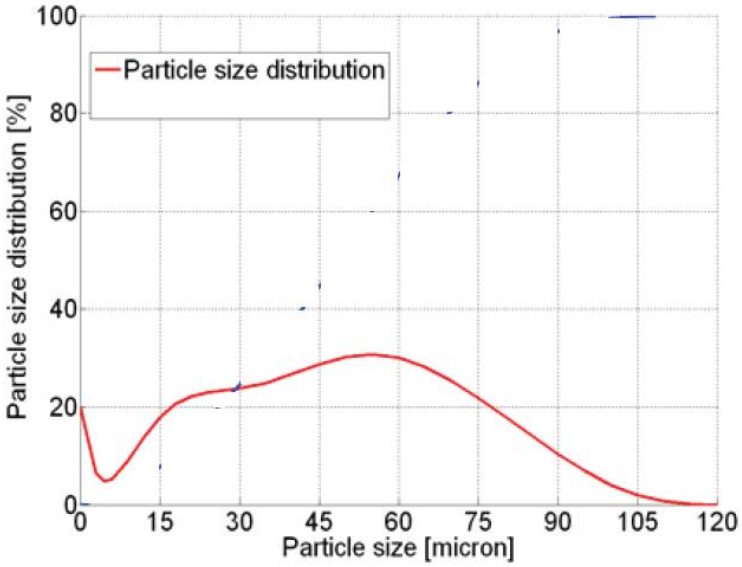

Figure 2-17: Typical particle size distribution of Duraform PA12[25]

- **Particle morphology**

The ideal powder for laser sintering is normally spherical or near-spherical with a regular morphology[23]. Powders with regular morphologies tend to arrange more efficiently during the laser sintering process, which increases the density of parts, while particles with irregular morphologies are not able to achieve this form of efficient arrangement resulting in low density parts. Moreover, spherical morphology can facilitate powder flow, by ensuring that a flat and thin powder layer is deposited during the sintering process[23,57]. Therefore, spherical powder particles are often preferred when available. Non-porous particles are evidently favoured. The study performed by Karapatis *et al*[55] illustrated the achievable density of parts built with particles of various shapes, shown in Figure 2-18, which showed that spherical powder resulted in higher density of laser sintered parts than irregular powder.

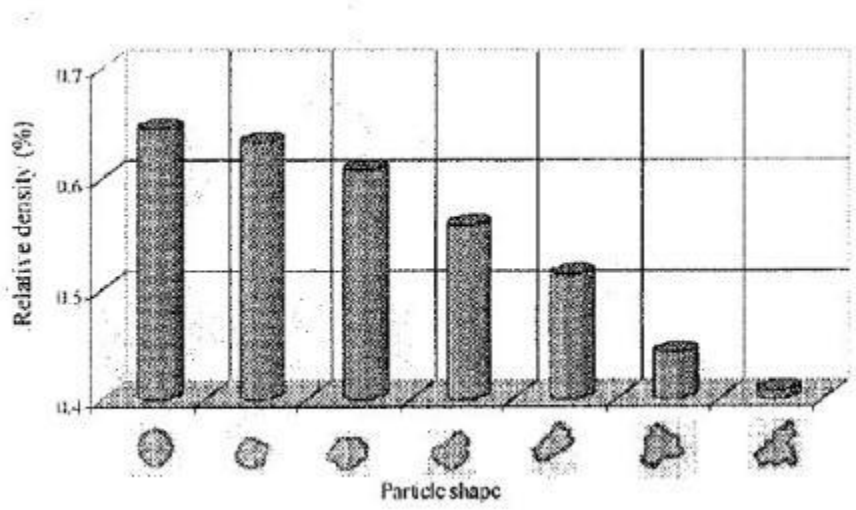

Figure 2-18: Effect of particle shape on the achievable relative density; spherical powder resulted in higher density of laser sintered parts than irregular powder[55]

Figure 2-19 shows the morphology of powder particles made from precipitation and cryogenic milling methods[25]. It can be seen that the powders produced using the precipitation method had near-spherical and regular shapes (Figure 2-19a); however cryogenic milling produced irregular and random-shaped powder (Figure 2-19b), which is not ideal for the laser sintering process.

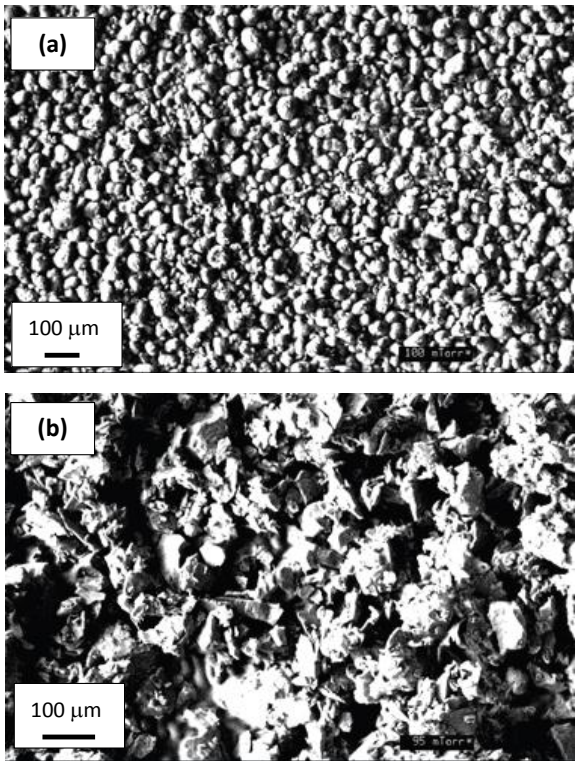

Figure 2-19: Morphology of powder particles made from (a) precipitation and (b) cryogenic milling methods[25]

- **Particle surface state**

Smooth particles will move easily within the powder bed during the powder deposition process, and will lead to a higher loose density. In addition, moisture-free surfaces can prevent the formation of clumps of powder, so that particle motion is not prevented[58].

2.3.2. Viscosity

In the laser sintering process, polymers melt and flow. Therefore the motion of liquid is very important in the process. A critical feature of material flow is

viscosity. For Newtonian flow, the viscosity μ is considered to be the constant of proportionality relating the shear strain rate $\dot{\gamma}$ to an applied shear stress τ[59]:

$$\tau = \mu\dot{\gamma} \qquad \text{Equation 4}$$

For most polymers, there is a similar non-Newtonian power law relationship in which $\dot{\gamma}$ is raised to a power *m* less than one. Viscosity is temperature dependent, decreasing with increasing temperature. Equation 5 shows the viscosity relationship for both liquid polymers and liquid metals:

$$\eta = \eta_0 \exp(\frac{Q}{RT}) \qquad \text{Equation 5}$$

where η_0 is a constant, Q is the activation energy of viscous flow, and R is the ideal gas constant. It can be seen that viscosity is lowered significantly by increasing the temperature[59].

For materials used in laser sintering, low viscosity is generally desirable, which means that the material will flow easily when scanned by the laser. Improved flow will lead to good interfusion of the polymer chains, sufficient particle necking and greater binding between layers, which can improve the mechanical properties of laser sintered parts. This is important for LS because layer binding is critical to successful processing[2].

To achieve full densification, the viscosity of laser sintering materials should be kept lower than a defined value. For example, under similar surface tension driving forces ($\gamma \approx 30$ mN/m), PA12 with a melt viscosity $\eta \approx 100$ Pa·s can be fully consolidated, however polycarbonate, which has a melt viscosity $\eta \approx 5000$ Pa·s cannot be fully densified[60]. However, low viscosity can lead to poor part

accuracy and high shrinkage. For polymer materials, higher viscosity could have the advantage of greater mechanical properties. Improved mechanical properties come from greater molecular weight, which brings higher viscosity. Molecular weight increase can also improve the dimensional accuracy of the laser sintered parts by reducing shrinkage. Therefore, there is a trade-off between these factors when developing a material for laser sintering.

2.3.3. Powder recycling in laser sintering

In the laser sintering process, only a small amount of powder material in one processing cycle is used to make parts and the rest remains as unsintered powder. Recycling of the unsintered supporting powder is necessary for economic (high cost of laser sintering powder) and environmental (minimising waste) reasons. However, holding polymers at elevated temperatures can change the molecular weight of the polymer, which changes the polymer powder properties when they are recycled and reused.

Reuse of the same powder repeatedly can result in continuous thermal degradation over time, which causes a drop in powder flowability and an increase in melt viscosity[25]. Melt flow index (MFI) is a measure of the flowability of a thermoplastic polymer, which can provide information on molecular weight and viscosity. Figure 2-20 shows the MFI of a commercial PA12 laser sintering powders following a given number of runs (reuse times). It can be seen that as the number of runs increased, the powder MFI dropped, due to the rise in melt viscosity of the powders[25].

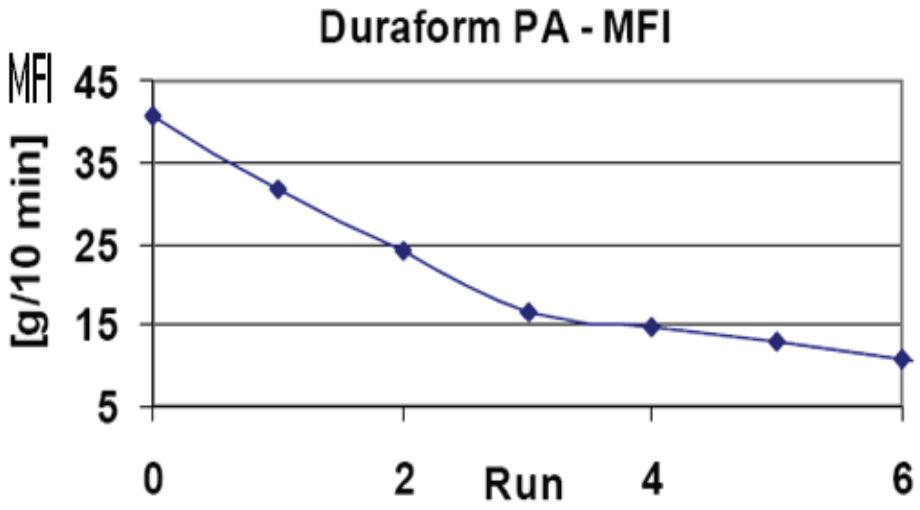

Figure 2-20: Graph showing a decrease in the MFI of a commercial laser sintering PA12 powder as the number of runs increases[25]

A decrease in MFI can prevent powder consolidation, resulting in a possible negative effect on the mechanical properties of laser sintered parts. Furthermore, continual reuse of powder can lead to a poor and rough surface finish for sintered parts. This is commonly referred to as 'orange peel', shown in Figure 2-21[61]. On the other hand, controlled polymer reuse has shown some positive affects in the laser sintering process. Zarringhalam[35] reported improved mechanical properties (mainly elongation at break) for used PA12 powders compared to virgin powders. He suggested that this improvement may have resulted from the increased molecular weight of the used powder.

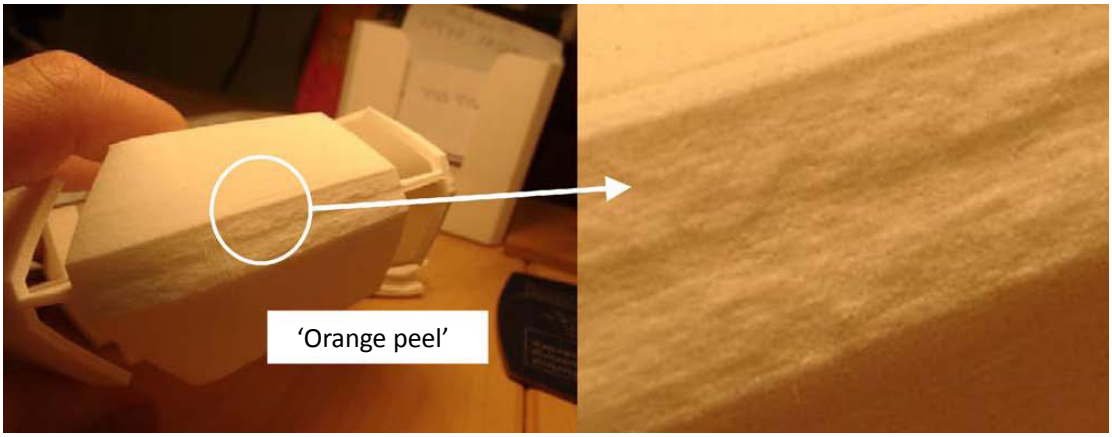

Figure 2-21: Laser sintering part with a poor surface finish known as 'orange peel', resulting from continual re-use of powder[61]

The simplest approach to address the decrease in properties with repeated reuse of the powder is to mix a specific ratio of unused powder with used powder. The ''refresh rate'' (amount of unused powder) is polymer specific. Table 2-4 shows the recommended refresh rates for commercially available polyamide laser sintering powders, as specified by the major manufacturers. It can be seen that for most of these materials, a high portion of fresh powder (>30%) is used in order to avoid poor surface finishing. By stabilising against thermal degradation, the refresh rate is improved to 15 – 25% for the PA12 powder made by Advanced Laser Materials (ALM)[62]. Some other laser sintering polymers, such as PEEK and PC (polycarbonate), have a 100% refresh rate, which hinders the extensive practical application for these new materials[23].

Manufacturer/ material name	Refresh rate fresh powder (%)	Additional recommendations
EOS PA2200 fine polyamide	30 to 50	Scrap the powder if there is severe "orange peel" texture
EOS PA3200 GF polyamide	50 to 70	
3D Systems DuraForm (polyamide)	30 +	Scrap the powder if there is severe "orange peel" texture, normally every 8-10 builds
3D Systems GF DuraForm	50 +	
ALM PA250 Fine polyamide	15 to 25	Stabilised against thermal degradation

Table 2-4: Recommended refresh rates for PA12 and PA12 composite laser sintering powders[61]

Although easy to implement, a simple fraction-based recycling approach will result in a certain amount of mixing inconsistencies due to different thermal history and part layout between different builds. In order to solve the inconsistencies and achieve more efficient recycling, another recycling methodology, based upon a powder's melt flow index (MFI), has been developed[63]. During the laser sintering process, unsintered powder is kept at an elevated temperature (normally above T_g but below T_m) for a certain time. The molecular weight could change during this process, which changes the MFI (viscosity) of the polymer[64]. Measuring the MFI of laser sintering powder is a relatively simple and accurate method to evaluate quality. It has become a standard technique to determine the suitable refresh rate for used polymer powders for achieving good part quality[61,65,66]. For example, in the research

carried out by Dotchev *et al.*[61], in order to produce parts of the required quality, a minimum recommended MFI level for PA12 powder was given as 25-26 g/ 10 min.

In this section 2.3., laser sintering powder properties, namely particle properties, viscosity and recyclability have been reviewed. It must be noted that the rules mentioned in this section for powder properties have been developed mainly through processing PAs, and may not be representative of all polymers. In the following section (2.4), materials which are currently used in laser sintering will be reviewed.

2.4. Polymers for laser sintering

2.4.1 Types of laser sintering polymer

Theoretically, almost any polymer available in powder form can be laser sintered using optimised processing parameters. However, in reality very few polymers are currently available for laser sintering, which is partly due to the complex thermal behaviour of polymers during the laser sintering process and a lack of understanding of how different polymers respond to this.

There are some current guidelines for polymer materials which can be processed by laser sintering. As the powder bed generally needs to be warmed up to a temperature close to the melting temperature (see section 2.2.3), it is difficult to process polymers with more than one tight melting range by laser sintering, which means that the polymers should have fixed controlled consolidation temperature or several very close peaks (typically 5^{o}C)[27]. Various kinds of commercial polymers often have multi-peak DSC curves, which is due to

special chain length design. The DSC diagram of a commercially available polymer blend without real full melting laser sintering processability is shown in Figure 2-22[25]. It can be seen that two different melting points exist for this material, which is not preferable for the laser sintering process.

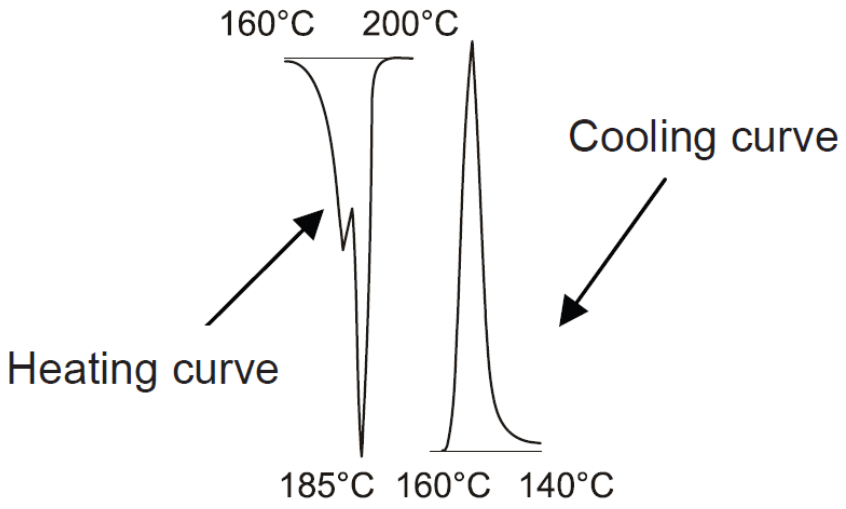

Figure 2-22: Commercially available polymer with no real laser sintering processability. (left) melting curve; (right) recrystallisation curve[25]

The consolidation process (solid – melt – solid) is fast in the laser sintering process. The melt viscosity of the polymer materials should be low enough to complete consolidation and achieve fully dense parts[25]. It was reported that polymers with a melt viscosity range from a few tens to a few thousand Pa·s could be laser sintered to near full density successfully[67]. However in reality, even the most commonly used laser sintering polymer material, PA12, cannot achieve 100% fully dense parts. It is believed that both partial melting and full melting occurs during the laser sintering process for PA12[26].

Laser sintering can process both amorphous and semi-crystalline polymers. Amorphous polymers do not exhibit a defined melting temperature (T_m), only a

glass transition temperature (T_g). In the laser sintering process, amorphous polymers are generally pre-heated near or above T_g, which is decided by the molecular weight and powder size[25]. When the temperature is increased above T_g by the energy from the laser, they soften gradually to a melt state without clear transition. Amorphous polymers normally only experience partial consolidation and thus their sintering rates are lower than that of semi-crystalline polymers. Higher residual porosity makes amorphous polymers parts suffering from inferior strength compared to traditionally processed counterparts[31]. Amorphous polymers normally have the advantage of low levels of volumetric shrinkage upon cooling (Figure 2-23), which enables the manufacture of components with high dimensional accuracy [68]. High dimensional accuracy and high degree of porosity makes them well suited for production of patterns/masters for casting/moulding applications[69].

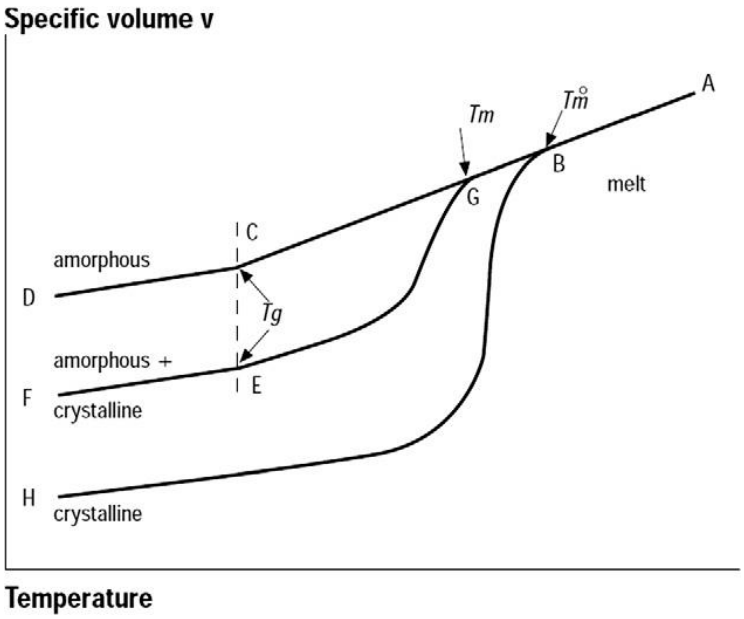

Figure 2-23: Volumetric variation with temperature for amorphous and crystalline polymers

In contrast with amorphous polymers, semi-crystalline polymers have both defined T_g and T_m. Unlike amorphous polymers which soften gradually when heated above T_g, semi-crystalline polymers change rapidly from solid state to viscous liquid when heated above T_m. Compared to amorphous polymers at a given temperature, semi-crystalline polymers are less viscous above the melting point temperature. This leads to a near-full consolidation for semi-crystalline polymers and near-full density laser sintered parts[23]. However, due to higher level of volume change upon cooling through T_m (Figure 2-23), semi-crystalline polymers exhibit greater shrinkage compared to amorphous materials. This leads to issues such as distortion of the part and part dimensional accuracy[28]. To prevent this, semi-crystalline polymer powders should be pre-heated and post-heated in a temperature range between the melting and crystallisation temperature. In this temperature range, parts will be cooled down slowly and no major part distortion will occur[27]. Therefore for laser sintering semi-crystalline polymers, it is recommended to have a clear temperature range between melting and crystallisation peaks. Figure 2-24 shows a DSC curve of PA12, where a relatively large temperature range between melting and re-crystallisation peak can be seen clearly[27].

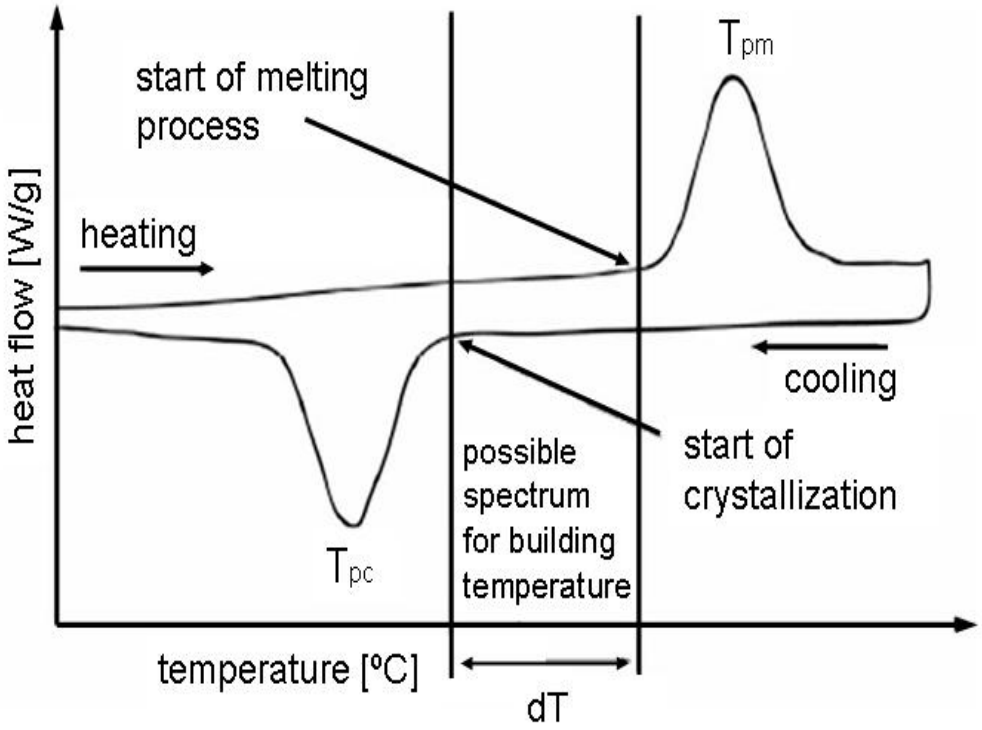

Figure 2-24: DSC-curve for melting and crystallisation of PA12[27]

Figure 2-25 shows the phases and transition temperature ranges of a selection of polymers. For amorphous polymers, T_n is the weakening temperature where polymers start to soften. T_f is the flow temperature range in which the polymer melts quickly. These polymer properties are very important in the laser sintering process, which can be used to guide the setting of the laser sintering parameters[25].

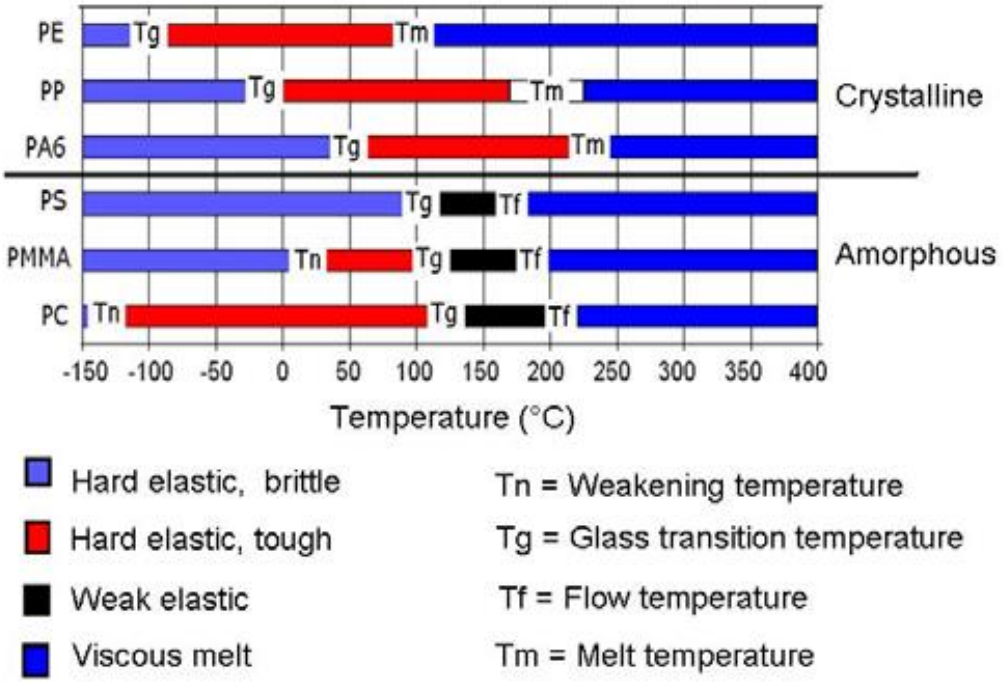

Figure 2-25: Phases and transition temperatures of some polymers[25]

2.4.2 Commercial polymers for laser sintering

Compared to traditional manufacturing process such as injection moulding, the range of available polymers for laser sintering is still very small at the moment. Figure 2-26 illustrates the common thermoplastic polymers (both amorphous and semi-crystalline) which have been used in laser sintering. Polyamides 11 and 12 (PA11/PA12) are by far the most commonly used laser sintering materials at present, making up more than 95% of the current laser sintering materials market[70]. Commercial PA powder has near-spherical morphology, even particle size distribution, clear melting and crystallisation temperature peaks, a defined temperature range between melting and crystallisation temperatures and low melting viscosity. These characteristics contribute to their ease of processing and history of use in laser sintering.

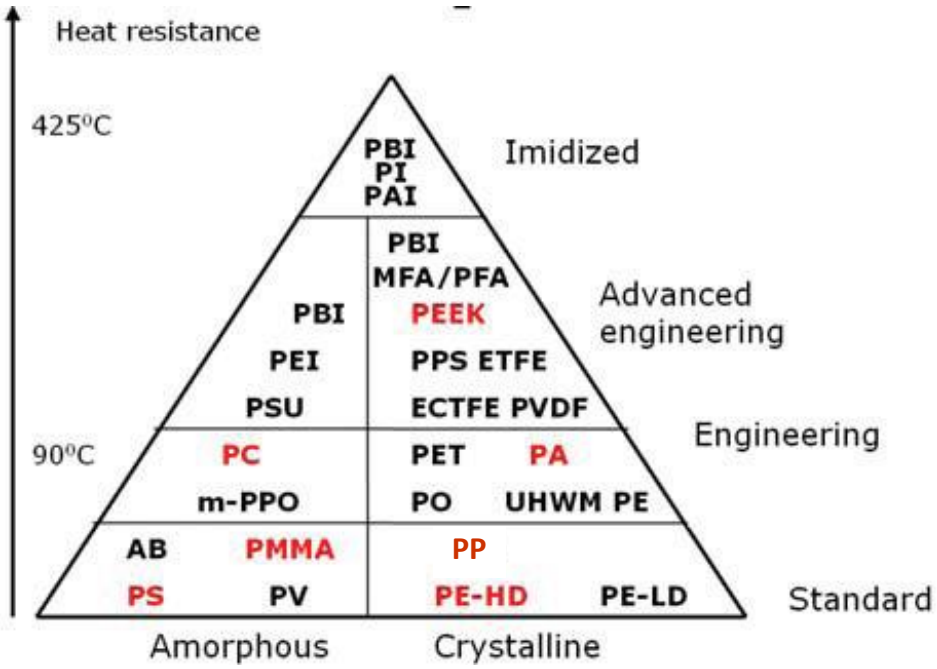

Figure 2-26: Thermoplastic polymers (red = materials currently used in laser sintering)[71]

Aside from polyamides, a handful of other polymers such as polypropylene (PP), polystyrene (PS), polycarbonate (PC), poly(ether-ether-ketone) (PEEK) have also been supplied by companies such as EOS, 3D systems and ALM for laser sintering[72,73]. A few thermoplastic elastomer polymers, such as DuraForm Flex® from 3D Systems, and TPE 210-S from ALM can also be processed by laser sintering. Table 2-5 lists a selection of major commercially available laser sintering polymers along with their key properties. EOS and 3D Systems also manufacture laser sintering machines. The mechanical properties of EOS and 3D Systems polymers listed in Table 2-5 were collected from samples made from their own brand laser sintering machines. The data for ALM materials were got from samples made on a Sinterstation 2500+ platform[76]. Due to the differences between various laser sintering machines (such as powder feeding or powder heating system), for the same material, the properties of sintered parts may vary if they are built by different laser sintering machines[23].

Materials	Trade name	Manufacturer	Tensile modulus (MPa)	Ultimate tensile strength (MPa)	Elongation at break (%)	Part density (g/cm^3)
PA12	PA2200	EOS	1700	50	24	0.93
	DuraForm PA	3D Systems	1586	43	14	1.00
	PA650	ALM	1700	48	14	1.00
PA11	PA1101	EOS	1600	48	45	0.99
	DuraForm EX	3D Systems	1517	48	47	1.01
	PA 860	ALM	1475	48	51	0.96
PS	PrimeCast 101	EOS	1600	5.5	0.4	0.77
	CastForm PS	3D Systems	1604	2.8	-	0.86
	PS 200	ALM	1604	2.8	-	0.86
PEEK	EOS PEEK HP3	EOS	4250	90	2.8	1.31
Elastomers	DuraForm Flex	3D Systems	1.8	7.4	110	-
	TPE 210-S	ALM	-	8.0	90 – 250	1.03

Table 2-5: Major commercially available laser sintering polymer materials and their key properties[74-76]

The polymers shown in Figure 2-26 and Table 2-5 are single polymers, which can meet the requirements of some applications. However, these polymers have limited use, particularly in more demanding engineering applications where improved mechanical properties are required or other properties (such as electrical conductivity) are desired. This has led to the development and research of composite materials for laser sintering, which will be discussed in the following section.

2.5. Composites in laser sintering

There are two main reasons for processing composites by laser sintering: 1. To combine different materials for achieving properties unachievable by a single material. 2. To facilitate the laser sintering process using liquid phase sintering (LPS) mechanisms. The first reason is the main purpose of developing polymer composites for laser sintering[77]. There are currently two main types of polymer composites being studied in laser sintering: polymer blends and polymer/filler composites.

2.5.1. Polymer blends

A polymer blend is a composite in which two or more polymers are blended together to create a new material with different physical properties[78-80].

According to the author's knowledge, few papers have been written on polymer blends for laser sintering. Salmoria *et al.*[80] investigated the processing of blends of PA2200 (PA) and high-density polyethylene (HDPE) by laser sintering. Depending on the blend ratio (80/20, 50/50 and 20/80 wt%), different phases and micro-structures were observed using SEM, EDX and XRD analysis. Results suggested that it is feasible to manufacture parts from polymer blends using laser sintering, by selecting the polymer properties, powder characteristics and optimum process parameters. However, the mechanical properties of the laser sintered parts were not reported. Fracture SEM images of laser sintered parts showed noticeable porous and unmelted powders remaining, which can lead to poor mechanical properties of laser sintered blend parts.

Each component in a blend has a different density and compatibility; therefore it is very difficult to blend them uniformly. Furthermore, different thermal properties, such as melting temperature, heat of fusion or thermal conductivity, could lead to incomplete powder melting (laser power too low) or polymer degradation (laser power too high) for different component of the blends. Due to these unfavourable factors, another polymer composite – polymer/filler composites has been utilised and studied more widely.

2.5.2. Polymer/filler composites

Polymer/filler composites have been more widely researched and commercialised for laser sintering[81-85]. Normally, there are two main types of polymer/filler composites in LS. In one case, the powder may be a mixture of polymer particles and reinforcement particles. However due to the morphology and density difference between polymer and reinforcement particles, it is difficult to mix them uniformly[86].

Alternatively, the single powder particles may already be a composite consisting of a polymer matrix containing filler particles or polymer coated filler particles. A single composite particle can achieve uniform mixing of polymer and reinforcement fillers and yields a uniform spread of composite components in the final product. However, it was found difficult to draw smooth layers of powder bed if long or continuous fibre fillers were used[77].

As the most common laser sintering material, PA12 has been compounded with other materials in order to further improve its mechanical or thermal properties[87]. Table 2-6 shows the mechanical properties of laser sintered neat PA12 and glass filled PA12 composites from EOS. Glass-filled PA12 parts showed

improved modulus and strength compared to neat PA12 parts, however the elongation at break decreased for glass-filled PA12.

Mechanical properties	Neat PA12 (PA2200)	PA12/Glass (PA3200 GF)
E-modulus (MPa)	1700	3200
Tensile strength (MPa)	50	51
Elongation at break (%)	24	9

Table 2-6: Overview of the mechanical properties of commercial available PA12 and glass filled PA12[88]

Polymer composites with macro-size fillers have shown their ability to enhance the strength of laser sintered parts[77]. However, problems such as uneven mixing, difficulty incorporating into processing and reduction in impact strength of laser sintered parts do exist[77]. To achieve improved processing and reinforcement effects, polymer nanocomposites have been introduced for laser sintering, which will be discussed in the following section 2.6.

2.6. Polymer nanocomposites

2.6.1. Background

As a hot research topic in recent decades, nanotechnology research is evolving and expanding very rapidly in nearly every science area. Nanotechnology refers widely to a field of applied science and technology, the theme of which is the

control of matter on the atomic and molecular scale (1 to 100 nanometres)[89-91]. It is a highly complex field which includes applied physics, interface science, materials science, mechanical engineering, electrical engineering and so on[92-95].

As a branch of nanotechnology, nanocomposites were discussed in the early 1950s[96], and became widely studied in academic and industrial laboratories after Toyota researchers began a detailed examination of silicate clay layered polymer composites[97-100]. Polymer nanocomposites (PNCs) are a class of composite that are nanofiller reinforced polymers for which at least one dimension of the dispersed filler is in the nanometre range. Nanoscale fillers have a very high surface-to-volume and aspect ratio, and the distance between the polymer and nanofiller components is extremely short. This results in a molecular interaction between the polymer and the nanofillers and gives polymer nanocomposites unusual material properties (mechanical, electrical, etc.) that conventional polymers do not have[94,101-105]. With extremely high surface-to-volume ratios, even a very small amount of nanofiller can have an observable effect on the macroscale properties of the composite[106]. Compared to macro-size fillers, the required nanofillers loading is typically much less[52].

Typically there are three types of nanofillers under investigation: fibrous, particle and layered nanofiller[107]. Figure 2-27 shows the representative geometry for each type and their surface-to-volume ratios. For fibrous and layered nanofillers, their surface-to-ratio is decided mainly by the fibrous diameter and layer thickness[108]. For fibrous nanofillers, their diameter is in the nano-meter range. They are mainly carbon or metallic materials in nature; carbon nanotubes and carbon nanofibres can be classified as fibrous nanofiller. The particle nanofillers have a nano-meter diameter. Silica nanoparticle and carbon black are examples of particle reinforcing nanofiller. Layered nanofillers

have a plate-like structure, and only one dimension (thickness) is in the nanometer range. These fillers are in the form of sheets of one to a few nanometres thick with a high aspect ratio (30 – 1000). The most widely used layered nanofillers are nanoclay (layered silicates)[108,109].

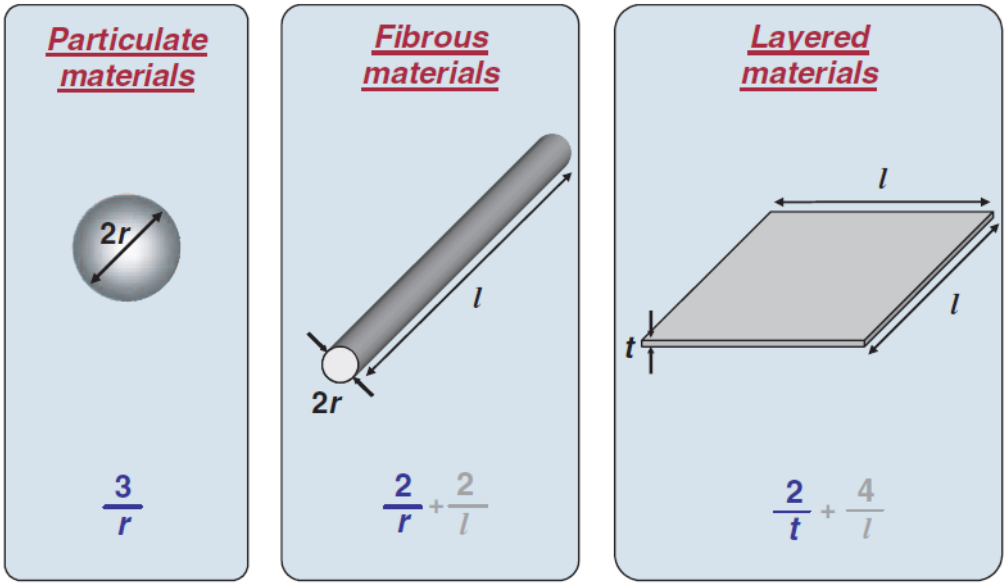

Figure 2-27: Common nanofiller reinforcements/geometrics and their respective surface area-to-volume ratios[107].

The essential components for optimal reinforcement in nanofiller-reinforced composite systems are filler dispersion, orientation, compatibility and reaggregation[110]. Dispersion of the nanofiller into a polymer matrix has been one of the largest challenges when producing polymer nanocomposites. For example, the Van der Waals force interactions between individual carbon nanotubes make them very easy to agglomerate, which could lead to an inconsistent dispersion of CNTs in the polymer matrix. Good dispersion of the reinforcing nanofillers throughout the matrix is very important, which leads to consistent load transfer from the matrix to nanofillers. Furthermore, good dispersion can also assist the realisation of a network for the conductivity of electrical and thermal energy[110,111]. A poorly dispersed nanocomposite may

degrade the mechanical properties[112]. For example, Figure 2-28 shows three different types of polymer/layered silicate nanocomposites. The properties of unseparated silicate composite (Figure 2-28a) will stay in the same range as a traditional microcomposite. The nanocomposite can be prepared with intercalated (Figure 2-28b) and exfoliated (Figure 2-28c) structure, and the physical properties of them are significantly different from microcomposite[113].

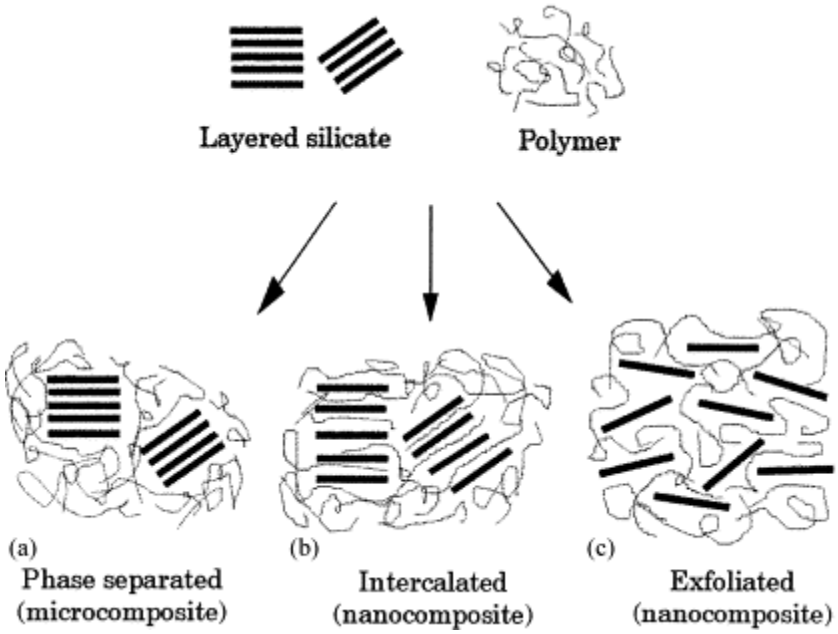

Figure 2-28: Schematic of different types of composite arising from the interaction of layered silicates and polymers: (a) phase-separated microcomposite; (b) intercalated nanocomposite and (c) exfoliated nanocomposite[113].

Nanofiller orientation also has an effect on the success of a nanocomposite. When the nanofiller is oriented in the direction of the applied force, the full potential of the nanofiller can be realised. Moreover, same direction oriented nanofiller could facilitate the transfer of electrical or thermal energy. Good compatibility between the nanofillers and the polymer matrix is also required to achieve strong interaction. It is common to functionalise nanofillers to improve their compatibility to the polymer matrix, however concerns have been raised

about the effect on the properties of the nanofiller through functionalisation[108,114]. During the processing stage, there is a possibility of reaggregation where the nanofillers clump together, which could also lead to unsuccessful nanocomposite production.

There are three common methods used to generate polymer nanocomposites: in-situ polymerisation, exfoliation-adsorption and melt compounding. By in-situ polymerisation technique, the nanofillers (normally layered nanofillers) are swollen within the liquid monomer (or a monomer solution), so the polymer formation can occur between the nanofillers. This process can facilitate the intercalation of high molecular weight polymer chains inside the clay interlayers[106]. Furthermore, this process also leads to much better interfacial contacts between the organic and inorganic phases. Polymerisation can be initiated by many ways, for instance, by heat or radiation, by the diffusion of a suitable initiator or by an organic initiator or catalyst fixed through cationic exchange inside the nanofiller before the swelling step by the monomer[115].

Exfoliation-adsorption method introduces a solvent as a medium to integrate the polymer and nanofiller molecules. The solvent used in the process should be able to dissolve the polymer, and the nanofillers can be swollen in the solvent. Common solvents for this method are toluene, chloroform and acetonitrile, in which the nanofillers such as layered nanosilicates, can be easily dispersed because of the weak forces between the layers. This method was used initially by the Toyota Research Group to produce polyamide nanocomposite[116]. However the shortcoming of the exfoliation-adsorption method is the use of large amount of solvent in the resin system, which makes the removal of the solvent after the process difficult. Furthermore, the use of solvents is also not environmentllay-friendly[115,117].

Melt compounding is the most widely used method for polymer nanocomposite production. This method is based on the molten state, in which the nanofillers are mixed with the polymer matrix. It is done simultaneously when the polymer is being processed through an extruder, injection moulder or other processing machine under elevated temperature. If the nanofillers are sufficiently compatible with the polymer matrix, the polymer can get into the interspace of the nanofiller and form either an intercalated or exfoliated structure. One advantage of this technique is that no solvent is required during the process. As the compounding process happens at elevated temperature, the processing time should be optimised to minimise any thermal degradation[106,108].

It has been widely reported that by adding nanofillers into the polymer matrix, the mechanical properties were improved. Okada *et al*[118] prepared PA6/clay nanocomposite via in situ polymerisation method. Compared to neat PA6, with incorporation of 1 wt% of nanoclay, the mechanical properties for PA6/nanoclay showed significant enhancement, as the tensile strength and modulus were increased by 55% and 91%. Heat distortion temperature was also increased by 134%. In the study carried out by Kearns *et al*[119], PP/CNT nanocomposites were produced with a combination of solvent processing and melt spinning for improved dispersion and orientation. Results showed that by adding 0.5 wt% and 1wt% CNT into PP matrix, the tensile strength and modulus were improved. At 1 wt%, the tensile strength and modulus were 40% and 55% higher than neat PP. However, additions of 1.5 wt% and 2 wt% made spinning of the fibres difficult and led to lower mechanical properties. The tensile strength of PP/CNT with 1 wt% loading was between high-strength industrial PP and Kevlar® fibers.

In addition to improving mechanical properties such as strength and modulus, multifunctional features of PNCs can also improve other properties such as

thermal resistance[94], flame resistance[128], optical properties [120], thermal conductivity[121], and biodegradability[122]. Furthermore, PNCs have been shown to improve the base polymer's properties while remaining processible by conventional processing techniques[123,124], and this potential is also expected for the laser sintering process. It is also believed that using PNCs materials in laser sintering processing could help change rapid prototyping into additive manufacturing[125].

2.6.2. Polymer nanocomposites for laser sintering

To enhance the mechanical, thermal, or electrical properties of current laser sintering materials, much research in recent years has focused on PNCs. Various reinforcing nanofillers combined with base polymers have been investigated for laser sintering[23,126]. Koo et al[127,128] used carbon nanofibres to improve the mechanical properties and flammability of PA11 parts made from injection moulding and laser sintering. Due to the insufficient density of the laser sintered parts, the success seen with the injection moulded PA11 nanocomposites was not translated to the laser sintered counterparts. Nanoclay has also been used to produce polymer nanocomposites for laser sintering[129-131]. Jain et al[131] carried out a study to examine the feasibility of processing blended PA12 and nanoclay using laser sintering. The nanoclay did not improve the mechanical properties of laser sintered PA12 parts. The authors suggested it was due to non-homogeneous dispersion of nanoclay and partial powder melting during the sintering process. Zheng et al[132] reported a PS/nano-Al_2O_3 nanocomposite made by emulsion polymerisation for laser sintering. Compared with the PS/nano-Al_2O_3 composite made from mechanical mixing, the composite made from emulsion polymerisation showed a core-shell structure, which had increased laser beam absorbance and improved tensile properties.

The starting point of all this research has been to prepare suitable PNCs powders for laser sintering. Besides the particle morphology and size distribution as discussed in section 2.3.1., uniform dispersion and good interfacial adhesion between nanofillers and polymer matrix is also crucial to lead to properties enhanced by PNCs. Different techniques have been used to prepare the PNCs powders for laser sintering, which are discussed below.

Mechanical mixing is a common method to prepare PNCs powder for laser sintering[126,133-136]. However, it is difficult to obtain well-dispersed PNCs powder by simple mechanical mixing or milling, and nanofiller agglomerates are normally observed[135,134]. In the research performed by Athreya *et al*[134], PA12/carbon black (4 wt%) nanocomposite powder was prepared by mechanical mixing. After laser sintering, the PA12/carbon black parts showed improved electrical conductivity but decreased flexural modulus compared to neat PA12 parts. SEM showed that the reduction in flexural modulus was due to agglomeration of the carbon black particles on the surface of PA12 powders, as shown in Figure 2-29.

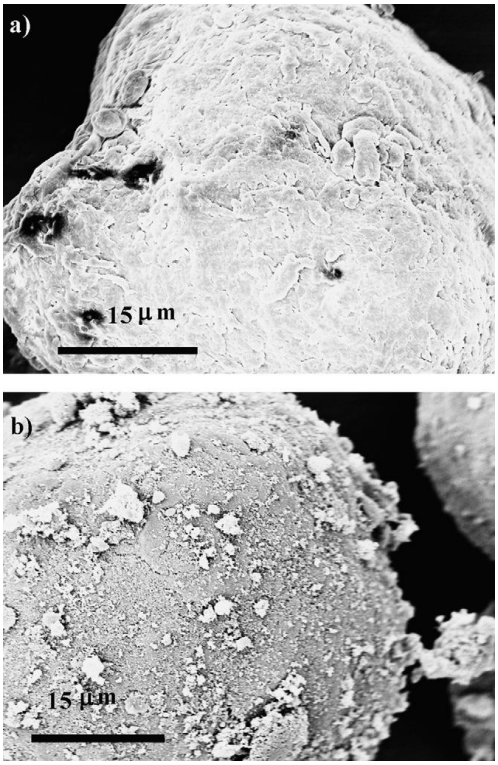

Figure 2-29: SEM images of (a) PA12 powder, and (b) carbon black-coated PA12 powder[134]

Salmoria *et al*[135] produced a PA12-CNT (0.5 wt%) nanocomposite for laser sintering by mechanical mixing, with the parts showing improved tensile strength (10%) compared to neat PA12 parts. However, there was a 9 - 11% reduction in elongation at break of the PA12-CNT parts compared to the neat PA12, which could be due to the CNT agglomerates acting as defects in the laser sintered parts. To achieve maximum properties for final parts, the nanofiller should not form aggregates and must be well-dispersed in the polymer matrix[136,137], otherwise aggregates could act as defects and there will be a weakening effect on the PNCs[138].

In an attempt to produce nanocomposite powders with near-spherical morphology, Wahab *et al.*[139] prepared a polymer nanocomposite powder using a spray drying process, which involved the atomisation of a liquid feedstock into

a spray of droplets. The process is shown in Figure 2-30. First, the PA6 powder and nano particles were dissolved in organic acid in separate containers and stirred for 3 hours. Then the dispersed nano particles were added into the PA6 solution and it was continued to be stirred. After that, the mixture solution was spray dried to powder form. A ball mill was used to separate any agglomerated powder. Finally, the powder was sieved to sub 70μm, and powders produced from this method were spherical in shape. However, the main problem found for this method was voids in the laser sintered parts, which reduced the parts density and strength. The authors proposed that the voids might be from the trapped gases generated from the residual solvent during the spray drying process.

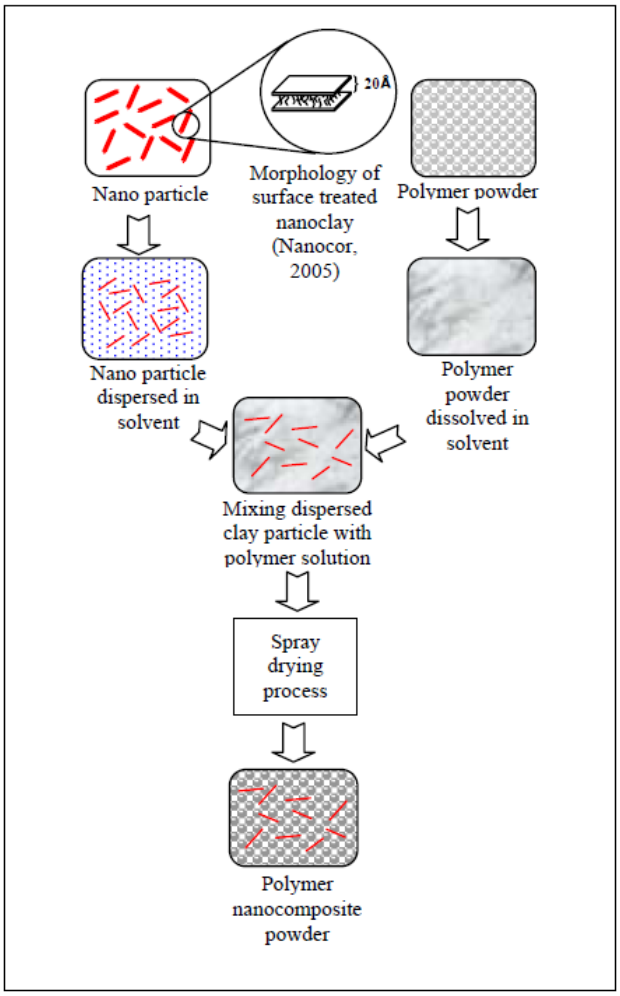

Figure 2-30: Schematic representation of the solution-spray drying process used to prepare polymer nanocomposite powders[139]

A cryogenic fracturing method has been used in some work to produce well-dispersed PNC powder for laser sintering[57,125]. In the research carried out by Goodridge *et al*[57], a well-dispersed 3 wt% PA12/carbon nanofibre (CNF) composite sheet was produced by melt mixing and compression moulding firstly. Then, the nanocomposite powder was produced by cryogenically fracturing the composite sheet. After laser sintering, the nanoparticles increased the base material's properties produced by the same cryogenically fracturing method, but not compared to non-cryogenically prepared powder, which can be seen from the DMA results in Figure 2-31.

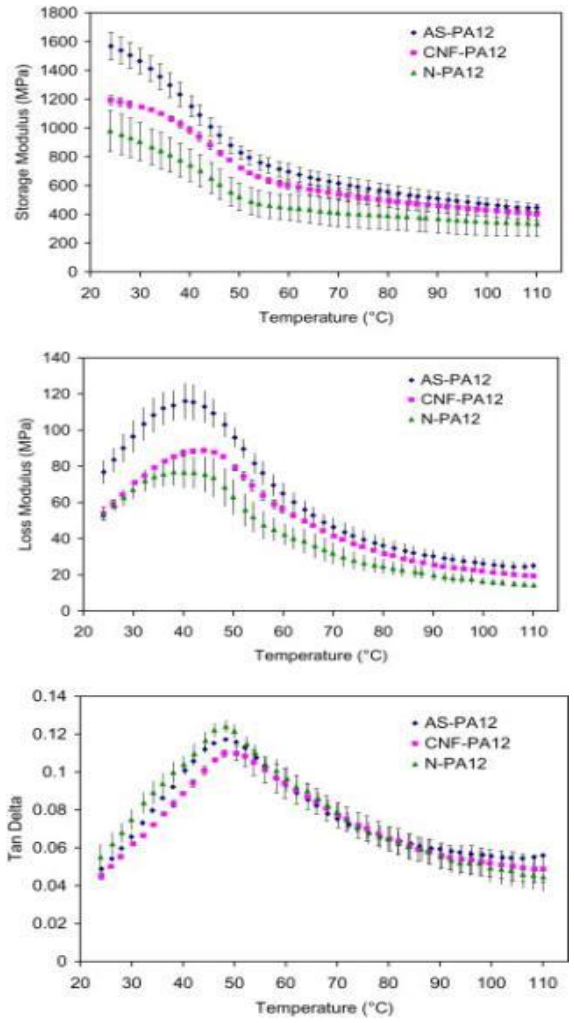

Figure 2-31: DMA results for three samples processed by laser sintering (AS-PA12: as-received neat PA12; CNF-PA12: carbon nanofibre-PA12 composite prepared by melt mixing; N-PA12: neat PA12 prepared by melt mixing process)[57].

In the same work, SEM observation showed that the nanocomposite powders produced by the cryogenic fracturing process had irregular powder morphology and a wide particle size distribution, shown in Figure 2-32. The authors hypothesised that the irregular powder morphology was responsible for the difference in properties between the cryogenically fractured and non-cryogenically fractured materials.

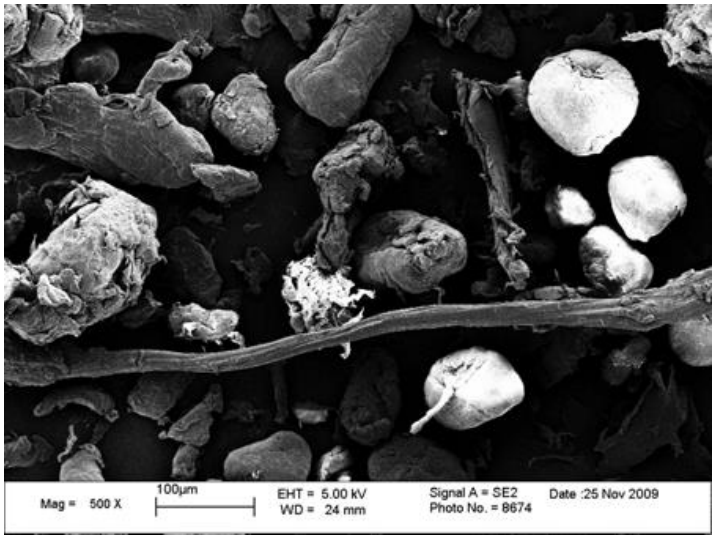

Figure 2-32: SEM of carbon nanofibre-PA12 powder (CNF-PA12) prepared by cryogenic fracturing, showing irregular powder morphology and wide particle size distribution[23]

Yan *et al* [126] used a dissolution-precipitation process to coat nanosilica (3 wt%) with PA12 to prepare nanosilica/PA12 nanocomposite powder. In their work, modified nanosilica was dispersed uniformly in the PA12 solution. Then, the mixture was gradually cooled, the PA12 crystallised and the nanocomposite powder was formed. The nanosilica was dispersed well in the PA12 matrix; however, the PA12/nanosilica powder prepared by this process also showed irregular particle shape (Figure 2-33). The composite laser sintered parts showed increased tensile strength, modulus and impact strength compared to neat PA12 which had been fabricated using the same dissolution-precipitation technique; however, the elongation at break decreased by about 3.65% compared to neat PA12.

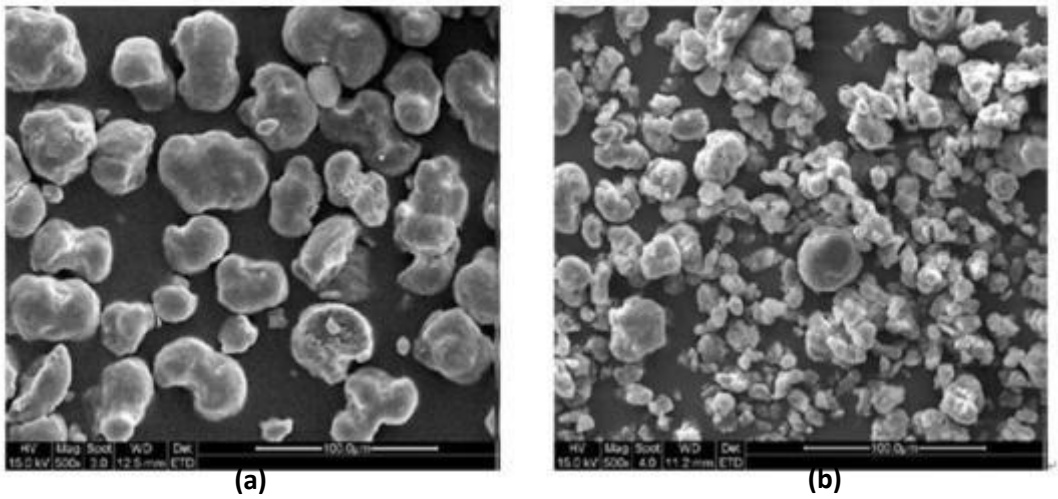

Figure 2-33: SEM micrographs of (a) original PA12 powder, and (b) Nanosilica/PA12 powder[126]

2.7. Summary

In this chapter, one of the most commonly applied additive manufacturing technology, laser sintering, was introduced and reviewed. The use of laser sintering permits the fabrication of polymer parts with greater design freedom compared to conventional manufacturing techniques. The effects of the laser sintering process parameters, such as laser power, laser scan speed and energy density, on the mechanical properties of sintered parts were discussed. Research has been carried out to utilise polymer nanocomposites for laser sintering to enhance the properties of sintered parts. From previous research it is known that it is very important to achieve both homogeneous and favourable powder morphology, as well as well-dispersed nanofillers when providing PNCs for laser sintering. However the methods used in the literature to prepare nanocomposite powders for laser sintering have shown drawbacks. The knowledge gaps found from the literature lead to the objectives of this study, which are stated in Chapter 3.

Chapter 3

Research novelty and objectives

3.1. Research novelty

From the literature review in the previous chapter, the use of laser sintering permits the fabrication of polymer parts with a complex internal and external structure which cannot be achieved by conventional manufacturing techniques. However, only a very limited range of polymer materials can currently be processed to build end-use parts with satisfactory mechanical properties using laser sintering. The utilisation of polymer nanocomposites provides a possible solution to this problem. It is well-known that achieving good dispersion of nanoparticles within the polymer matrix is crucial for the successful preparation of polymer nanocomposites. For laser sintering, it has also been shown that maintaining the correct powder morphology can be just as crucial. Research has been carried out in this area, and some promising results have been obtained, however so far there is not an effective method to prepare suitable nanocomposite powders for laser sintering.

In an attempt to achieve this, the current study introduces a novel procedure to prepare polymer nanocomposite (PNC) powder for laser sintering. Following optimisation of processing parameters to produce parts, mechanical and material characterisation was carried out, with characterisation techniques such

as dynamic oscillatory melt rheology and three dimensional transmission electron microscopy being used to investigate PNCs for laser sintering for the first time.

3.2. Research objectives

In this context, the main research objectives of the study were to:

- Understand the requirements of polymer nanocomposite powders for use in laser sintering and develop a way to fabricate homogeneous and near-spherical PA12/nanofiller nanocomposite powder, in which nanofillers are well-dispersed.

- Optimise the laser sintering process parameters for the PA12/nanofiller nanocomposite in order to maximise the mechanical properties; evaluate the dispersion of CNTs in the laser sintered PA12-CNT nanocomposite parts and the influence of the nanofillers on the mechanical properties of the laser sintered PA12 nanocomposite.

- Investigate the reinforcement mechanism of the nanofillers on the properties of laser sintered PA12 nanocomposite, and understand the relationship between structure and properties of the laser sintered nanocomposite.

Chapter 4

Methodology

4.1. Preparation of PA12-CNT nanocomposite powders

The literature work reported in Chapter 2 highlighted the importance of preparing homogeneous and near-spherical polymer nanocomposite powder, in which the nanoparticles are well dispersed, in order for the nanocomposite powders to be used in the laser sintering process. In this work, it was proposed that a novel patented method developed at Loughborough University[140] could be used to prepare suitable powders for laser sintering. The original patent[140] was modified in this work to produce homogeneous, spherical and well-dispersed nanocomposite powders for laser sintering. By this modified method, the nanofiller could be coated on the surface of individual polymer particles, providing a more effective way to add the nanoparticle to the base polymer, whilst maintaining the optimum powder morphology already achieved by commercial laser sintering polymer powders.

4.1.1. Materials

In this work, polyamide 12 (PA12) powder was supplied by EOS GmbH, Germany (trade name PA2200™). These PA12 powder particles have near-spherical

morphology, with an average particle size of 57.5 µm (measured in section 5.1). This material was chosen as the base polymer material due to its established use in the laser sintering process, commercially and academically.

Carbon nanotubes (CNTs) were chosen as the nanofiller in this study. CNTs are carbon allotropes with a cylindrical nanostructure (Figure 4-1)[141], which have a great length-to-diameter ratio. They have generated a great deal of interest in developing functional composites due to their potential for nanoscale mechanical reinforcement, thermal reinforcement and their low aspect ratio[136,137,142-145]. Compared to other nanofillers, CNTs show extremely good thermal conductivity, shown in Table 4-1. It can be seen that the thermal conductivity of CNTs is between 2000 – 6000 W/mK, compare this to copper, a metallic filler well known for its good thermal conductivity, which transmits 483 W/mK. Laser sintering is a heat transfer and conduction process, and improved thermal conductivity could potentially facilitate the sintering process, which makes the CNTs the most promising nanofiller candidate in the current work.

Material	Thermal Conductivity (W/mK)
Carbon Nanotubes	2000 - 6000
Carbon black	6 – 174
Graphite	100 – 400 (on plane)
Copper	483
Aluminum	204
Nanosilicate	0.5 – 1.1

Table 4-1 : Thermal conductivity of various nanofillers at 25°C [146,147]

There are two types of CNTs: single-walled CNTs and multi-walled CNTs. Single-walled CNTs are more suitable for electrical applications, such as the development of the first intermolecular field-effect transistors[148]. Compared to single-walled CNTs, multi-walled CNTs have improved functionalisation ability (chemical functions at the surface of the nanotubes), which is important to achieve well-dispersed CNTs in a solution. Furthermore, the cost of the single-walled CNT is much more than the multi-walled CNT, particularly when scaled up. In this work, a multi-walled CNT water dispersion (3 wt%) was obtained from Nanostructured & Amorphous Materials Inc, USA. The average length of the CNTs was 1.5 μm, and the average diameter was 10 nm.

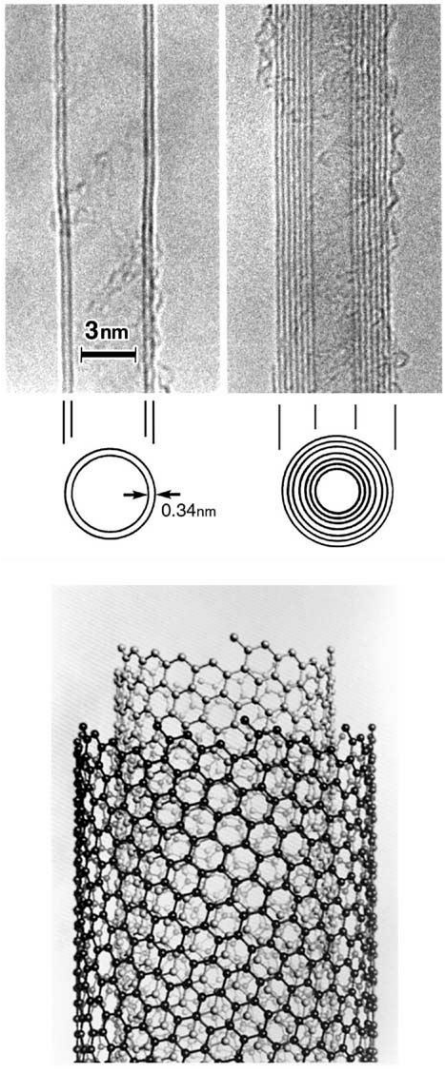

Figure 4-1: Multi-wall carbon nanotubes discovered in 1991[149]

From here-on, the PA12-CNT nanocomposite will be referred to simply as PA12-CNT, and the neat PA12 as PA12.

4.1.2. Calculation of the theoretical loading of CNTs required

To obtain an initial idea of the amount of CNTs that should be used when preparing the PA12-CNT nanocomposite powders, a mathematical calculation was carried out. In the PA12-CNT nanocomposite powder preparation process, CNTs distribute on the surface of PA12 powder particles. The calculation below

was used to determine how many CNTs were required theoretically to fully cover the surface of each PA12 powder particle.

Assuming that the PA12 powder particles were spherical and the CNT particle was cylindrical in morphology, the physical properties of PA12 and CNT are shown below.

Properties	PA12	CNT
Diameter	57.5 µm	10.0 nm
Length	N/A	1.5 µm
Density	$0.45\ g/cm^3$ (Powder density)	$2.10\ g/cm^3$

Table 4-2: Physical properties of PA12 and CNT

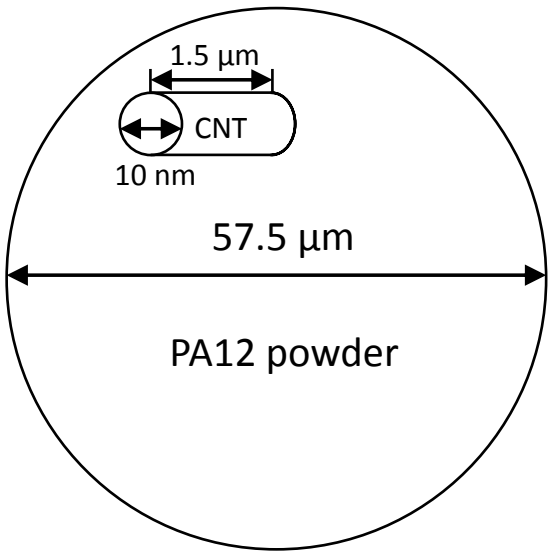

The surface area for one single PA12 powder particle:

$$S_{PA} = 4\pi R_{PA}^2$$

The shadow area for one single CNT particle on the PA12 surface is:

$$\mathrm{S_{CNT}} = 2\mathrm{R_{CNT}} \times \mathrm{L_{CNT}}$$

The number of CNTs to fully cover one PA12 powder particle is:

$$N = \frac{S_{PA}}{S_{CNT}}$$

PA12 powder / CNT volume ratio:

$$\frac{V_{PA}}{V_{CNT}} = \frac{\frac{4}{3}\pi R_{PA}^3}{N \times \pi R_{CNT}^2 \times L}$$

PA12 powder/ CNT weight ratio:

$$\frac{m_{PA}}{m_{CNT}} = \frac{V_{PA} \times \rho_{PA}}{V_{CNT} \times \rho_{CNT}}$$

Therefore,

$$\frac{m_{PA}}{m_{CNT}} = \frac{S_{CNT}}{S_{PA}} \frac{\frac{4}{3}\pi R_{PA}^3}{\pi R_{CNT}^2 \times L} \times \frac{\rho_{PA}}{\rho_{CNT}} = 784.2$$

Therefore, theoretically the percentage of CNTs used to fully cover the surface of an average PA12 particle is:

$$m_{CNT} = \frac{1}{784.2} = \frac{1}{784.2} = 0.13\ wt\%$$

According to this calculation, 0.13 wt% CNT can completely cover the PA12 particles surface. In this work, 0, 0.1, 0.2 and 0.4 wt% CNT loading were attempted to produce PA12-CNT nanocomposite powders.

4.1.3. Production of PA12-CNT powders

The nanocomposite powder preparation process was developed from a patented method[140]. It was modified in this work to meet the specific requirement of powders for laser sintering. The main modification was the process temperature when mixing PA12 powders and CNTs. In the original patent a pressure reactor was used to achieve processing temperature higher than 100^{o}C;while in the current work basic laboratory glassware (as opposed to the pressure reactor method) was applied to provide 100^{o}C processing temperature. This is discussed in the detailed process description below.

Firstly, the as-received CNT water dispersion mixture was diluted and subjected to strong mechanical stirring for 20 minutes to disperse the CNT. Then, the CNT/water mixture was subjected to strong ultrasonic treatment for 20 minutes in a 100^{o}C water bath to disperse the CNT further. Figure 4-2 shows the CNT/water mixture after mechanical stirring and ultrasonic vibration. It can be seen that the CNT was dispersed well in the water, with no noticeable agglomerates.

Figure 4-2: A photograph of the well-dispersed CNT/water mixture

At the same time, as-supplied PA12 powder was mixed with deionised water at a weight ratio of 1:2 to form a PA12 powder suspension. Then, the CNT/water dispersion was mixed with the PA12 powder suspension with CNT loadings of 0, 0.1, 0.2, 0.4 wt%.

After brief mixing, the PA12-CNT mixture was heated to soften the surface of the polymer, and strong mechanical stirring was used during this step. The original patent used a pressure reactor to increase the mixing temperature to above 100^{o}C. However it was found in this work that the PA12 powders could agglomerate if a pressure reactor was used, which was due to the excessive melting with an overheated mixing process. Melting of the surface of the polymer particles must be distinguished from complete melting of the polymer particles. When only the surface of the polymer particles is melted, the polymer particles could remain as discreet particles. The softening or melting occurs to a degree suitable to enable the nanofillers to attach to the polymer particles. Then a lowered mixing temperature, 100^{o}C was attempted using basic laboratory glassware (as opposed to the pressure reactor method), and the PA12 and CNT were mixed successfully without PA12 particles caking under this

temperature. Therefore 100^{o}C was set as the mixing temperature in this process. After the mixing temperature was reached, the temperature was maintained for 20 minutes for the nanofillers to be adhered on the surface of the polymer particles. Then, the water was separated from the PA12-CNT mixture using a filter.

After this process, the recovered PA12-CNT powder was dried in an oven at 80^{o}C. Moisture analysis was performed using a Moisture Analyser MX-70 (A&D Ltd.) at 100^{o}C testing temperature, to ensure that the powder was dry enough (less than 1.00 wt%) before laser sintering. Figure 4-3 shows the process chain for the preparation of PA12-CNT powder.

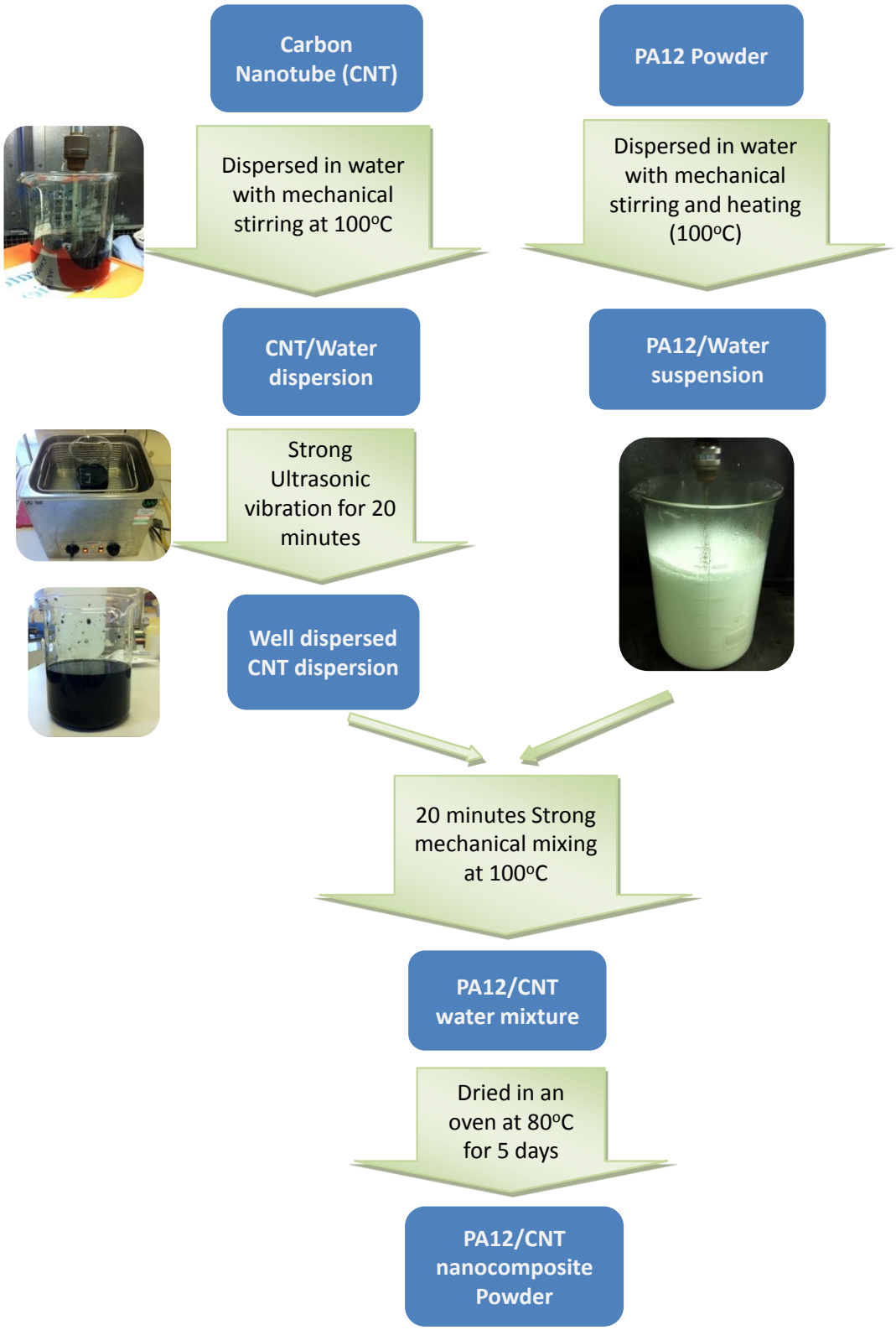

Figure 4-3: Process chain for the production of PA12-CNT powders

4.2. Laser sintering

The laser sintering machine used in this research was a FORMIGA P100, a commercial polymer laser sintering system manufactured by EOS GmbH, shown in Figure 4-4. The FORMIGA P100 was used due to its small build volume (200 mm x 250 mm x 330 mm), and thus has suitability for research into new materials which are costly to produce in large quantities. Furthermore, if the PA12-CNT nanocomposite powders can be processed in the commercialised laser sintering machine P100 (as opposed to an experimental machine), there is more likelihood that the powders can also be laser sintered with other commercial laser sintering machines.

The P100 machine used in the work had been modified to allow chamber heating at all temperatures from ambient to 180^{o}C. The laser used in the P100 is a CO_2 laser, which has a wavelength of 10.2 to 10.8 μm, and can generate power up to 25W. The laser scan speed during the build process is up to 5 m/s. Typically layer thickness is 0.1 mm[150]. A recoating blade is used to coat new layers of powders across the build area, and the deposited powders are heated by a radiant heater that is above the powder bed.

The prepared PA12-CNT, as well as PA12 powder (for comparison purposes), was laser sintered to produce mechanical and thermal testing specimens. Various powder bed temperatures, laser powers and energy densities were attempted to optimise the laser sintering process (details of these will be provided in section 5.2.).

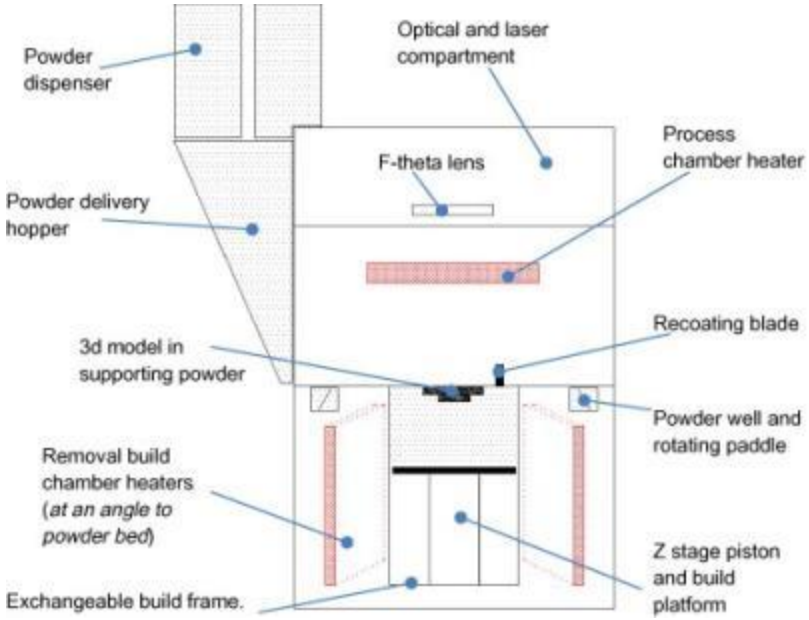

Figure 4-4: Schematic of the FORMIGA P100 Laser Sintering Machine[23]

4.3. Characterisation techniques

4.4.1. Differential scanning calorimetry

Differential scanning calorimetry (DSC) is a thermal analytical technique which measures the temperatures and heat flows associated with transitions in materials[151]. Through DSC experiments, a curve of heat flow versus temperature or time can be obtained, which is used to determine the heat of fusion, glass transition temperature, melting temperature, crystallisation temperature and crystallinity of the samples[152,153]. In this work, the thermal behaviour of PA12 and PA12-CNT powders and laser sintered parts were studied using a SHIMADZU DSC-60 machine. Samples weighing 5mg were heated and cooled at a rate of 10^{o}C/minute.

4.4.2. Particle size distribution analysis

The particle size distribution of powdered materials is very important in understanding its physical behaviour during the laser sintering process. In this work, the particle size distributions of the PA12 and PA12-CNT powders were analysed using a laser diffraction particle size analyser - Malvern Mastersizer 2000® (Malvern Instruments). During the laser diffraction measurement, dry PA12 and PA12-CNT powder particles were passed through a focused laser beam. The angle of diffraction increased as the particle size decreases. The angular intensity of the scattered light was then measured by a series of photosensitive detectors, which provides the information of the particles size.

4.4.3. Melt rheology

The rheological properties of PA12 and PA12-CNT were examined by melt flow index and small amplitude sinusoidal oscillatory testing. Melt flow index is a relatively simple experiment which provides information about the ease of flow of thermoplastic polymers. Compared to melt flow index, the amplitude oscillatory test is more comprehensive and studies the viscous and elastic properties of polymers.

- **Melt flow index**

To measure the ease of flow in the melted state, the melt flow index (MFI) of PA12 and PA12-CNT powders was measured using a Tinius Olsem® MP600 Extrusion Plastometer at 235^{o}C with a 2.16 kg weight according to ASTM D1238[154]. The MFI was calculated using the conversion:

$$MFI\ (T, w) = \frac{m \times 600}{t} \qquad \text{Equation 6}$$

where MFI is in g/10 min, T is the test temperature in degrees Celsius, w is the net testing load in kilograms, m is the mass of the extrudate in grams, and t is the cut-off time-interval in seconds.

- **Small amplitude sinusoidal oscillatory testing**

Small amplitude sinusoidal oscillatory testing was used, with the measurements conducted on a RADII instrument (Rheometrics®, Inc), to measure the viscous and elastic properties of the polymer and polymer nanocomposite simultaneously. In this study, the parallel disk method (parallel plates diameter: 25mm) was used. PA12 and PA12-CNT powders were formed into sheets by hot pressing at 210°C under 3 ton pressures for 3 minutes. Then the sample discs with a diameter of 25 mm and thickness of ~1 mm were cut from the pressed sheets. A time dependent strain is represented as:

$$\gamma = \gamma_0 \sin(\omega t) \qquad \text{Equation 7}$$

where γ is the strain, γ_0 is the strain amplitude, ω is the test frequency and t is the time. The result shear stress is:

$$\sigma(t) = \gamma_0 [G' \sin(\omega t) + G'' \cos(\omega t)] \qquad \text{Equation 8}$$

where G' is the in-phase, elastic, or storage modulus, G'' is the out-of-phase, viscous, or loss modulus, which is a measure of the energy dissipated per cycle of deformation per unit volume. To keep a linear response, a strain amplitude 10%

was used to obtained reasonable signal intensities at elevated temperature or low frequency. The master curves were obtained at a reference temperature 220^{o}C by using a time-temperature superposition principle.

4.4.4. Dynamic mechanical analysis

To examine the modulus (stiffness) and damping (internal frication) of laser sintered samples, dynamic mechanical analysis (DMA) was applied. DMA applies an oscillatory force at a set frequency to the sample[155]. The tests were performed on a RDAII® instrument for both PA12 and PA12-CNT laser sintered samples (35mm x 12mm x 1mm) with the testing parameters shown in Table 4-3:

Parameter	Value
Frequency	6.2832 s^{-1}
Initial temperature	-150^{o}C
Final temperature	180^{o}C
Heating rate	2 ^{o}C/min
Strain amplitude	0.05%
Auto-tension sensitivity	1.0 gm

Table 4-3: DMA testing parameter for PA12 and PA12-CNT laser sintered parts.

4.4.5. Scanning electron microscopy

To examine the powder morphology, CNT dispersion and fracture surface of laser sintered parts, a field emission gun scanning electron microscopy (FEGSEM) (LEO 440 Scanning Electron Microscopy, Leo Electron Microscopy Ltd) was used. The FEGSEM is an ultra-high resolution Schottky field emission scanning electron microscopy and is ideal for looking at materials on the nanometre scale. The powders and laser sintered samples were placed on a specimen holder using double-sided carbon conductive tape, and the whole part was coated with gold before SEM characterisation to prevent charging.

4.4.6. Transmission electron microscopy

Transmission electron microscopy (TEM) was used to analyse the dispersion of CNTs in the polymer matrix after laser sintering. Besides normal two dimensional observations, TEM can also be used to make three-dimensional images of samples. In this study two and three dimensional images were acquired on a JEOL 2100F TEM at an accelerating voltage of 200 kV. Focus ion beam (FIB) etching was used to prepare the samples (~100 nm thickness). For 3D TEM tomography observation, multiple images were acquired by rotating the sample to the desired angle (2^{o} in this study). With a 2^{o} increment, a series of 2D projection images with tilt angles ranging from $+60^{o}$ to -60^{o} were collected. Then, three dimensional images were obtained by computational alignment and reconstruction.

4.4.7. Density measurement

The density of laser sintered parts has been seen to have a direct relation to the mechanical properties of the parts[50]. The densities of laser sintered PA12 and PA12-CNT parts were measured using a liquid displacement method. Five specimens were tested for each material to obtain an average value.

4.4.8. Thermal conductivity measurement

The thermal conductivities of the PA12 and PA12-CNT samples were measured by a thermal conductivity apparatus P5697 (Cussons Technology Ltd, UK). The apparatus consists of a vertical stack of specimens clamped between an electrically heated source at the top and a water cooled base, all located within a Dewar vessel and furnished with a radiation shield and anti-convection baffle[156], shown in Figure 4-5a.

The sample specimen was designed as a hollow cylinder (height = 38 mm, diameter = 20mm, wall thickness = 0.5 mm) and produced by laser sintering, in which the testing materials were stored, shown in Figure 4-5b. Two small thermocouples were inserted into the specimen cylinder to contact with the testing specimens inside. The inlet and outlet water temperatures were recorded. The heating current was supplied from a variable voltage power pack, which was used to vary the testing temperature. In this work, the testing temperature was chosen from 100 – 175^{o}C, with an interval of 25^{o}C.

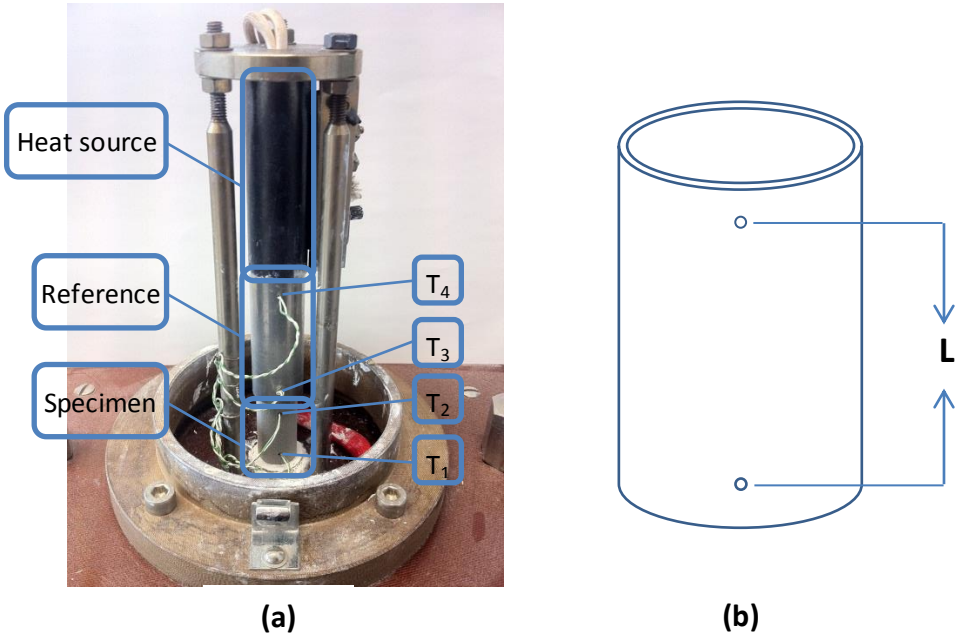

Figure 4-5: Schematic of (a) internal structure of the Dewar vessel. T_1 – T_4 are the thermocouples, (b) hollow cylinder specimen made by laser sintering

The thermal conductivity is calculated as:

$$K = \frac{C_P \times M \times L \times (W_2 - W_1)}{A \times t \times (T_4 - T_3)} \qquad \text{Equation 9}$$

where C_P is the specific heat capacity of water (4186 Joules/Kg), M is the mass of water collected in a certain time (t), L is the distance between the two thermocouples (T_1 and T_2), W_1 is the water inlet temperature, W_2 is the water outlet temperature, A is the cross-section area of the specimen, t is the time for collection of M, T_1 to T_4 are the thermocouple temperatures[156].

4.4.9. Tensile testing

Tensile tests were carried out to determine the ultimate tensile strength (UTS), tensile modulus and elongation at break of the laser sintered PA12 and PA12-CNT parts. A Zwick® 103 test machine was used in this work. Laser sintered PA12 and PA12-CNT parts, which were produced in accordance with ASTM D638-99, were tested with a 10 KN load cell and a cross-head speed of 5 mm/min at room temperature. Five samples were tested each time to obtain average values.

4.4.10. Impact testing

To measure the amount of energy absorbed by a laser sintered part at high-rate loading, impact tests were carried out on a RAY-RAN® Universal Pendulum Impact System at room temperature, with a hammer weight of 1.796 kg and impact velocity 3.5m/s. PA12 and PA12-CNT Izod impact test specimens were built via laser sintering according to ISO 180-2000[157]. Ten specimens were tested in each batch to achieve an average value.

4.4.11. Flexural testing

The flexural properties of the PA12 and PA12-CNT laser sintered parts, which were produced according to ASTM D790, were tested on a Zwick 103 (Zwick/Roell Corporation) testing machine at a test speed of 5 mm/min at room temperature.

Chapter 5

Characterisation and laser sintering of PA12-CNT nanocomposites powders

There are two main parts to this chapter. Firstly, in Section 5.1, characterisation of the PA12-CNT powders prepared by the novel method described in Chapter 4 is reported. Powder size, powder morphology, CNT dispersion, thermal and rheology analysis were carried out to evaluate the suitability of the PA12-CNT powders for laser sintering, as well as the effect that CNTs have on the polymer matrix. Secondly, the PA12-CNT composites powders, along with PA12, were laser sintered with various powder bed temperature and laser powers; this is described in Section 5.2. Section 5.3 provides an overall discussion of the results.

5.1. Characterisation of PA12-CNT nanocomposite powder

5.1.1. Particle size distribution

The particle size distributions of PA12 and PA12-CNT are shown in Figure 5-1. Each powder was tested three times to get an average curve. It can be seen that the two curves are identical, indicating that there was no change in the powder size distribution of PA12-CNT compared to PA12; both PA12 and PA12-CNT nanocomposite powders had an average particle size of 57.5 µm, which lies in the optimum particle size range for laser sintering[54]. This evidence suggests that the method used in this work to prepare the PA12-CNT powders did not alter the powder size or size distribution of the original PA12 powders.

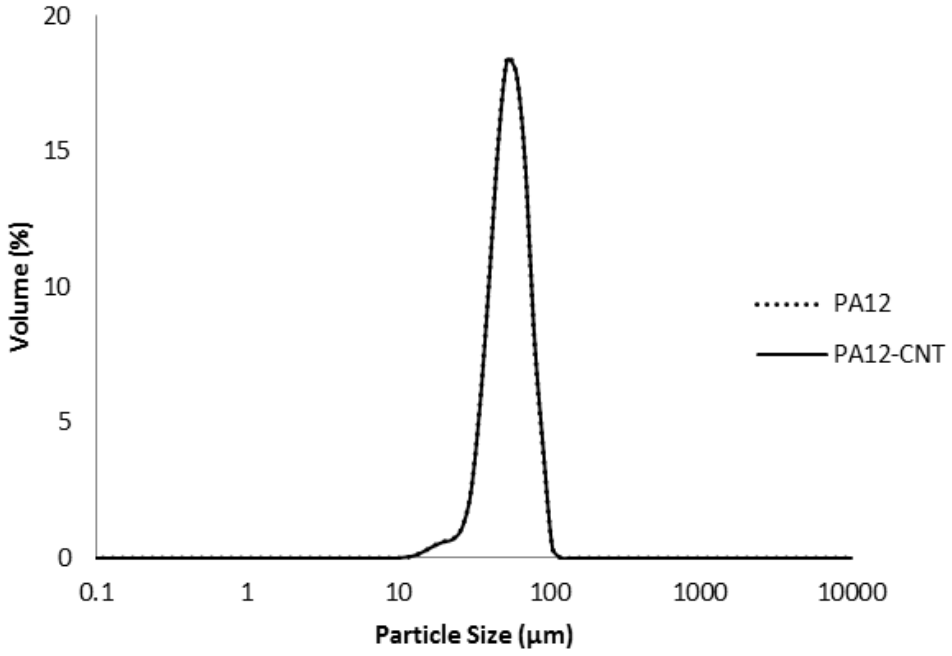

Figure 5-1: Particle size distribution of PA12 and PA12-CNT powder

5.1.2. Powder morphology

SEM micrographs of the PA12 and PA12-CNT powders are shown in Figures 5-2 and 5-3. The commercial PA12 powder had a near-spherical morphology (Figure 5-2a). Compared to PA12, it can be seen that the PA12-CNT powder maintained the same near-spherical morphology (Figure 5-2b). Figure 5-3 shows that this particle morphology was typical of the powder. Combined with the results shown in Figure 5-1, it is reasonable to suggest that the method used in this work to prepare the PA12-CNT powder did not change the size, size distribution and morphology of the original PA12 powder.

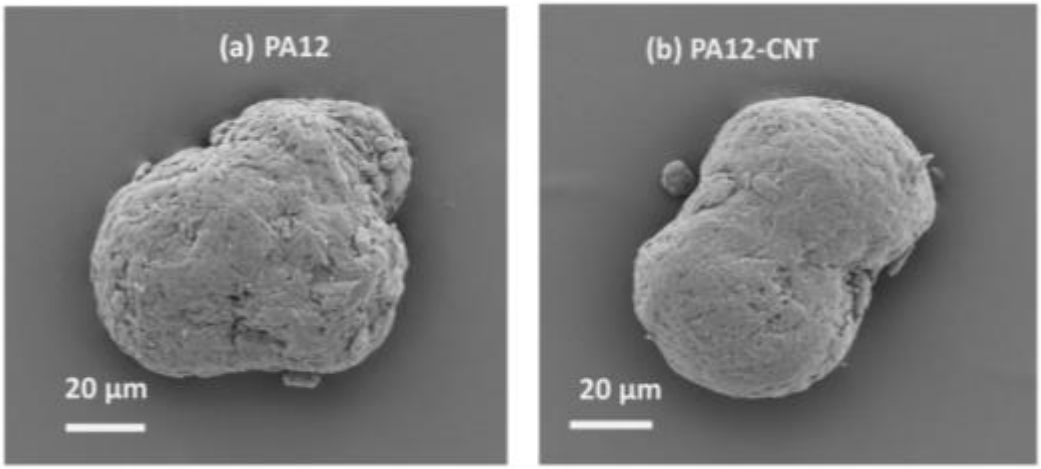

Figure 5-2: SEM micrographs of a typical single (a) PA12 powder and (b) PA12-CNT powder particle

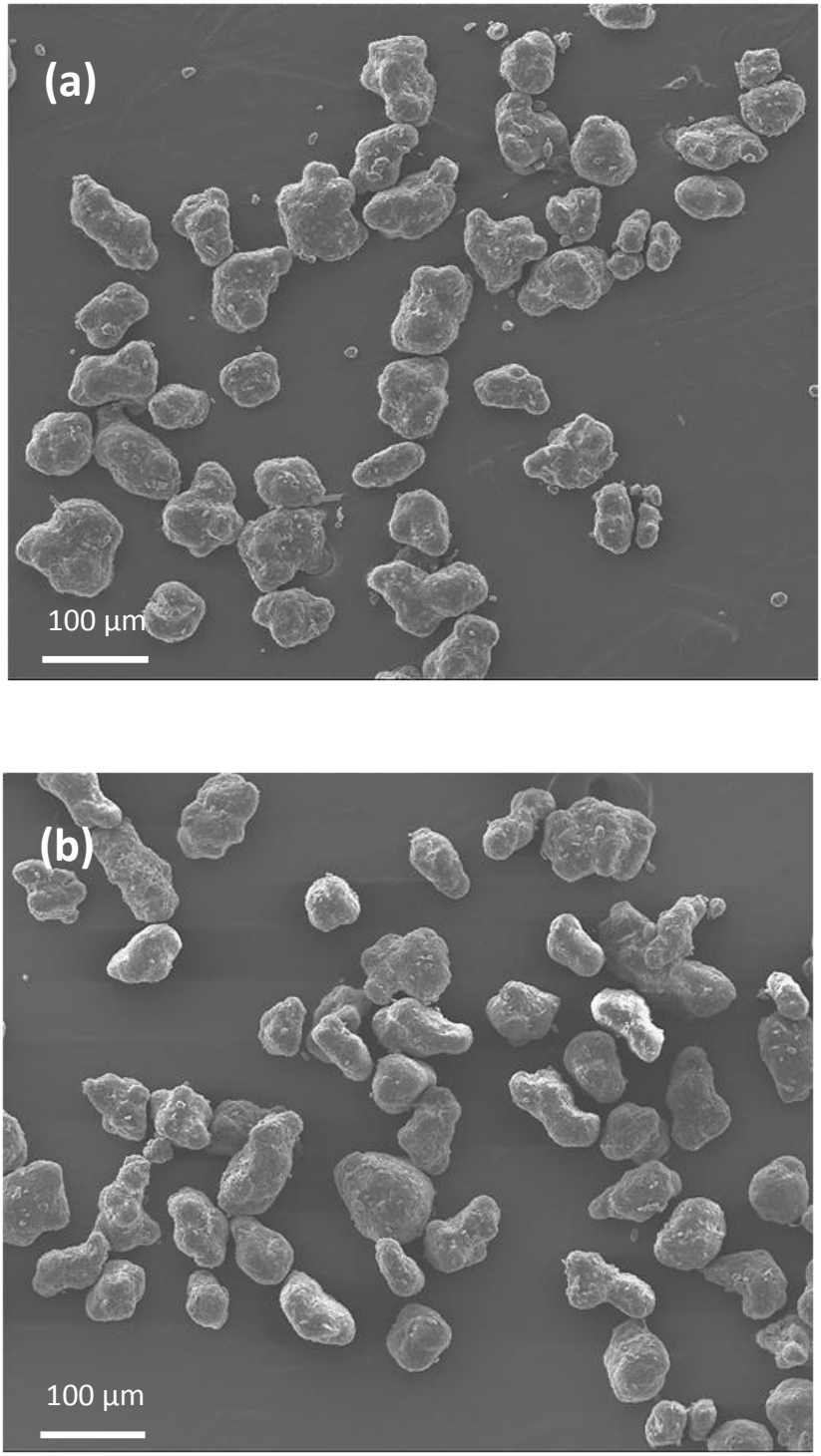

Figure 5-3: SEM micrographs of a number of (a) PA12 and (b) PA12-CNT powder particles

5.1.3. Dispersion of carbon nanotubes

High magnification SEM micrographs of a typical PA12 powder particle and PA12-CNT powder particles which were produced with 0.1 wt%, 0.2 wt% and 0.4 wt% CNT loadings are shown in Figure 5-4a, 4b, 4c and 4d. In Figures 5-4b, 4c and 4d, single CNTs (visible as white strands) can be easily seen, and there was no obvious variance for the densities of the CNTs between these three figures. This suggested that compared to the PA12-CNT produced with 0.1 wt% CNT, the nanocomposites prepared with higher CNT loading (0.2 wt% and 0.4 wt%) did not result in a noticeable increase of the CNTs introduced in the nanocomposites.

In Figures 5-4b and 4c, no obvious CNT agglomerates were detected, which indicated that the CNTs were dispersed uniformly. In Figure 5-4d which had higher CNT loading, most of the CNTs were well-dispersed, however small agglomerates can be seen occasionally. Nanofillers tend to form agglomerates very easily, which could weaken the mechanical properties of the final nanocomposites part, thus achieving uniform dispersion of the nanofillers is crucial when producing polymer nanocomposites.

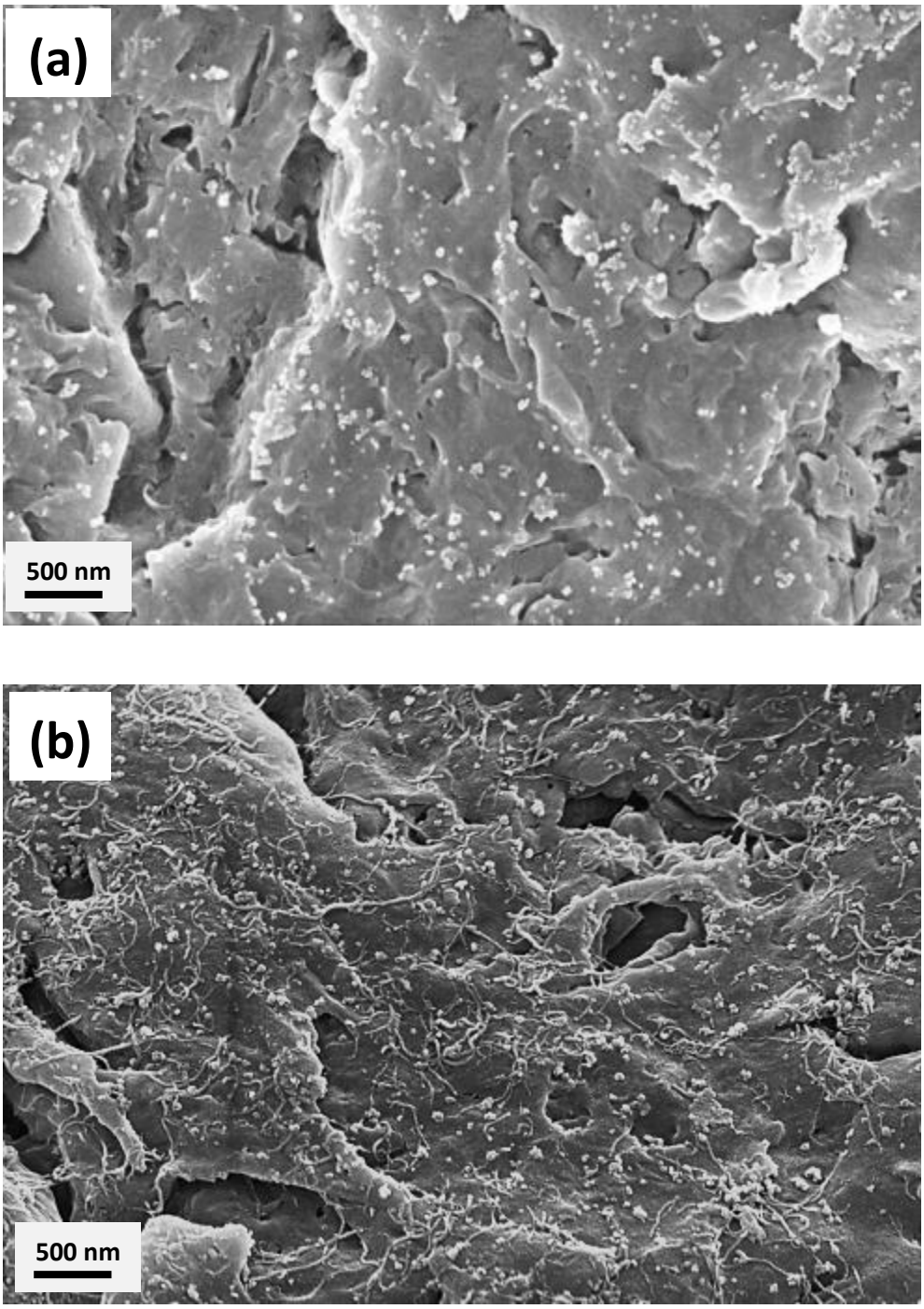

Figure 5-4a: SEM micrographs of the surface of (a) PA12 powder particle, (b) PA12-CNT powder particle prepared with 0.1 wt% CNT, (c) PA12-CNT powder particle prepared with 0.2 wt% CNT and (d) PA12-CNT powder particle prepared with 0.4 wt% CNT. The white strands visible in (b), (c) and (d) are the CNTs. The small white particles shown in all images are artefacts commonly seen on the surface of commercial PA2200™ powders

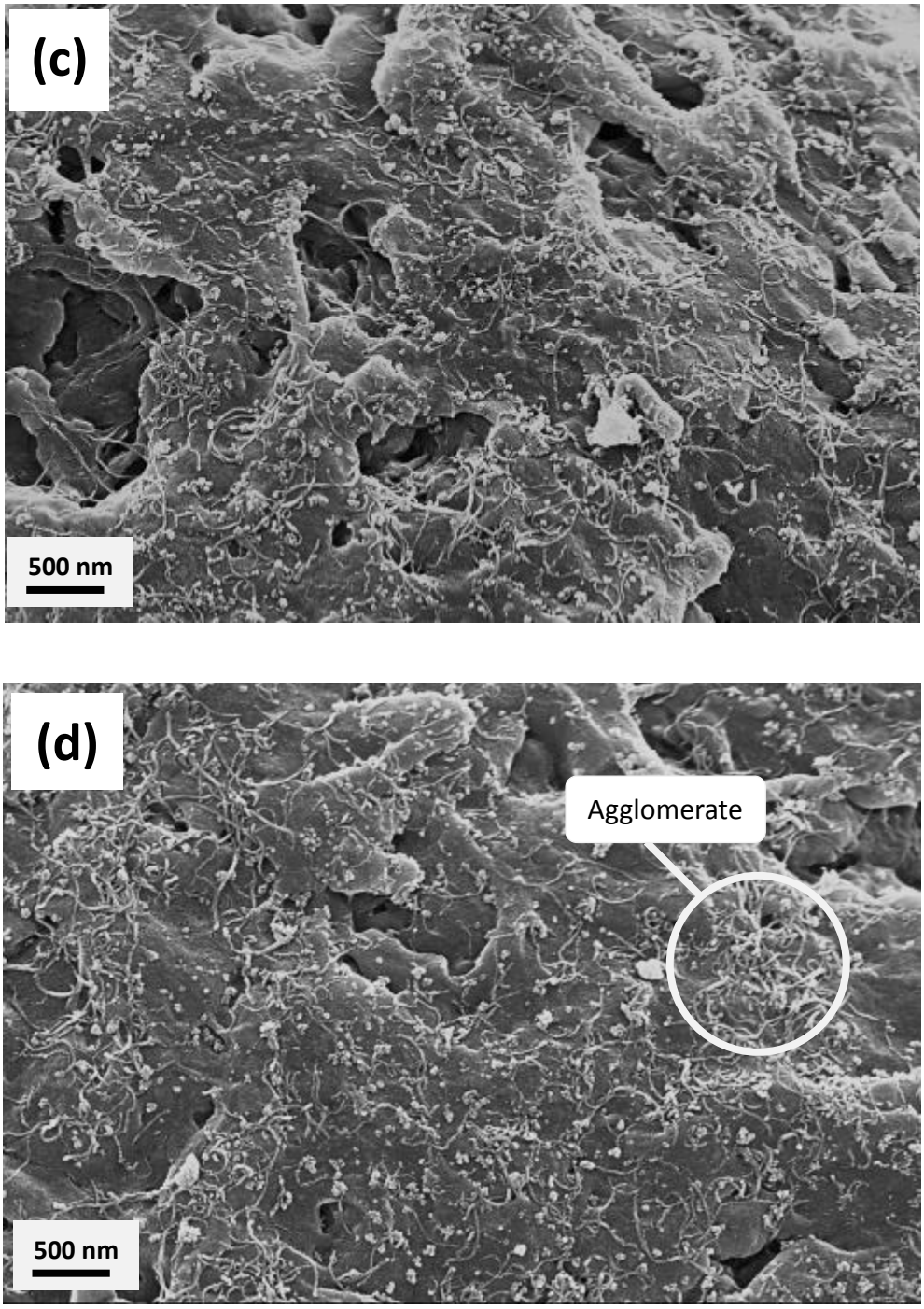

Figure 5-4b: SEM micrographs of the surface of (a) PA12 powder particle, (b) PA12-CNT powder particle prepared with 0.1 wt% CNT, (c) PA12-CNT powder particle prepared with 0.2 wt% CNT and (d) PA12-CNT powder particle prepared with 0.4 wt% CNT. The white strands visible in (b), (c) and (d) are the CNTs. The small white particles shown in all images are artefacts commonly seen on the surface of commercial PA2200™ powders[158].

Combined with the mechanical characterisation results for the laser sintered PA12-CNT in section 6.1.1, it was found that there was no significant difference (conditions for laser sintering, actual amount of CNTs introduced in the nanocomposites and mechanical properties) between the PA12-CNT nanocomposites produced by the three CNT loadings. Furthermore, higher CNT loading 0.4 wt% showed a greater chance of forming CNT agglomerates in the PA12-CNT nanocomposite, which could reduce the reinforcement effect of the CNT to the polymer matrix. It should be noted that the 0.1 wt% was the amount of CNT used in the PA12-CNT powder preparation process calculated in a theoretical manner, and the actual CNT loading on the surface of the produced powder was not measured. The original patent[140] used the amount of nanofiller in the preparation process as the stated nanofiller loading when the nanocomposite powder was produced by this method, which was also applied in this work. Bearing this in mind, 0.1 wt% of CNT was found to be the most optimum and effective CNT loading in this work. Based on these observations and results, the PA12-CNT prepared with 0.1 wt% CNT loading, which was shown to introduce sufficient well-dispersed CNTs in the PA12 matrix, was thus chosen for the rest of the studies described from this point on.

5.1.4. Thermal analysis

- **DSC**

The DSC curves of the PA12 and PA12-CNT powders are shown in Figure 5-5. The melting and crystallisation temperatures of both PA12 and PA12-CNT powders are listed in Table 5-1. Both materials showed clear melting and crystallisation peak with a certain temperature range between these two peaks. Compared to PA12 which had a melting point at 183.4^{o}C, there was a very small

increase in melting point for PA12-CNT (184.0°C). However, the crystallisation temperature of the PA12-CNT powder was 5°C higher than PA12. CNTs increased the crystallisation temperature of PA12 and narrowed the width of the crystalline peak. This implied that the CNTs increased the crystallisation rate and had a heterophase nucleation effect on PA12, similar to that observed by Yan *et al*[159] and Liu *et al*[160].

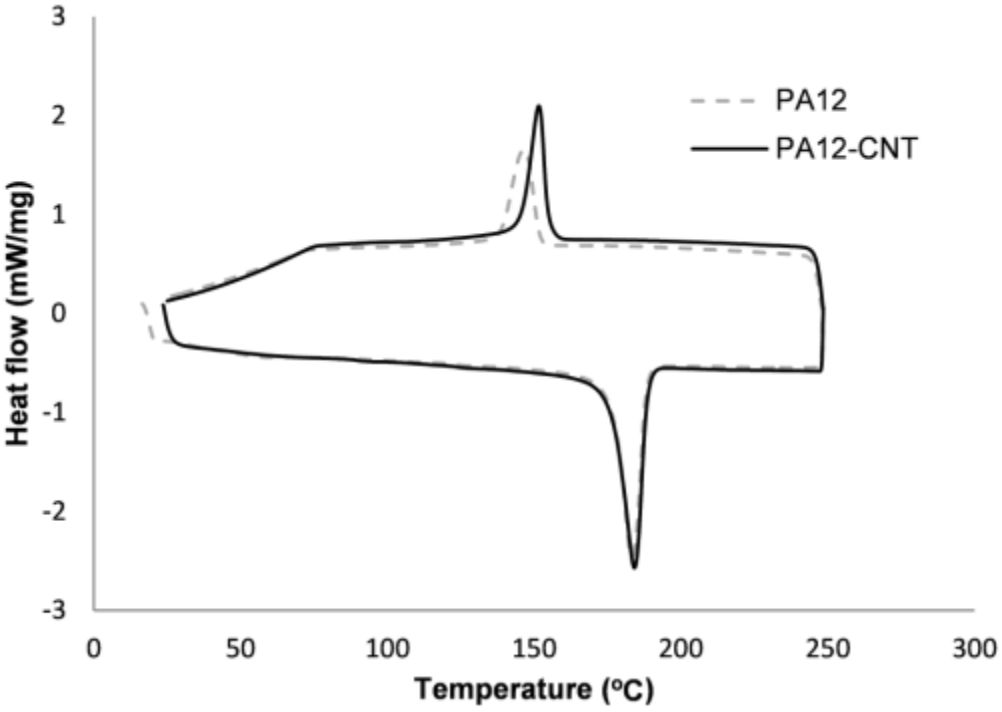

Figure 5-5: DSC curves of PA12 and PA12-CNT powders

Sample	Melting point (°C)	Crystallisation Temperature (°C)
PA12	183.4	146.6
PA12-CNT	184.0	151.6

Table 5-1: Melting and crystallisation temperatures of PA12 and PA12-CNT powders

- **Melt flow index**

The MFI results for PA12 and PA12-CNT powders are presented in Table 5-2. Each powder was tested three times to get average results and standard deviation. Compared to PA12, the viscosity of the PA12-CNT powder was higher, suggesting that the CNTs decreased the melt flow rate for PA12. This may be due to the interfacial force between the CNTs and PA12 hindering the movement of PA12 chains, which could cause increased resistance when a load is applied.

Property	PA12	PA12-CNT
Flow rate (g/10 min)	28.6 ± 2.3	20.9 ± 1.6
Volume Rate (cc/10 min)	40.3 ± 3.9	24.2 ± 4.6
Viscosity (Pa·s)	265.5 ± 19.6	443.5 ± 23.8
T: 220°C, Weight: 2.16 Kg		

Table 5-2: MFI results for PA12 and PA12-CNT powder with standard deviation

- **Thermal conductivity**

The results of the thermal conductivity of the PA12 and PA12-CNT are shown in Figure 5-6. PA12-CNT had an average 14.2% greater thermal conductivity than that of PA12. It can be seen that as the temperature rose, the thermal

conductivity for both PA12 and PA12-CNT increased very slightly.

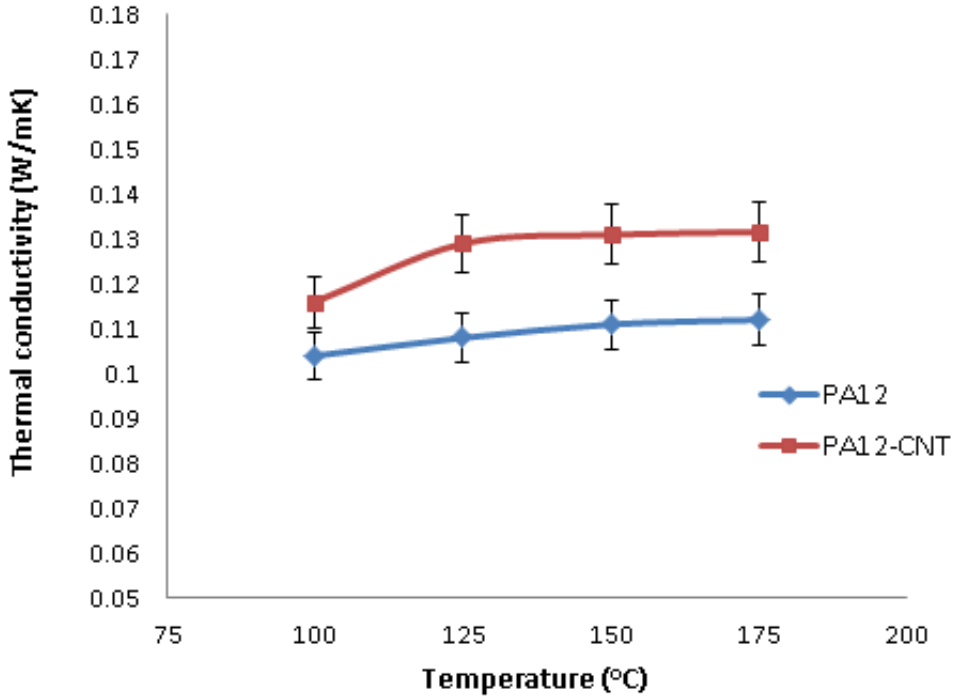

Figure 5-6: Thermal conductivity of PA12 and PA12-CNT powders

5.2. Laser sintering

5.2.1. Determining the powder bed temperature

During the laser sintering process, the powder bed temperature is controlled to prevent curling or caking. The powder bed should be kept uniform, agglomerate-free and constant to achieve repeatable results. In this work, to determine the optimum powder bed temperature, it was initially set to 100°C (based on previous processing experience of PA12) and increased in 10°C increments until the powder bed became hard or agglomerate lumps formed. When this occurred the temperature was reduced 1 - 2°C at a time until free

powder flow and a smooth, soft powder bed was obtained again. Using this method, the suitable powder bed temperatures for PA12 and PA12-CNT were determined as 171^{o}C and 172^{o}C respectively.

5.2.2. Determining the laser power

As PA12-CNT prepared in this study was a new material, different laser powers were tried in an attempt to find suitable processing laser powers.

The laser powers trialled for PA12-CNT are shown in Table 5-3. The laser speed and laser scan spacing were kept at 2500 mm/s and 0.25 mm respectively. Initial attempts to build parts using relatively low laser powers, 13W and 15W, produced parts that curled at the very beginning of each build, which led to failure of the build as the recoater could not pass over the raised section. Then, the laser power was increased to 17W, and there was considerably less curl and parts were built successfully. This suggested that to build PA12-CNT laser sintered parts successfully, the lowest laser power/energy density used should be 17W/0.0272 J/mm^2. Then, the laser power was increased further to 25W with a 2W interval, which is the highest laser power that the EOS P100 laser sintering machine can achieve.

Laser speed: 2500 mm/s, Laser scan spacing: 0.25 mm		
Laser power (W)	**Energy Density (J/mm^2)**	**Note**
13	0.0208	Curling, build failed
15	0.0240	Curling, build failed
17	**0.0272**	**A little curling, success**
19	**0.0304**	**A little curling, success**
21	**0.0336**	**Hardly any curling, success**
23	**0.0368**	**No curling or distortion, success**
25	**0.0400**	**No curling or distortion, success**

Table 5-3: Laser sintering parameters trialled for PA12-CNT

5.2.3. Preparation of test specimens

After determining suitable laser sintering processing parameters for PA12 and PA12-CNT, mechanical and thermal testing specimens were built for both materials. Laser powers from 17 – 25W with a 2W interval were used, and the powder bed temperature was set as 171^{o}C for PA12 and 172^{o}C for PA12-CNT. The optimised laser sintering parameters used in this work for PA12 and PA12-CNT are summarised in Table 5-4.

	PA12	PA12-CNT
Laser power (W)	17 – 25	17 – 25
Laser scan speed (mm/s)	900 – 2500 (most builds with 2500)	900 – 2500 (most builds with 2500)
Laser scan spacing (mm)	0.25	0.25
Powder bed temperature (°C)	171	172

Table 5-4: Laser sintering processing parameters for PA12 and PA12-CNT

In this research, flexural test specimens were built according to ASTM D790[161], tensile test specimens were produced in accordance with ASTM D638-99[162], impact test pieces were built according to ISO 180-2000[157], and dynamic mechanical analysis specimens were produced with dimensions 35mm x 12mm x 1mm[163]. All test specimens were oriented with the longest dimension aligned vertically to the direction of the movement of the recoating blade (shown in Figure 5-7), and were built with a cross-scanning laser. Due to the cost and time scale limitation for powder preparation, parts orientated in the Z-axis were not produced. However, for the future work, further study is worth carrying out to see the effect of CNTs on the properties of laser sintered parts in the Z-axis. From the literature (section2.3.3.), recycled unsintered laser sintering powders have been shown to deteriorate and changed their properties with each re-use. To maintain consistency, only virgin powders of both PA12 and PA12-CNT were used to make parts in this work.

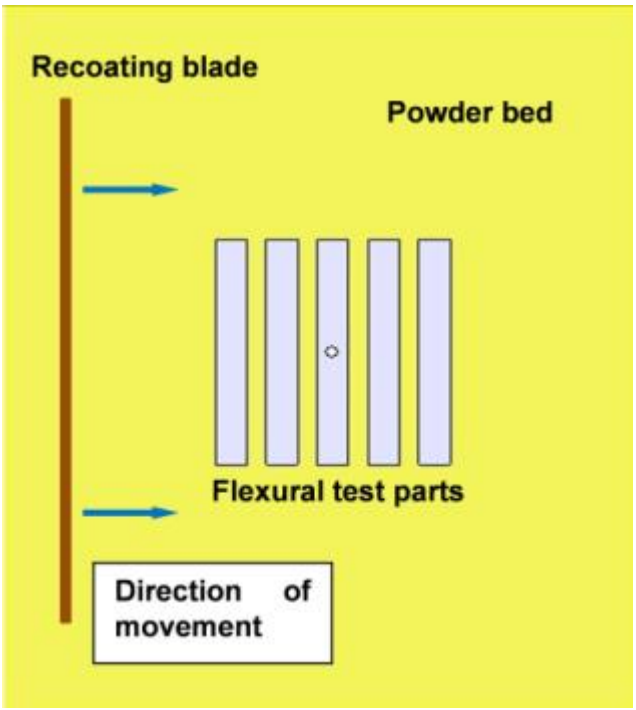

Figure 5-7: Schematic of the powder spreading direction in relation to the orientation of the laser sintered parts

- **Impact and flexural tests specimens**

Impact and flexural tests specimens were laser sintered with optimised laser sintering parameters. The powder bed and laser sintered parts of PA12 and PA12-CNT are shown in Figure 5-8. It can be seen that the flexural specimens for both PA12 and PA12-CNT were built successfully with good definition. Apart from the colour difference as a result of the presence of the CNTs, there were no obvious differences between the PA12 and PA12-CNT laser sintered parts visible by eyes.

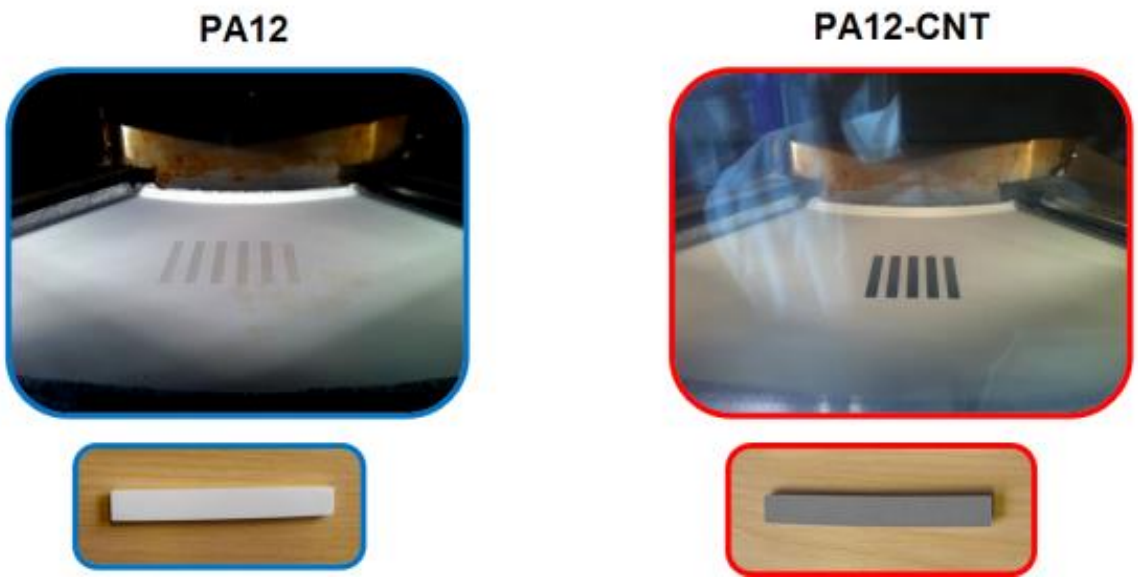

Figure 5-8: Photographs of the impact and flexural specimens of PA12 (left) and PA12-CNT (right); top pictures show the laser sintering process in machine.

- **Tensile test specimens**

To examine the tensile properties of PA12 and PA12-CNT laser sintered parts, tensile test pieces were produced with optimised laser sintering parameters. The PA12 and PA12-CNT during the laser sintering process are shown in Figure 5-9. Tensile test specimens were built successfully at laser powers ranging from 17W – 25W with good definition, shown in Figure 5-10.

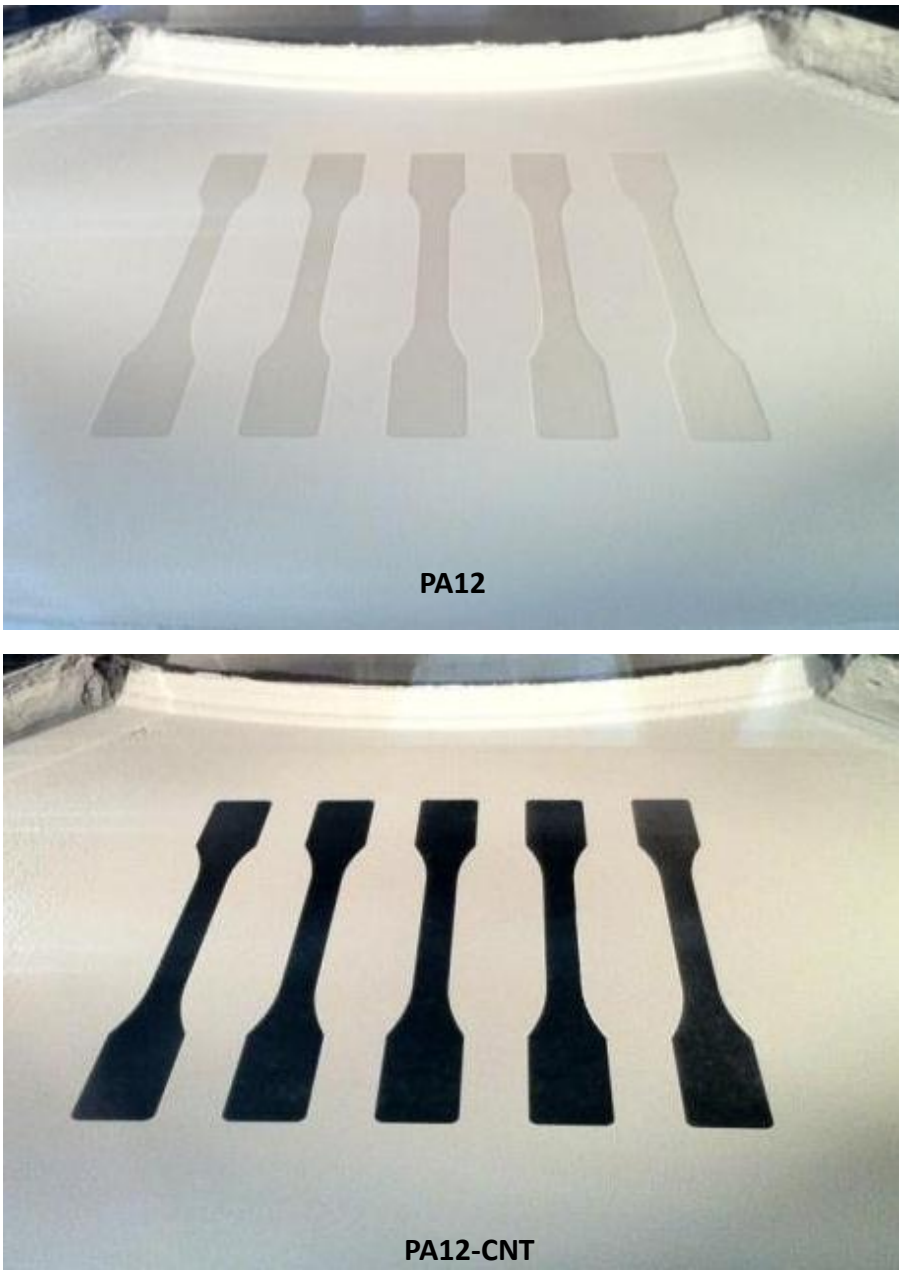

Figure 5-9: Photographs of PA12 (top) and PA12-CNT (bottom) parts during laser sintering

Figure 5-10: A photograph of the completed PA12 and PA12-CNT tensile test specimens

5.3. Discussion

In this chapter, PA12-CNT powder prepared by a novel method was characterised by a number of different techniques. Results showed that well-dispersed (nano-scale), uniform, near-spherical and agglomerate-free CNT coated PA12 nanocomposite powder was achieved.

It is well-known that achieving good dispersion of nanoparticles within the polymer matrix is crucial for the successful preparation of polymer nanocomposites[57,85,164,165,166]. For laser sintering, it has also been shown that maintaining the correct powder morphology can be just as crucial. In this study, a novel method was used to prepare PA12-CNT powder by coating the CNTs onto the surface of PA12 powder particles. This allowed the optimised size and near-spherical morphology of the commercial laser sintering PA12 powder to be retained.

Powder morphology, size and size distribution have been found to play a key role in both the ability to process powders by laser sintering (e.g. ease of deposition and spreading over the powder bed) and the quality of laser sintered parts (e.g. surface roughness, density/porosity)[23]. Powder particles with too small diameter exhibit poor bulk flow at high temperatures, presumably due to the higher interparticle friction found in extremely fine powders. On the other hand, particles that are too large have a negative influence on surface finish and part density. The optimum particle size in terms of processing ability is generally around 45 – 90 μm for laser sintering of macro-sized parts[54].

Besides particle size, the ideal powder for laser sintering is normally near-spherical with a regular morphology. Powders tend to arrange themselves more efficiently with spherical morphology, which increases the density of parts, while powders with irregular morphology are not able to achieve this form of efficient arrangement resulting in low density parts. Moreover, spherical morphology can facilitate powder flow, by ensuring that a flat and thin powder layer is deposited during the laser sintering process. The PA12 powder used in this study was PA2200®, produced by EOS GmbH, which had near-spherical particles and suitable particle size (Figure 5-2a and Figure 5-3a) for laser sintering. After the process used to coat the CNTs onto the surface of the PA12 powder, the spherical morphology and particle size distribution of PA12-CNT powder remained the same as the as-received PA12 powder, as shown in Figure 5-2b and Figure 5-3b.

In addition to powder size and morphology, to achieve maximum properties for laser sintered parts the nanofillers should be well-dispersed in the polymer matrix, otherwise they may have a weakening effect on some properties[80,133]. In the current work, well-dispersed CNTs in the nanoscale were coated uniformly

on the surface of PA12 powder (Figure 5-4). The visual evidence from SEM images suggested that the CNTs were adhered to the surface of the PA12 powder particles very well. Melt flow index tests (Table 5-2) showed that the viscosity of the PA12-CNT composite powder was higher than the PA12, which may indicate the interfacial interaction between the CNTs and PA12.

The melting and cooling processes for PA12 and PA12-CNT powders were analysed with DSC. From the DSC result (Figure 5-5), the crystallisation temperature of the PA12-CNT powder was 5^{o}C higher than PA12. This implied that the CNTs increased the crystallisation rate and had a heterophase nucleation effect on PA12. However this difference did not have an obvious effect on the laser sintering process and the powder bed temperature. To prevent shrinkage and distortion during the laser sintering process, powders should be pre-heated and post-heated in a temperature range between the melting and crystallisation temperature. In this temperature range, parts will be cooled down slowly and no major parts distortion will occur[27]. Therefore for semi-crystalline polymers, it is recommended to have a clear temperature range between melting and crystallisation peaks. From Figure 5-5, it can be seen that PA12-CNT, along with PA12, showed clear melting and crystallisation peak with a certain temperature range between them. This helps to achieve successful processing by laser sintering and accurate parts to be produced.

The optimum laser sintering processing parameters were determined for both PA12 and PA12-CNT. Both PA12 and PA12-CNT can be laser sintered successfully using a laser power from 17 – 25 W. The laser scanning speed and scan spacing were set at 2500 mm/s and 0.25 mm respectively for most builds. As the highest laser power for the P100 laser sintering machine was 25 W, to further increase the energy density, the laser scanning speed was reduced to as low as 900 mm/s

for some builds.

The outstanding thermal properties of CNTs, which comes from the nearly perfect crystalline lattice structure and free length of path for phonon and electron transport, make it a promising material in thermal management[167]. It was reported that the thermal conductivity *k* of CNTs is as high as over 3000 W/mK[168]; this value is remarkably higher than that of PA12, which is about 0.11 W/(mK). Due to their superb thermal conductivity, CNTs have been considered as nanofillers to improve the thermal conductivity of polymer matrix. From Figure 5-6, it appears that by adding the CNTs into the PA12 powder, the thermal conductivity was increased. With increased thermal conductivity, the heat from laser beam could be conducted more efficiently by the powder. This could increase the fusion of the powder and flow of melted PA12, resulting in denser and stronger parts (see section 6.1.4. and 6.3.1.).

After characterisation, PA12-CNT powder, along with PA12 powder, was laser sintered to produce various test specimens to evaluate the mechanical and thermal properties of laser sintered parts, which are reported in the next chapter.

Chapter 6

Characterisation of laser sintered PA12-CNT nanocomposite

The laser sintered PA12-CNT parts, along with PA12 laser sintered parts, were characterised by mechanical, thermal and microscopy experiments. All the characterisation results for laser sintered parts are presented and discussed in this chapter. In Section 6.1., the mechanical properties, including flexural, tensile, impact, dynamic and density are presented. The thermal properties of laser sintered PA12 and PA12-CNT parts are reported in Section 6.2. In Section 6.3., the microstructure of laser sintered PA12-CNT parts were examined by SEM and TEM.

6.1. Mechanical analysis

6.1.1. Impact properties

Izod impact tests were carried out to study the toughness of PA12 and PA12-CNT laser sintered parts. Toughness is the ability of a material to absorb energy during plastic deformation. Figure 6-1 shows the impact strength of PA12 and

PA12-CNT (0.1, 0.2 and 0.4 wt% CNT loadings) laser sintered parts. All three PA12-CNT parts had enhanced impact strength compared to PA12, and there was no noted difference between the three PA12-CNT laser sintered parts with the three different CNT loadings.

Compared to PA12, which had a maximum impact strength of 49.8 KJ/m^2 when 25W was used as the laser power, the maximum value for PA12-CNT increased to 111.6 KJ/m^2 for PA12-0.1CNT, 115.7 KJ/m^2 for PA12-0.2CNT and 107.8 KJ/m^2 for PA12-0.4CNT. This significant increase demonstrated that more energy was absorbed by PA12-CNT laser sintered parts during the impact tests compared to PA12, and indicated that adding CNT into PA12 can improve the toughness of laser sintered parts.

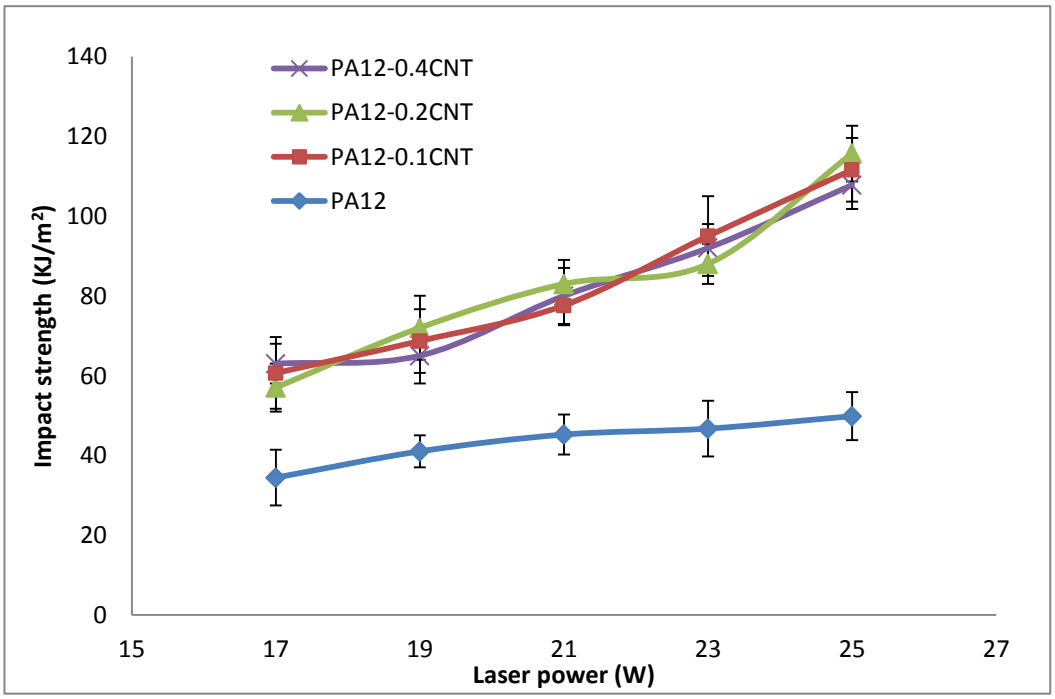

Figure 6-1: Impact strength of PA12 and PA12-CNT (0.1, 0.2 and 0.4 wt% CNT loading) produced by laser sintering

Table 6-1 shows the mean and standard deviation of the impact properties of PA12 and PA12-CNT0.1 laser sintered parts. In Figure 6-1, the error bars represent the standard deviation for each data point, which is the mean value from 10 samples. In considering the standard deviation, the impact strength was still higher for PA12-CNT compared to PA12. Also, no obvious difference in the standard deviation was noticed between PA12 and PA12–CNT, which suggests that CNT do not have an influence on the repeatability of the laser-sintered parts.

			PA12		
	17W	19W	21W	23W	25W
Mean (KJ/m^2)	34.4	41.0	45.2	46.7	49.8
Standard deviation (KJ/m^2)	7.1	2.2	3.3	6.9	4.5
			PA12-CNT0.1		
	17W	19W	21W	23W	25W
Mean (KJ/m^2)	60.6	68.6	77.6	88.6	111.6
Standard deviation (KJ/m^2)	8.1	4.5	3.1	6.4	8.3
Number (N): 10					

Table 6-1: Statistic analysis of impact strength results of laser sintered PA12 and PA12-CNT

6.1.2. Flexural properties

The effect of laser power on flexural modulus and strength for both PA12 and PA12-CNT laser sintered parts is illustrated in Figure 6-2. The data points were the mean value from 6 specimens, and the error bars were the standard deviation for each mean value. It can be noted that as the laser power was

increased, the general trend of flexural modulus and strength increased for both PA12 and PA12-CNT. Compared to PA12, PA12-CNT laser sintered parts exhibited an average improvement of 16.1 ± 0.5% in flexural modulus and 11.4 ± 1.2% in flexural strength. It is also seen that the increase with laser power was not a consistent trend for both PA12 and PA12-CNT, as dips were observed in the curves. This might be due to the standard deviation of the experiments.

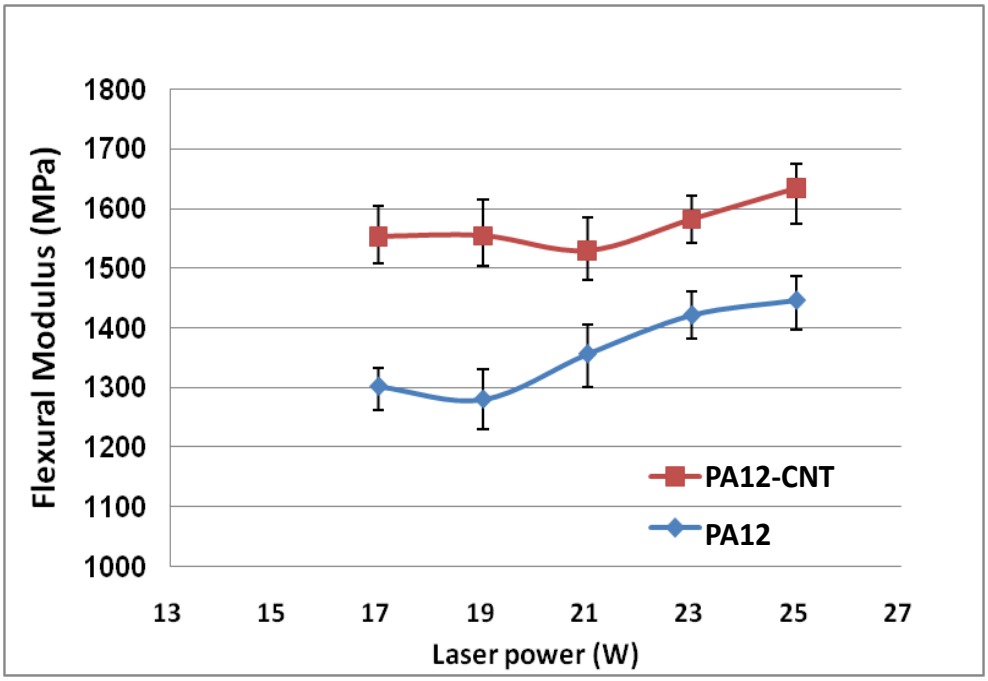

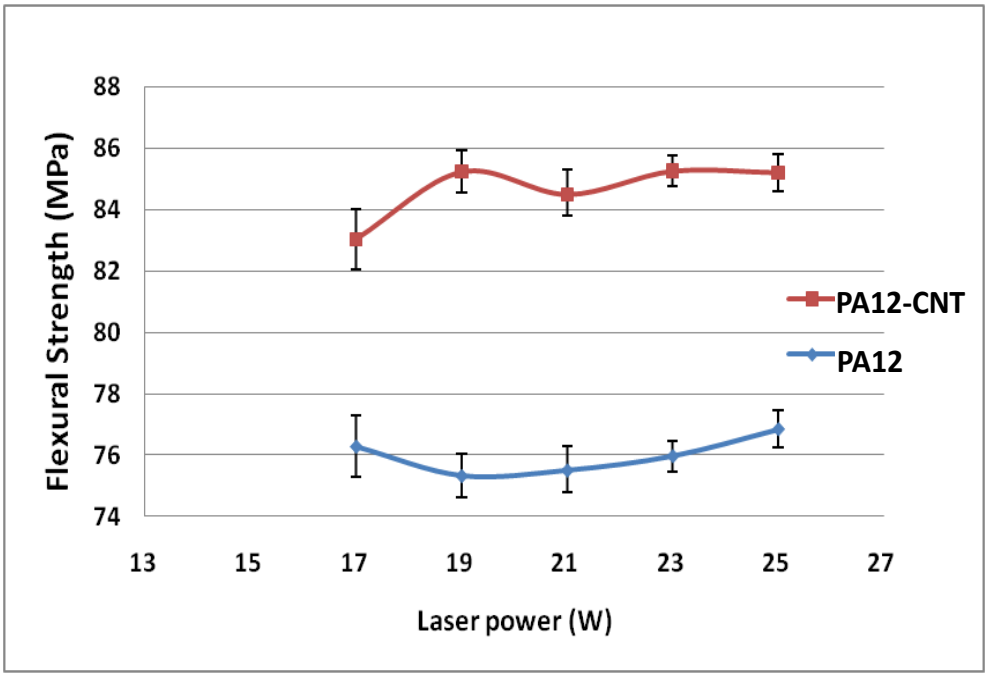

Figure 6-2: Flexural modulus and strength of PA12 and PA12-CNT laser sintered parts

The highest laser power that the P100 laser sintering machine can achieve is 25 W which with a laser scan speed of 2500 mm/s and laser scan spacing of 0.25 mm, gives an energy density of 0.04 J/mm. In an attempt to examine the flexural modulus and strength of PA12 and PA12-CNT laser sintered parts at higher energy densities, the laser scan speed was decreased. The dependence of flexural modulus and strength of laser sintered parts on laser energy density is shown in Figure 6-3. The data points were the mean value from 6 specimens, and the error bars were the standard deviation for each mean value. It can be seen that for both PA12 and PA12-CNT laser sintered parts, there was an optimum laser energy which corresponded to the best flexural modulus and flexural strength. The decrease in strength and modulus after optimum laser energy could be explained by the degradation of the polymer materials with excessive laser energy.

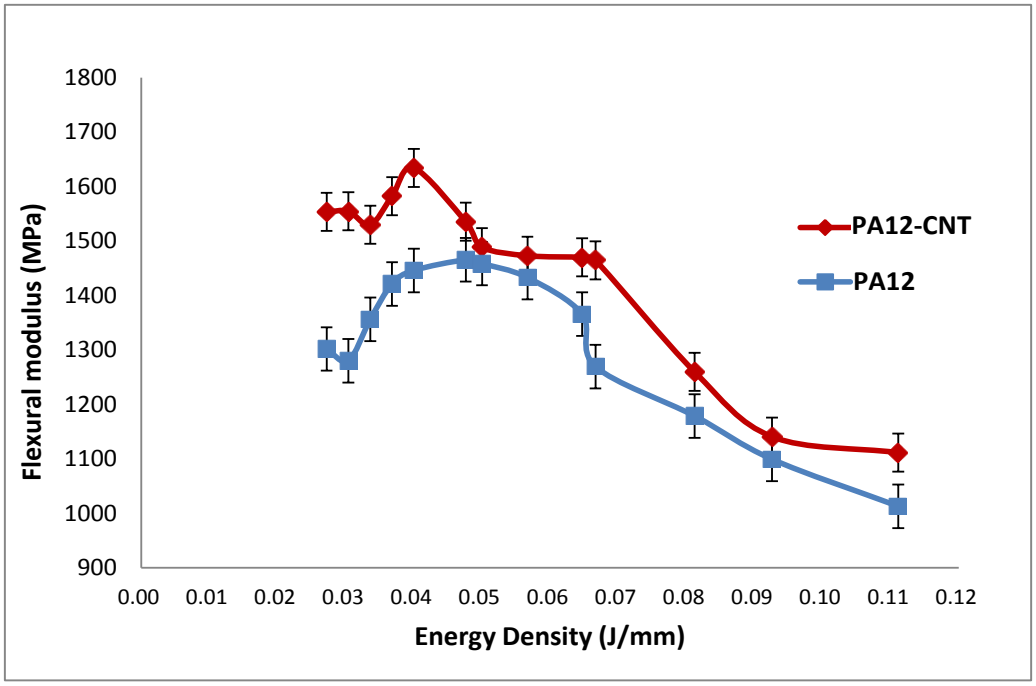

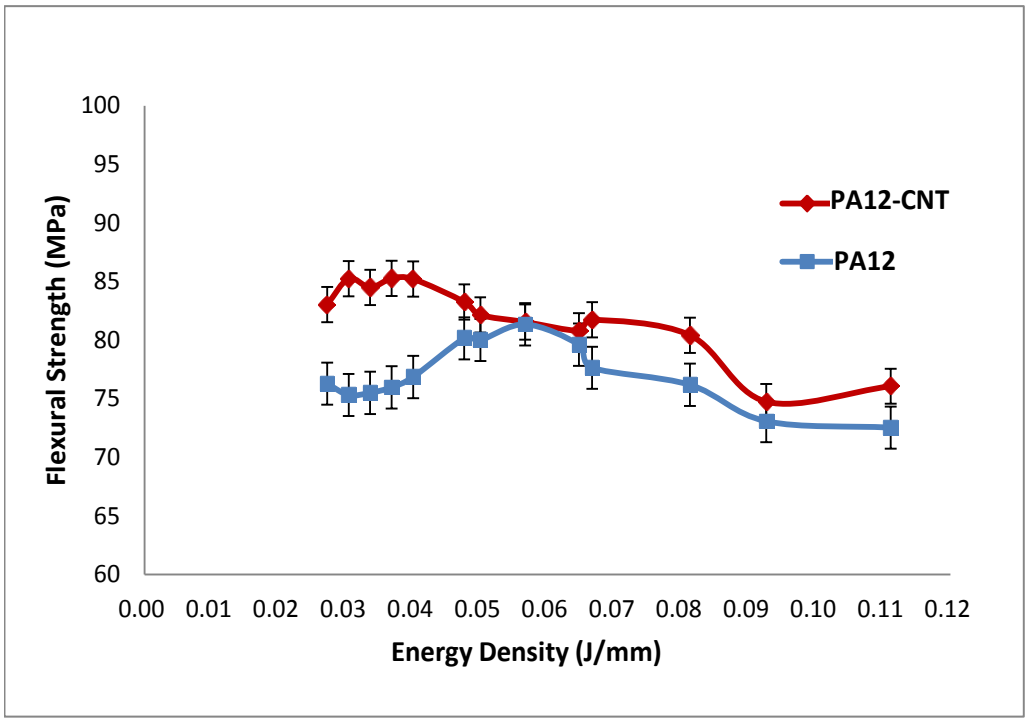

Figure 6-3: Effect of energy density on flexural modulus and strength of PA-CNT and PA laser sintered parts

Table 6-2 shows the flexural properties and corresponding energy densities for PA12 and PA12-CNT laser sintered parts. It can be seen that the flexural modulus and flexural strength of PA12-CNT laser sintered parts were greater than that of PA12 laser sintered specimens. Compared to PA12, a lower energy density was used to achieve the highest flexural properties for PA12-CNT.

Material	Energy Density (J/mm^2)	Highest flexural modulus (MPa)	Highest flexural strength (MPa)
PA12	0.0480	1465.27±45.3	-
PA12	0.0570	-	81.35±3.5
PA12-CNT	0.0400	1634.05±56.2	-
PA12-CNT	0.0368	-	85.27±3.2

Table 6-2: Highest flexural modulus and strength (with standard deviation) for PA12 and PA12-CNT laser sintered parts achieved in this work

6.1.3. Tensile properties

Figure 6-4 illustrates the Young's modulus and ultimate tensile strength (UTS) from the tensile tests of PA12 and PA12-CNT laser sintered parts. Each data point was the mean value of 5 specimens, and the error bars were the standard deviation for each mean value. The highest/average Young's modulus and UTS values achieved for each of the materials are listed in Table 6-3. Compared to PA12, PA12-CNT laser sintered parts showed an average improvement of 48.5% in Young's modulus and 7.9% in UTS. Both PA12 and PA12-CNT laser sintered

parts showed a decrease for Young's modulus and UTS after an optimum laser power, this could be due to the polymer degradation.

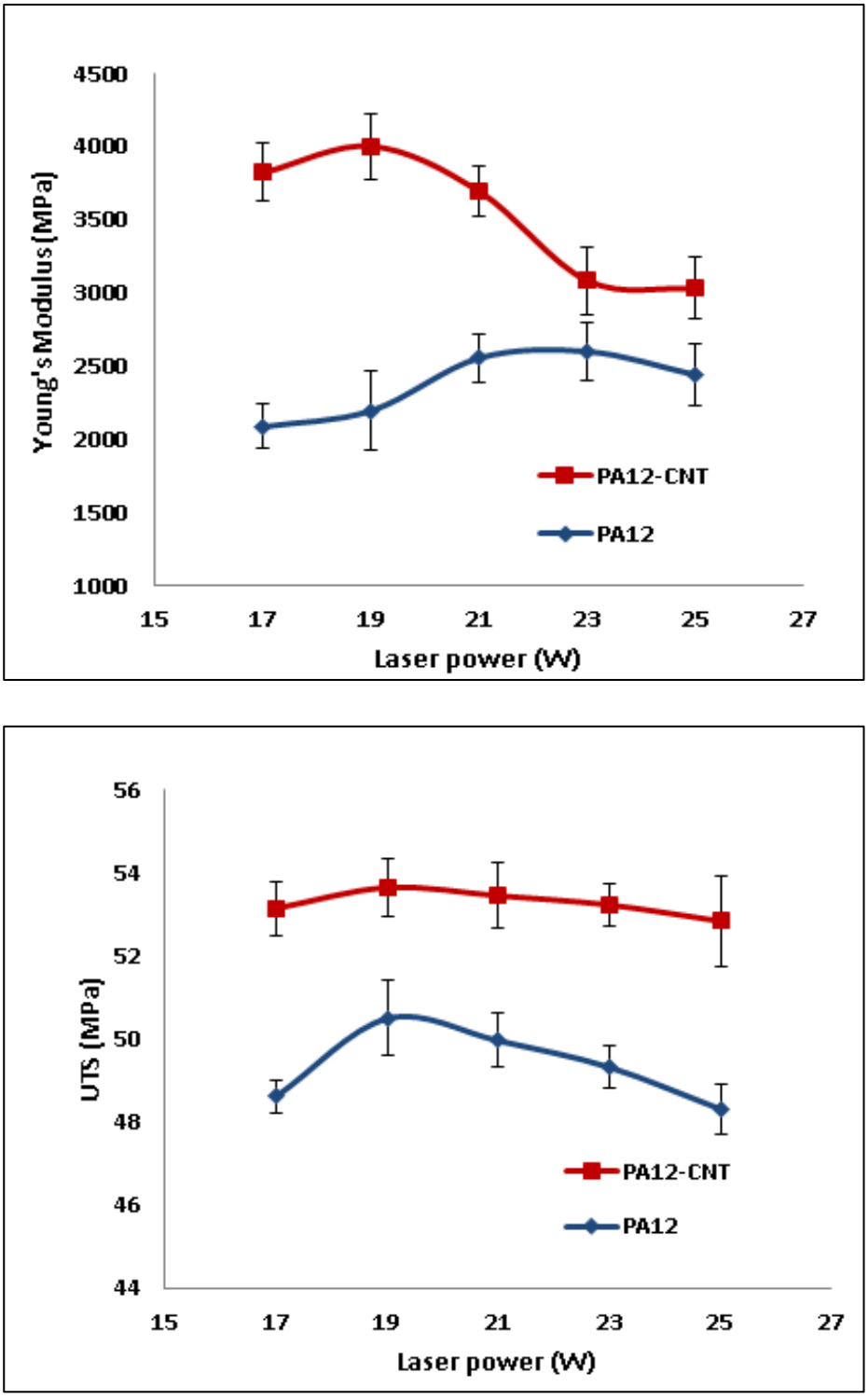

Figure 6-4: Young's modulus and UTS for PA12 and PA12-CNT laser sintered parts

Tensile properties		PA12	PA12-CNT
Young's modulus (MPa)	Average	2373.75 $\pm$ 78.59	3524.56 $\pm$ 92.51
	Highest	2598.30	4001.85
UTS (MPa)	Average	49.34 $\pm$ 1.37	53.26 $\pm$ 1.25
	Highest	50.50	53.65

Table 6-3: Average and highest values of Young's modulus and UTS achieved for PA12 and PA12-CNT laser sintered parts

The elongation at break of the PA12 and PA12-CNT laser sintered parts was also characterised; the results can be seen in Figure 6-5. The data points were the mean value of 5 specimens, and the error bars were the standard deviation for each mean value. It has been reported in the literature that elongation at break can become decreased when filler is added into laser sinter polymer powder to make a composite [169, 170]. Poor dispersion of the filler may cause filler agglomerates, which can become defects when a force is applied. In this research, it can be seen that compared to PA12, the elongation at break of PA12-CNT laser sintered parts did not decrease. This may be attributed to the good dispersion (see section 5.1.3.) and the small amount of CNTs in the PA12 matrix.

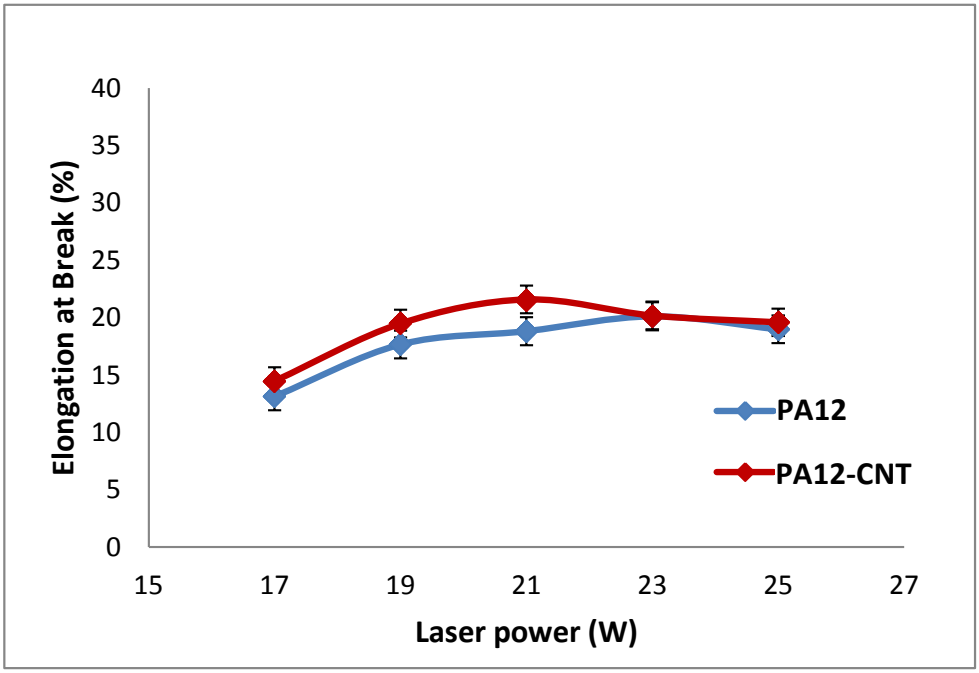

Figure 6-5: Elongation at break of PA12 and PA12-CNT laser sintered parts

6.1.4. Density

The density of the PA12 and PA12–CNT laser sintered parts is shown in Figure 6-6. The data points were the mean value of 6 specimens, and the error bars were the standard deviation for each mean value. It can be seen that the density of the PA12–CNT laser-sintered parts was higher than that of PA12 under each laser power. Compared to the PA12 laser sintered parts with an average density of 959.59 kg/m^3, the average density of PA12–CNT parts increased 4.1% to 999.32 kg/m^3. Density has been found to have a major influence over the mechanical properties (fracture, strength, ductility, and modulus) of laser sintered parts, with higher density parts having better mechanical properties[171], which corresponds to the results recorded in the previous Impact, Flexural and Tensile properties sections (section 6.1.1. – 6.1.3.).

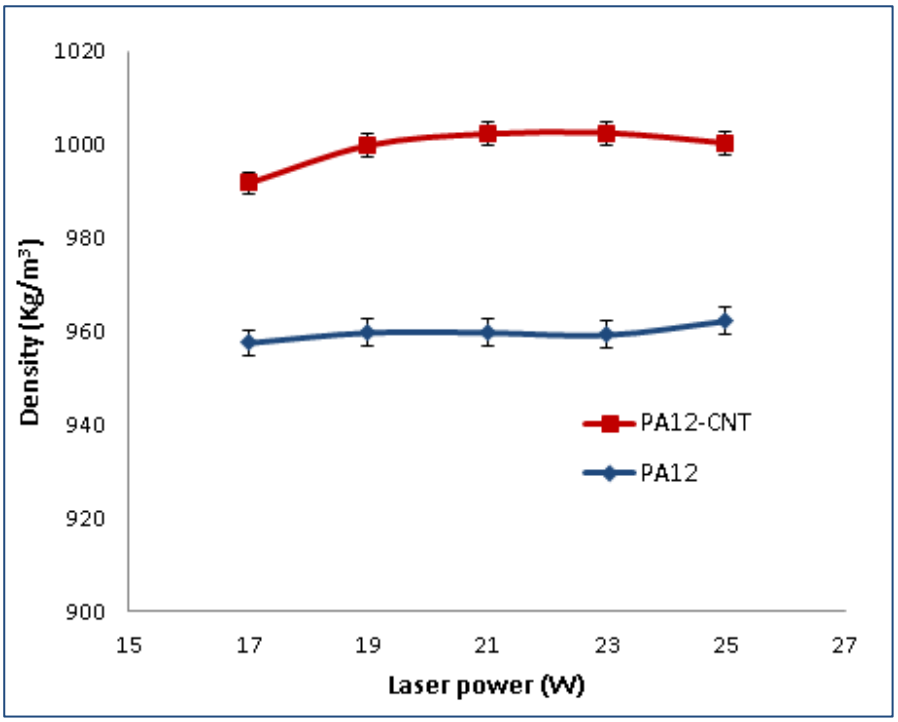

Figure 6-6: Density of PA12 and PA12-CNT laser sintered parts

6.1.5. Part accuracy

Shrinkage is a relatively common phenomenon for laser sintered parts, which happens due to the temperature difference during and after laser sintering. Shrinkage can cause inaccuracies in the dimensions of the laser sintered parts. The dimensional accuracy of PA12 and PA12-CNT laser sintered parts was therefore investigated. Figure 6-7 shows the cross sectional errors of the PA12 and PA12-CNT laser sintered parts. It can be seen that for both materials, the cross sectional area of the laser sintered parts expanded more as the laser power increased. Each data point was the mean value from 6 specimens, and the error bars were the standard deviation for each mean value. Compared to PA12, the cross sectional error of PA12-CNT laser sintered parts was lower. This indicated that with the same laser power input, PA12-CNT laser sintered parts

showed better dimensional accuracy than PA12. This might be due to the higher viscosity/lower shrinkage of the PA12-CNT during laser sintering process.

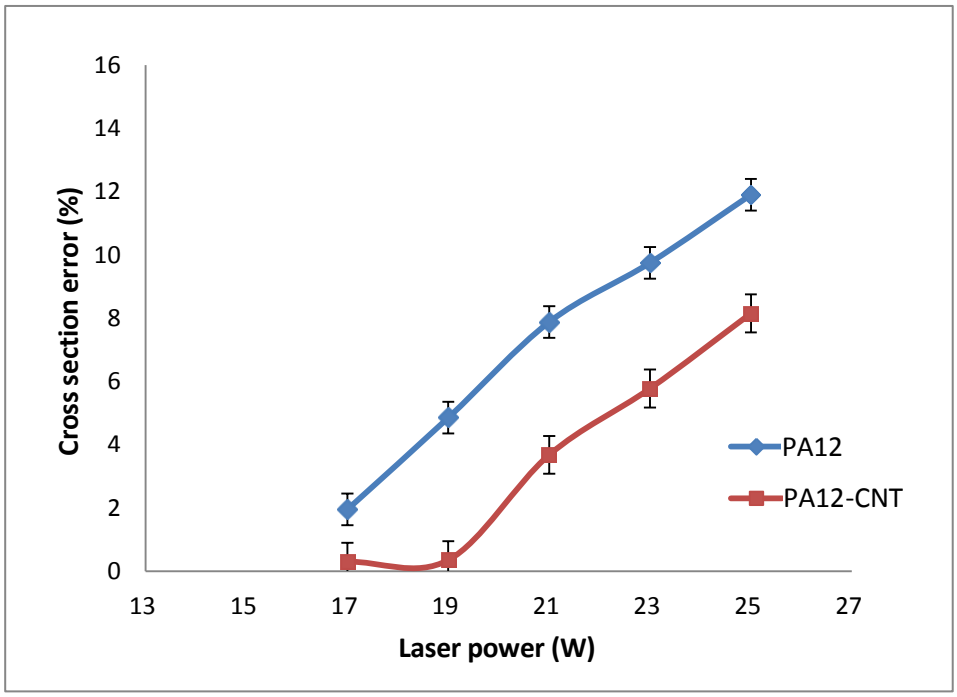

Figure 6-7: The cross-sectional error of PA12 and PA12-CNT laser sintered parts

In all the mechanical testing results figures shown here in section 6.1.1 – 6.1.5., the error bars for each data point were plotted for both PA12 and PA12–CNT laser sintered parts. No obvious difference in the relatively small error bars was noticed between PA12 and PA12–CNT, which suggests that CNT do not have an influence on the repeatability of the laser-sintered parts.

6.1.6. Dynamic mechanical analysis

Dynamic mechanical analysis (DMA) was carried out to determine the elastic modulus (G'), loss modulus (G'') and thermal expansion coefficient (α) of laser sintered PA12 and PA12-CNT parts as a function of temperature. Figure 6-8

records the temperature dependence of G' for the PA12 and PA12-CNT laser sintered parts. Compared to PA12, PA12-CNT showed improved elastic modulus over the experiment temperature range. The enhancement effect was significantly below the glass translation temperature (T_g), where an average reinforcement of 16.9% was achieved. With the rise in temperature above T_g, the reinforcement effect declined and the modulus of the PA12-CNT approached that of PA12. This suggested that at elevated temperature, the modulus of the PA12-CNT composites was mainly decided by the PA12 matrix, which also has been reported for other polymer composites[172,173,174].

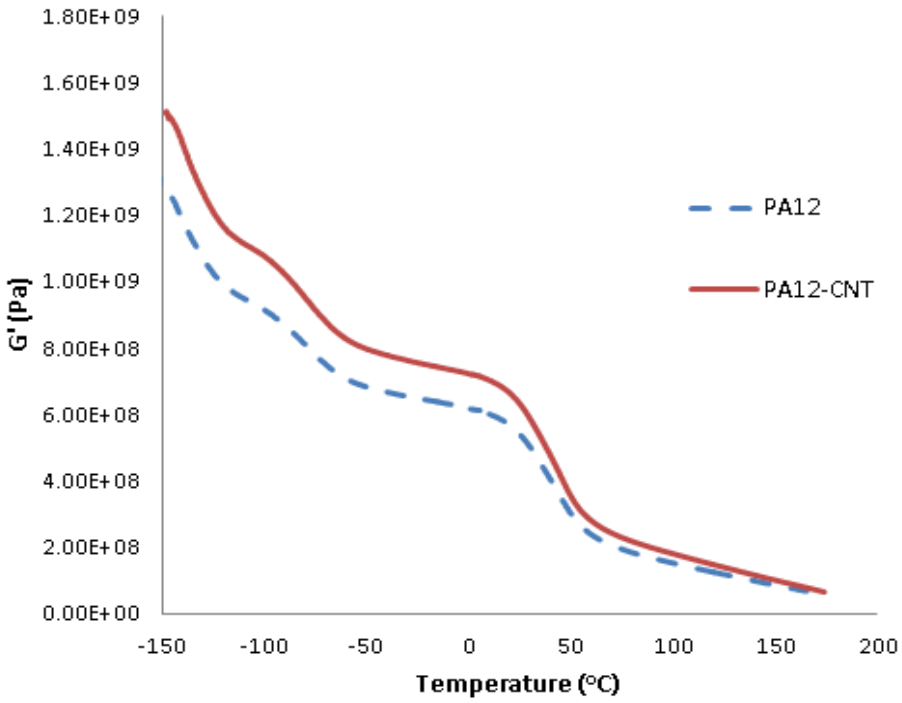

Figure 6-8: Elastic modulus vs. temperature for PA12 and PA12-CNT laser sintered parts

Figure 6-9 plots the loss modulus G'' of the PA12 and PA12-CNT laser sintered parts as a function of temperature, in which three peaks can be noticed obviously. The first peak at a temperature of about -140^{o}C is called 'γ relaxation',

which is from the movement of a few methylene groups between amide groups in the amorphous regions. The second peak temperature (around -80°C), which is defined as 'β relaxation', is caused by the segmental motions of the weak bonded amide groups and methylene groups[175]. As the temperature increased, the polymer chains in the amorphous regions started to move, which is defined as T_g, the third peak (around 40°C). PA12-CNT composite samples showed higher G'' compared to PA12, especially at the peak temperatures. G'' is the dissipated energy within the materials every circle during the test. Higher G'' could be due to the interaction between the CNT and polymer matrix, which hindered the motions of functional groups and chains. This phenomenon was also noticed in other polymer nanocomposites studies[176].

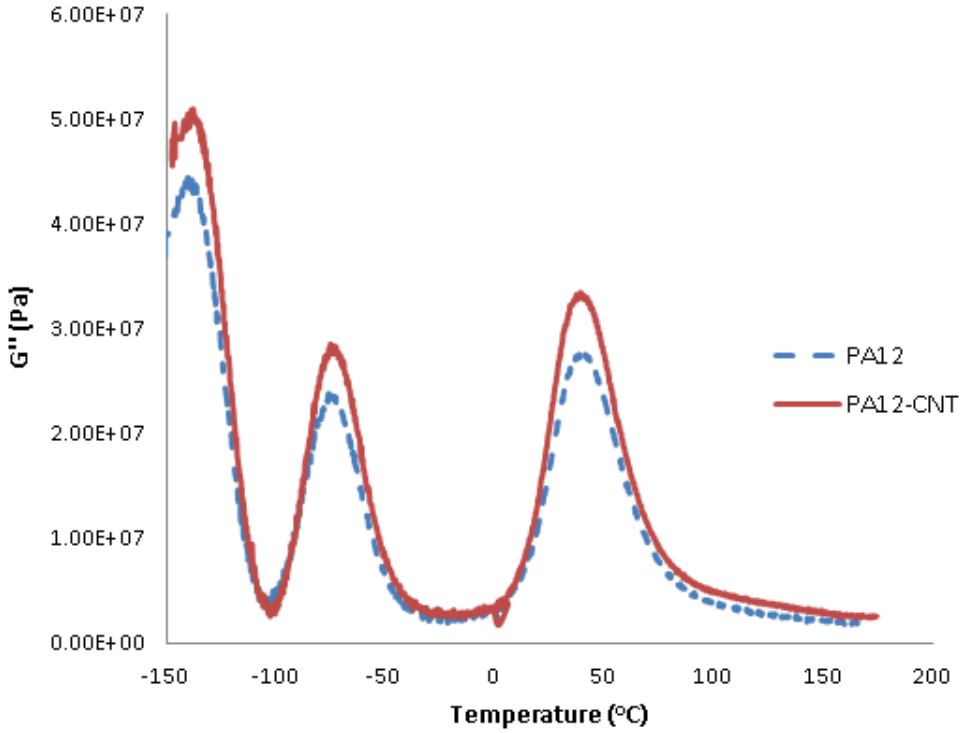

Figure 6-9: Loss modulus vs. temperature for PA12 and PA12-CNT laser sintered parts

From G' and G'', the tanδ (ratio of G''/G') was calculated and is shown in Figure 6-10. Tanδ is used to evaluate the energy loss of materials from segment rearrangements and internal friction during the test. There was a notable increase in tanδ for PA12-CNT at temperatures between 90°C and 160°C, which was due to the damping effect of the CNT fillers, as the CNTs restricted the molecular motion and increased the internal friction.

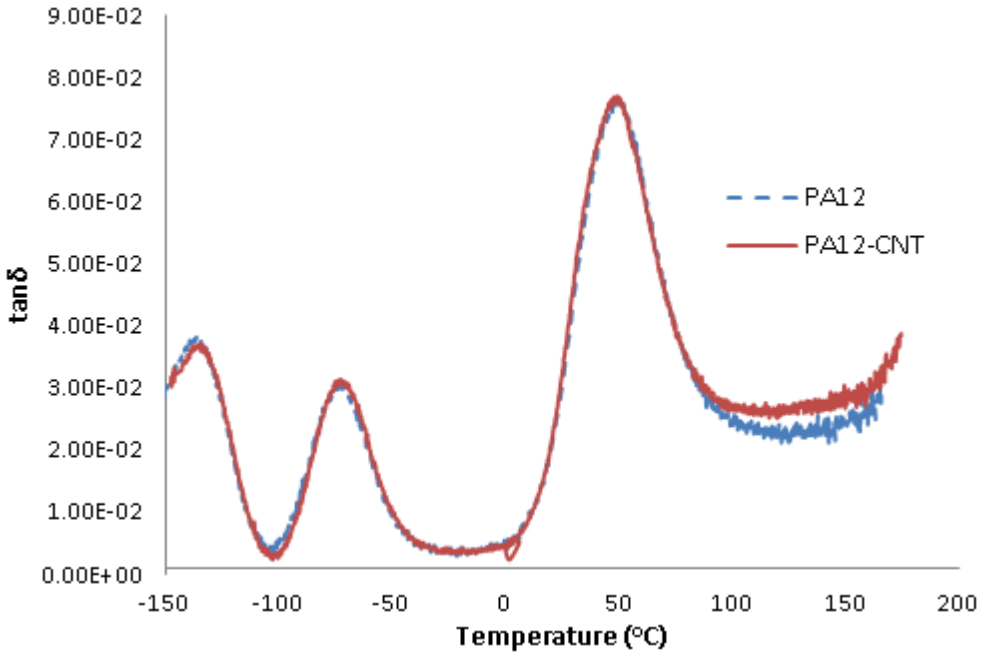

Figure 6-10: tanδ vs. temperature for PA12 and PA12-CNT laser sintered parts

Thermal expansion coefficient (α) is used to describe how the volume of a sample changes as a function of temperature, which is calculated as:

$$\alpha = \Delta L/(\Delta T \cdot L_0) \qquad \text{Equation 10}$$

where ΔL is the length change of the sample, ΔT is the change in temperature

and L_0 is the original sample length[177]. The average value of thermal expansion coefficient (α) from -150°C to 20°C for PA12 and PA12-CNT samples is shown in Table 6-4. For PA12-CNT, the α values were reduced compared to PA12. This decrease could be explained by the mechanical constraint of the CNT in the polymer matrix.

Sample	PA12	PA12-CNT
α (°C)	1.61×10^{-4}	1.39×10^{-4}

Table 6-4: Thermal expansion coefficient of PA12 and PA12-CNT laser sintered parts

6.2. Thermal analysis

6.2.1. DSC

DSC results of the PA12 and PA12-CNT laser sintered parts are plotted in Figure 6-11. The PA12 laser sintered parts showed two melting peaks around 180°C whereas the PA12-CNT parts only showed one. Double melting peaks were also observed previously by Zarringhalam[178], who suggested the smaller peak was the unmelted PA12 powder remaining in the laser sintered parts. In this study, the PA12-CNT sintered parts did not show this smaller peak that correlates to unmelted powder, which indicates that the CNTs increased the laser heat conduction and melting of the PA12 powder during the laser sintering process, resulting in denser laser sintered parts with enhanced mechanical properties (as reported in Section 6.1.)

Compared to PA12, the crystallisation temperature of the PA12-CNT laser sintered parts was 5.5°C greater, which indicated the nucleation effect of the CNTs on the PA12 polymer matrix. Nanofillers are commonly recognised as heterogeneous parts in the polymer matrix, which could have nucleating ability for semi-crystalline polymers.

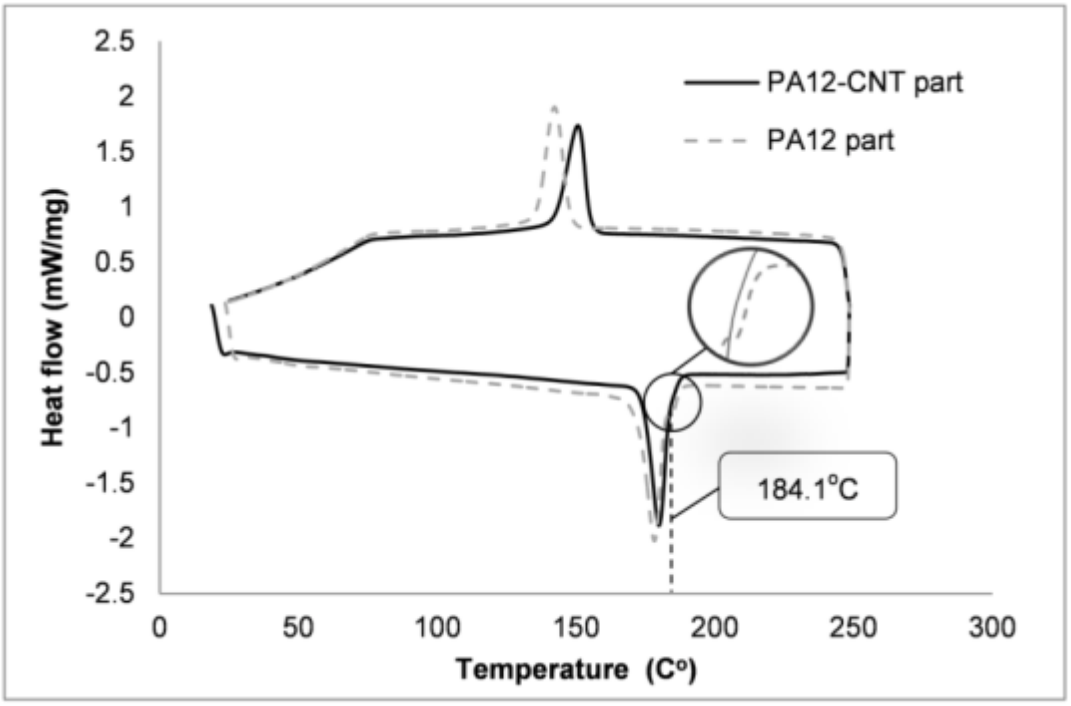

Figure 6-11: DSC curves of PA12 (dashed line) and PA12-CNT (solid line) parts.

6.2.2. Melt rheology properties

A parallel disc oscillatory shear test is a small amplitude deformation test, which does not change the material structure during the test. This is a major advantage for a small deformation test, especially for multiphase composites systems[179]. In this work, the parallel disc shear rheology tests were performed as a function of frequency and a function of temperature.

Figure 6-12 shows the G' and G'' of PA12 and PA12-CNT as a function of frequency at 230°C. At 230°C, the samples were in the molten state, and it acted as a viscous liquid, which can explain the G' < G'' for both PA12 and PA12-CNT. Compared to the PA12 samples, PA12-CNT showed an increase in storage modulus (G') and loss modulus (G''). It is observed that even though the CNT loading (0.1 wt%) was very low, the effect on the matrix rheology were still noticeable. An increased G' meant a more elastic structure, which indicates the restriction of the PA12 polymer chain motion due to the CNT nanofillers.

It is known that for linear mono-dispersed polymer melts, where polymer chains are fully relaxed, there is an approximate relation of $G' \sim \omega^2$ and $G'' \sim \omega$[180]. When the frequency is low, there is enough time for the molecular relaxation process, which makes the measurement of the G' and G'' more sensitive. Table 6-5 shows the power relations of G' and G'' at low frequency region for PA12 and PA12-CNT nanocomposite.

	G' ~ ω	**G'' ~ ω**
PA12	$G' \sim \omega^{1.28}$	$G'' \sim \omega^{0.73}$
PA12-CNT0.1	$G' \sim \omega^{0.72}$	$G'' \sim \omega^{0.65}$
PA12-CNT0.2	$G' \sim \omega^{0.65}$	$G'' \sim \omega^{0.64}$

Table 6-5: Power relations of G' and G'' at low frequency region for PA12 and PA12-CNT nanocomposites

The slopes of G' and G'' for PA12 were smaller than 2 and 1 respectively, which might be affected by the polydispersity of the polymer chain lengths[181]. Compared to the PA12, the slopes of G' and G'' for PA12-CNT were lower, which

could be explained by the polymer-nanotube and nanotube-nanotube interaction in the matrix leading to a modified matrix microstructure[182,183].

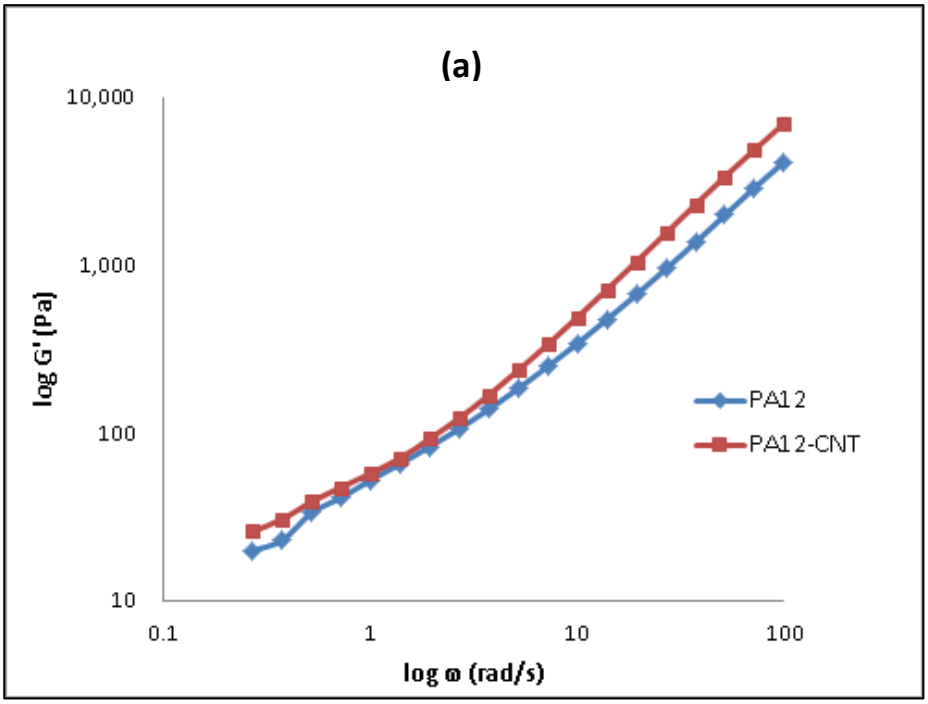

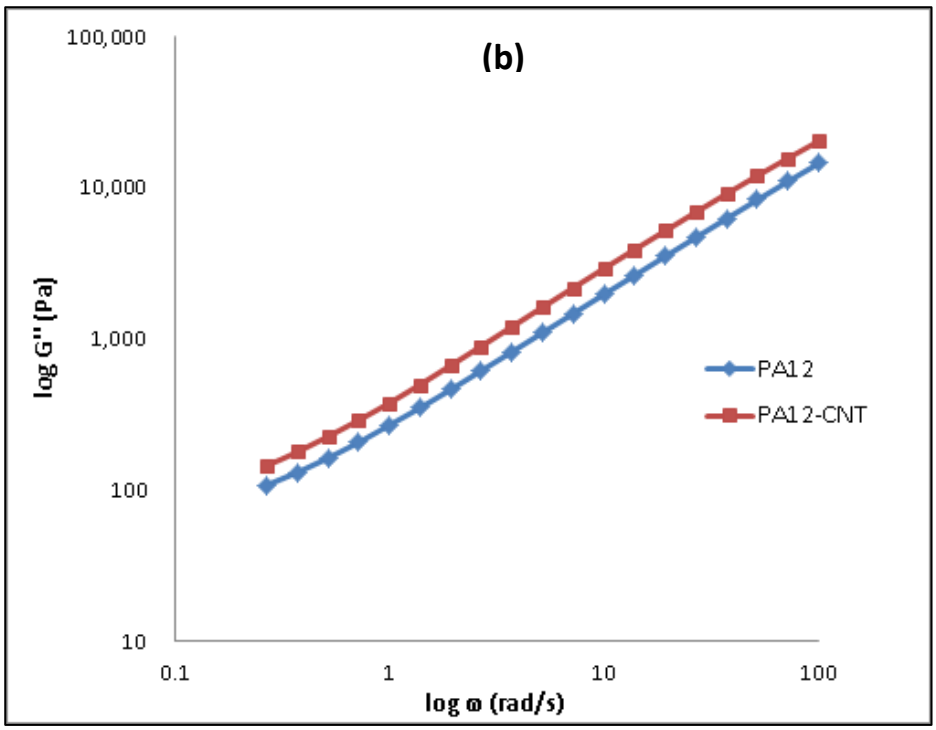

Figure 6-12: (a) Storage modulus G', and (b) loss modulus G'' as a function of frequency of PA12 and PA12-CNT at reference temperature 230°C

The viscosity η for PA12 and PA12-CNT as a function of frequency at 230°C is presented in Figure 6-13. It can be seen that with the increase in frequency, the viscosity for both samples decreased, which is also called shear thinning. This can be explained as the greater the shear rate, the more quickly two molecules move relative to each other, which leads to reduced chain entanglement density. As a result, fewer polymer chains remain in the entanglement state for a sufficiently long time, which caused the drop in viscosity[179]. For the PA12-CNT, the shear thinning effect was as obvious as it was for PA12, which indicated good dispersion of CNTs, as dispersed CNTs aligned with the flow direction and cause the viscosity to decrease. The shear thinning effect will weaken if CNTs agglomerates exist[172]. Compared to PA12, the viscosity of PA12-CNT was raised. Increased viscosity for PA12-CNT is a common phenomenon for filler enforced polymer, which can be explained by the interaction between the CNTs and PA12 hindering the movement of the PA12 chains.

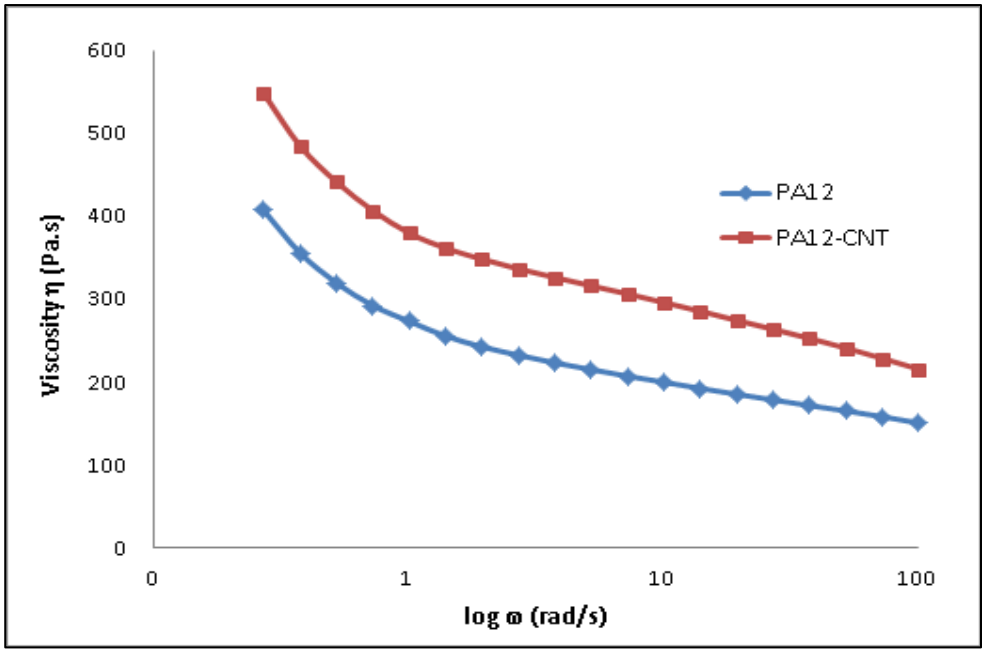

Figure 6-13: Viscosity η as a function of frequency of PA12-CNT at reference temperature 230°C

The variation in viscosity at different temperatures at ω = 1 rad/s for PA12 and PA12-CNT nanocomposites is plotted in Figure 6-14. The viscosity of PA12-CNT remained higher than that of PA12 at all temperatures. The most notable result in Figure 6-14 is the viscosity increase with the increase in temperature for both PA12 and PA12-CNT nanocomposites. This was a converse result compared to common polymers and polymer nanocomposites[106,179,184].

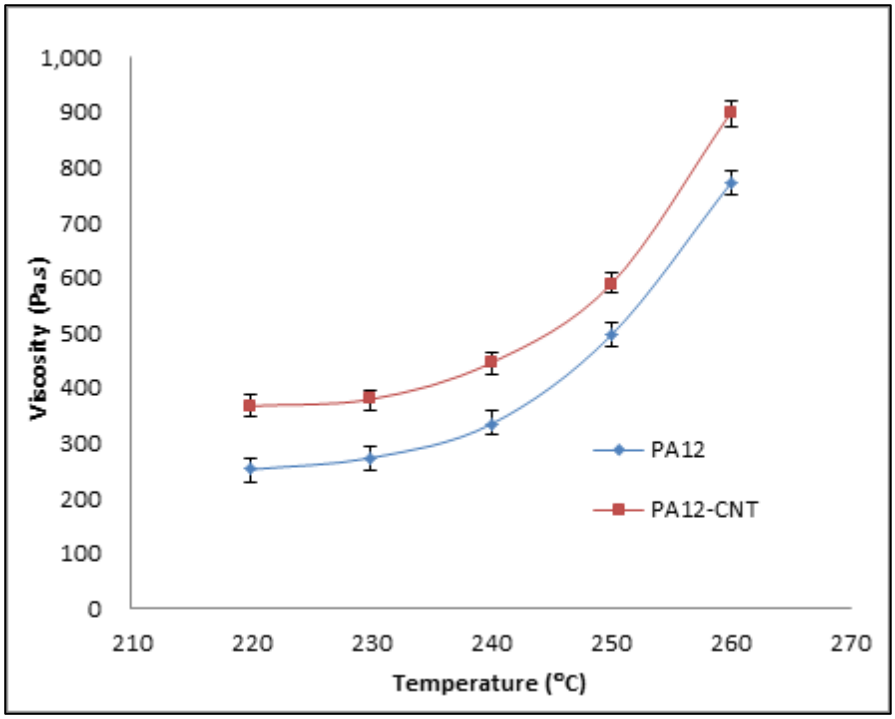

Figure 6-14: Viscosity of PA12 and PA12-CNT nanocomposites at different temperatures with frequency ω = 1 rad/s

6.3. Electron microscopy analysis

6.3.1. Scanning electron microscopy (SEM)

Scanning electron microscopy (SEM) was used to observe the fracture surfaces of the PA12 and PA12–CNT laser sintered parts, shown in Figure 6-15. It can be seen that voids were clearly visible in the PA12 laser sintered parts; No obvious defects were detected in the PA12–CNT parts. This could explain the density difference between the PA12 and PA12-CNT composites parts shown in section 6.1.4.

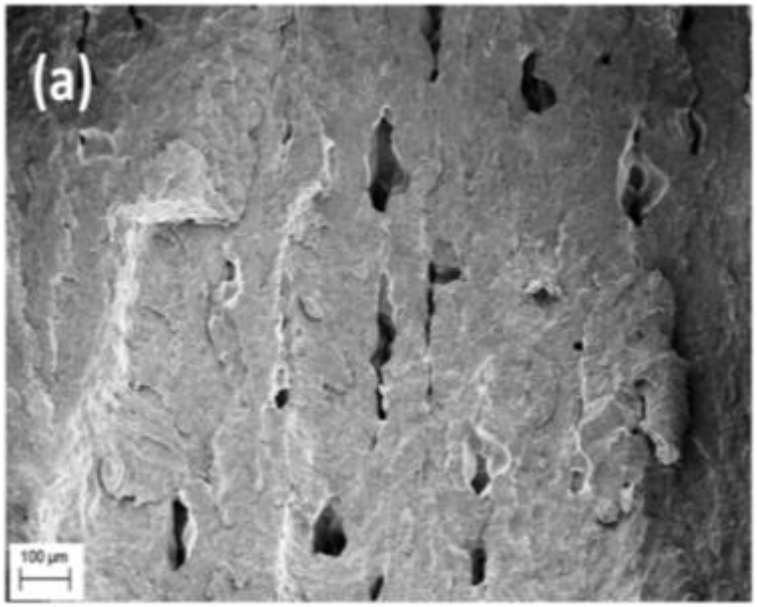

Figure 6 15a: Fracture surface of (a) PA12 sintered part

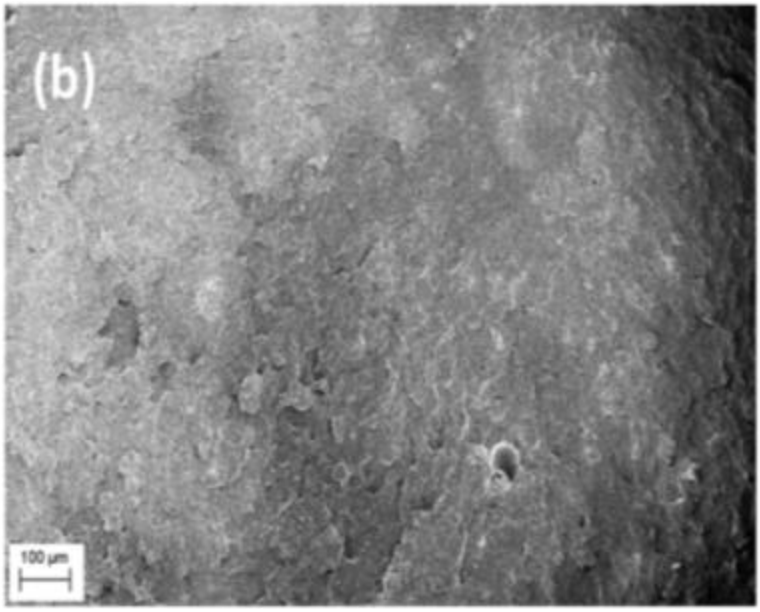

Figure 6-15b: Fracture surface of (b) PA12-CNT laser sintered part

Figure 6-16 shows a higher magnification SEM image of the fracture surface of a laser sintered PA12–CNT part. Only a few CNTs can be observed in the centre of the image; it is thought that most of the CNTs were encased within the PA12 matrix and therefore cannot be detected.

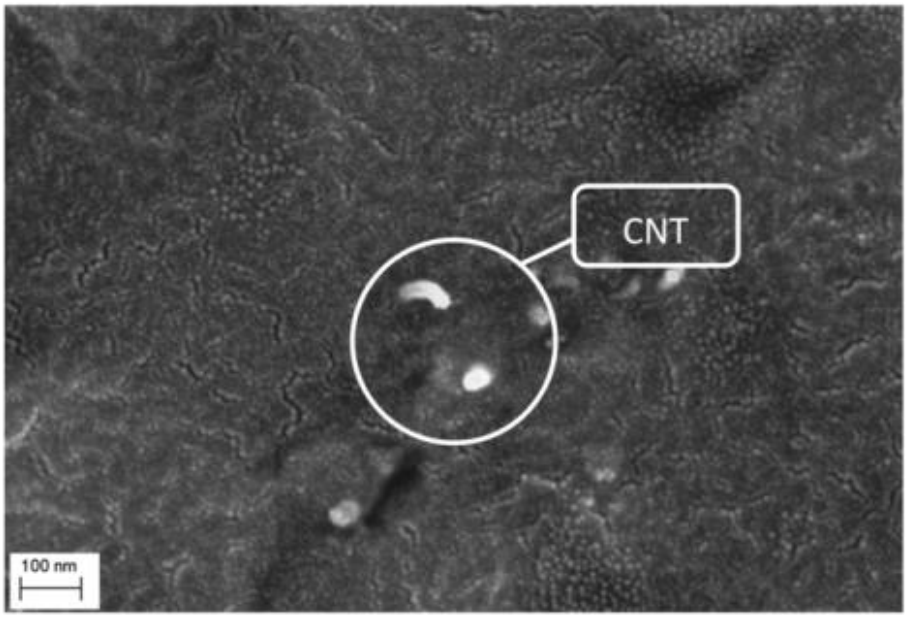

Figure 6-16: Fracture surface of the PA12–CNT laser-sintered part at higher magnification (x200 K).

6.3.2. Three dimensional transmission electron microscopy (3D TEM)

Three dimensional TEM (3D TEM) is a useful method which can provide nano size 3D characterisation of both the surface and internal structure of a material. With this technology, a 3D observation image can be gained by reconstructing a series of 2D TEM projections, which are collected at different tilt angles. In this work, for the first time, 3D TEM technology is used to examine laser sintered polymer nanocomposite parts. The 3D nano-structural observation of the CNTs dispersion in the laser sintered PA12 nanocomposite parts was carried out successfully.

- **Sample location identification**

For TEM observation, preparing high quality specimens is of great importance. Focused ion beam (FIB) milling is a powerful method for preparing TEM specimens. The biggest advantage of using FIB is that site-specific TEM specimens can be prepared. Identifying the TEM lamella location from a bulk sample is a very important step, which is a major advantage of using the FIB method to prepare TEM samples in this study.

The cross section of a laser sintered PA12-CNT is shown in Figure 6-17. It can be seen that the cross section is uniform and no obvious CNTs are observed in most areas. However, in a few regions, some clustered small white spots are observed (section B in Figure 6-17), which might be a CNT rich region. TEM lamellae specimens were prepared in two locations, one is in a random region (section A in Figure 6-17) where no intensive white spots were observed, shown in Figure

6-18a, and the other is in a clustered white spots region (section B in Figure 6-17), which is shown in Figure 6-18b. Figure 6-18c and 6-18d show the thin TEM samples cut loose by ion milling and ready to be lifted out. After ion milling, the lamella was ex-site lifted out using a micromanipulator, and transferred to a TEM sample holder.

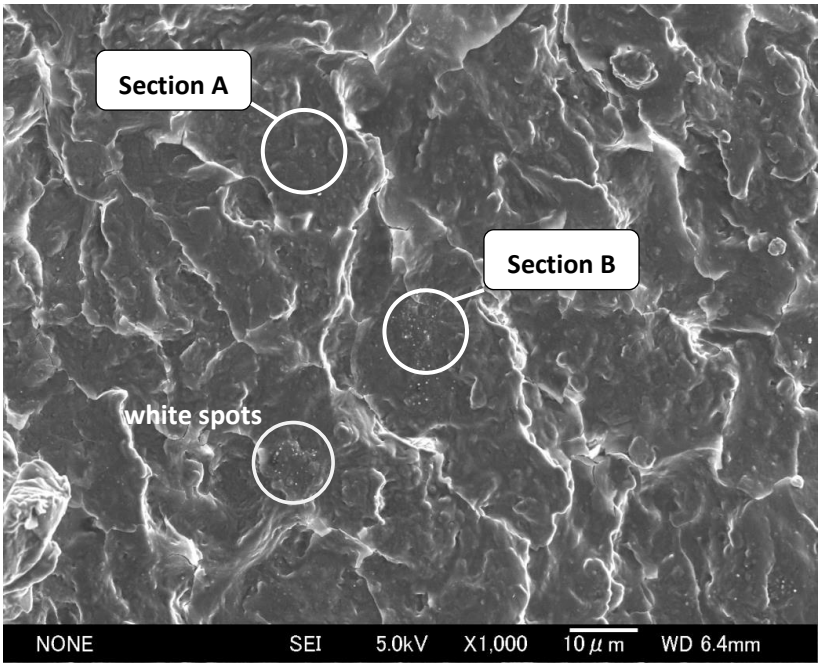

Figure 6-17: Fractured cross section of PA12-CNT laser sintered part. White spots: possible CNT rich region

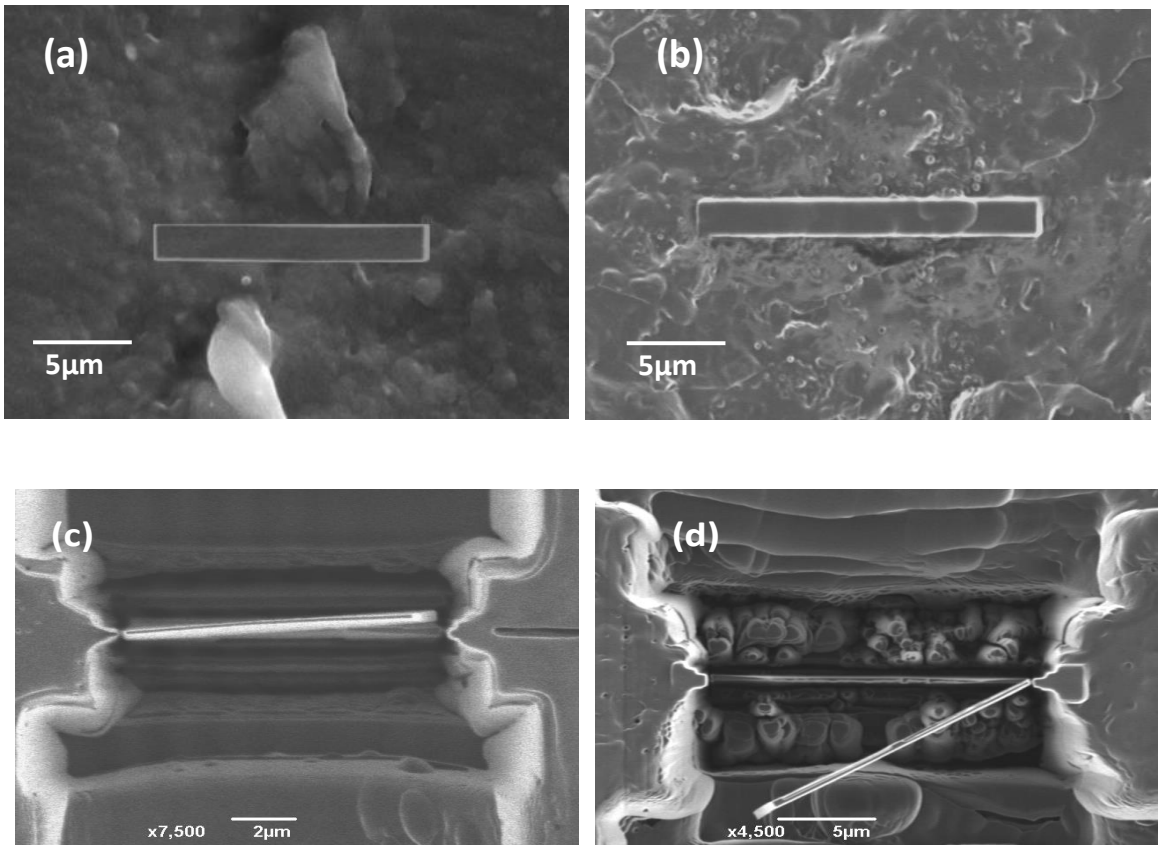

Figure 6-18: TEM sample prepared by FIB, (a) protective deposition at random area (section A in Figure 6-17), (b) protective deposition at intensive white spots region (section B in Figure 6-17), (c) thin TEM lamella sample prepared by ion milling at random region, (d) thin TEM lamella sample prepared by ion milling at intensive white spots region.

- **Initial assessment by 2D TEM**

Before 3D TEM observation, samples were examined by 2D TEM to check the density of CNTs in the PA12 matrix, as well as the sample quality for 3D TEM. The 2D TEM images of samples prepared from random a region and a rich white spots area are shown in Figures 6-19 and 6-20 respectively. It can be seen that both images show good contrast between the PA12 matrix and the CNT fillers.

In Figure 6-19, which is the sample prepared from a random region, CNTs were observed, but only a few. In Figure 6-20, which was the rich white spots region, intensive well-dispersed CNTs can be seen clearly throughout the TEM sample. This proves that the observed clustered white spots regions (Figure 6-18) were CNTs embedded in the PA12 matrix.

Figure 6-19: TEM image of a random region of PA12-CNT as prepared in Figure 6-18a

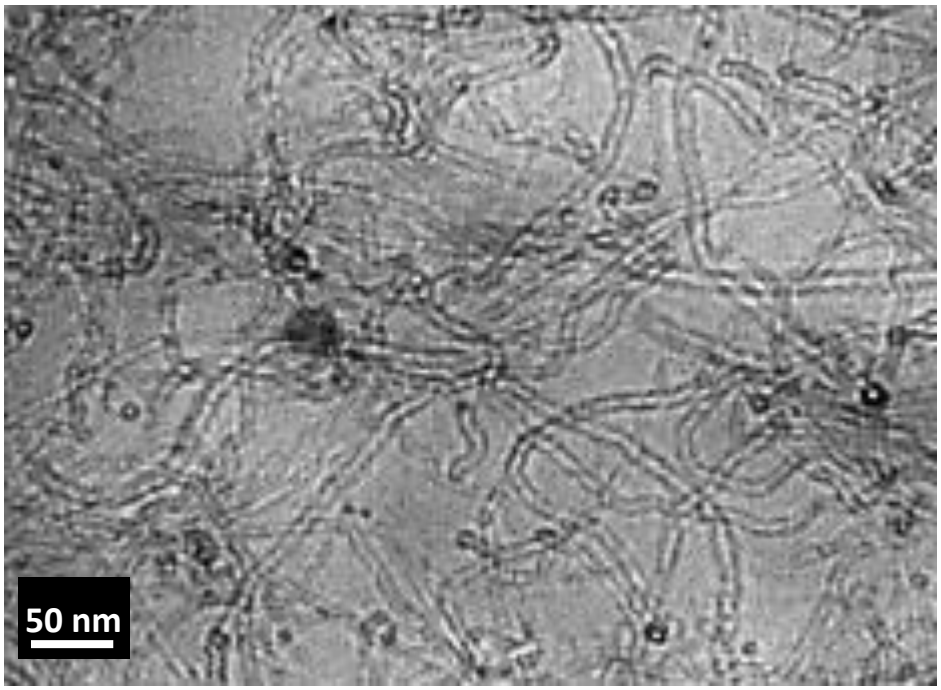

Figure 6-20: TEM image of rich white spots region as prepared in Figure 6-18b.

- **3D TEM observation**

As most CNTs were located intensively in the white spots region (Figure 6-20), the three dimensional TEM observation was carried out with the sample prepared from this region. During the characterisation, when tilting the sample to a different angle, there was a sample shifting and focus change, therefore alignment was applied manually across all tilt angle range (+60^{o} to -60^{o}) before data acquisition. Then, with a 2^{o} increment, a series of 2D projection images with tilt angles ranging from +60^{o} to -60^{o} were collected. In total, 61 2D TEM projection images data from the same sample area were taken. In Figure 6-21a and b, eight typical 2D TEM images of the PA12-CNT laser sintered specimens at various tilt angles are shown. Several CNTs can be observed clearly at each angle. A computer 3D reconstruction was then carried out based on these 2D tomography images.

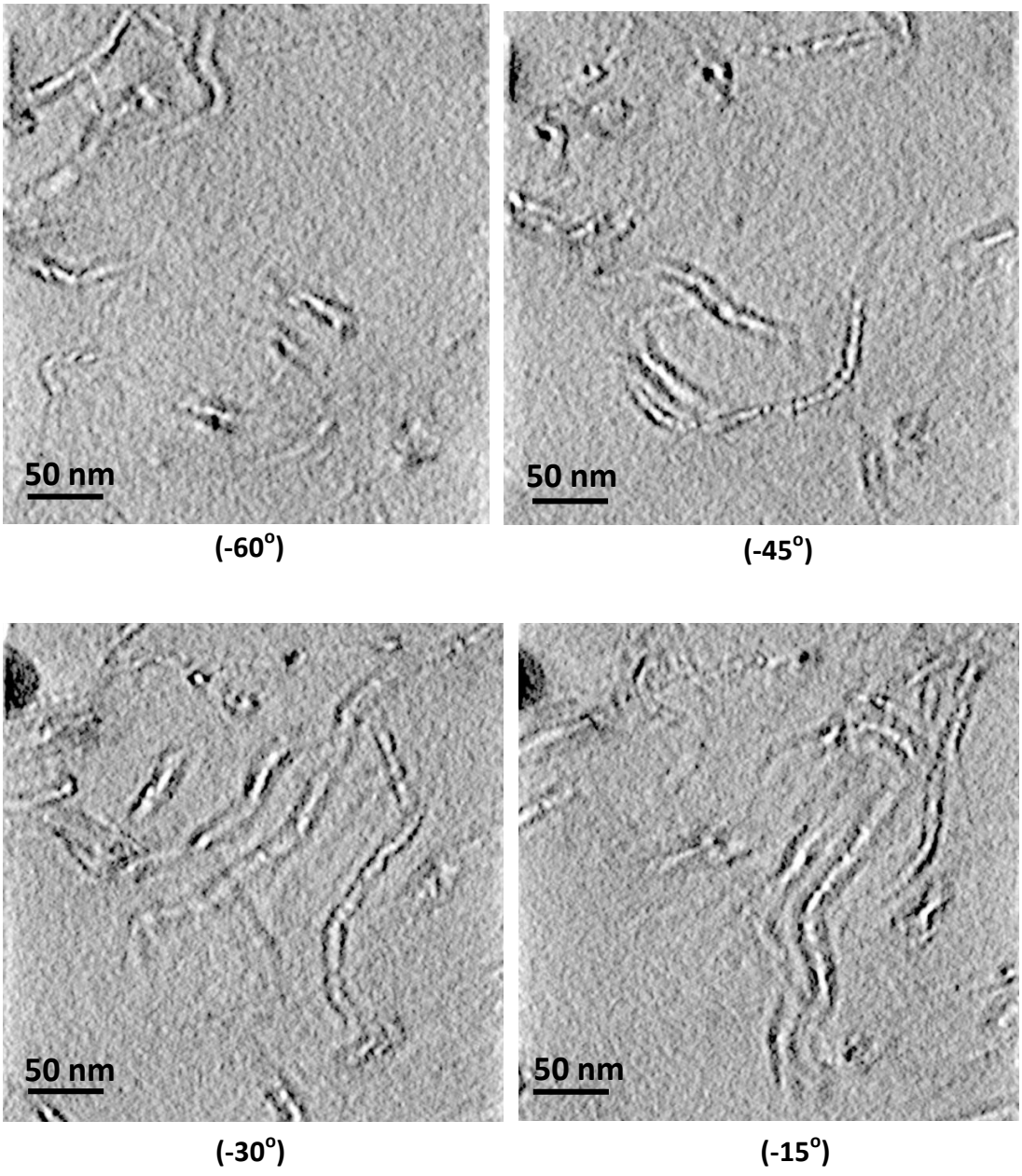

Figure 6-21a: 2D TEM images of a PA12-CNT laser sintered part at various tilt angles

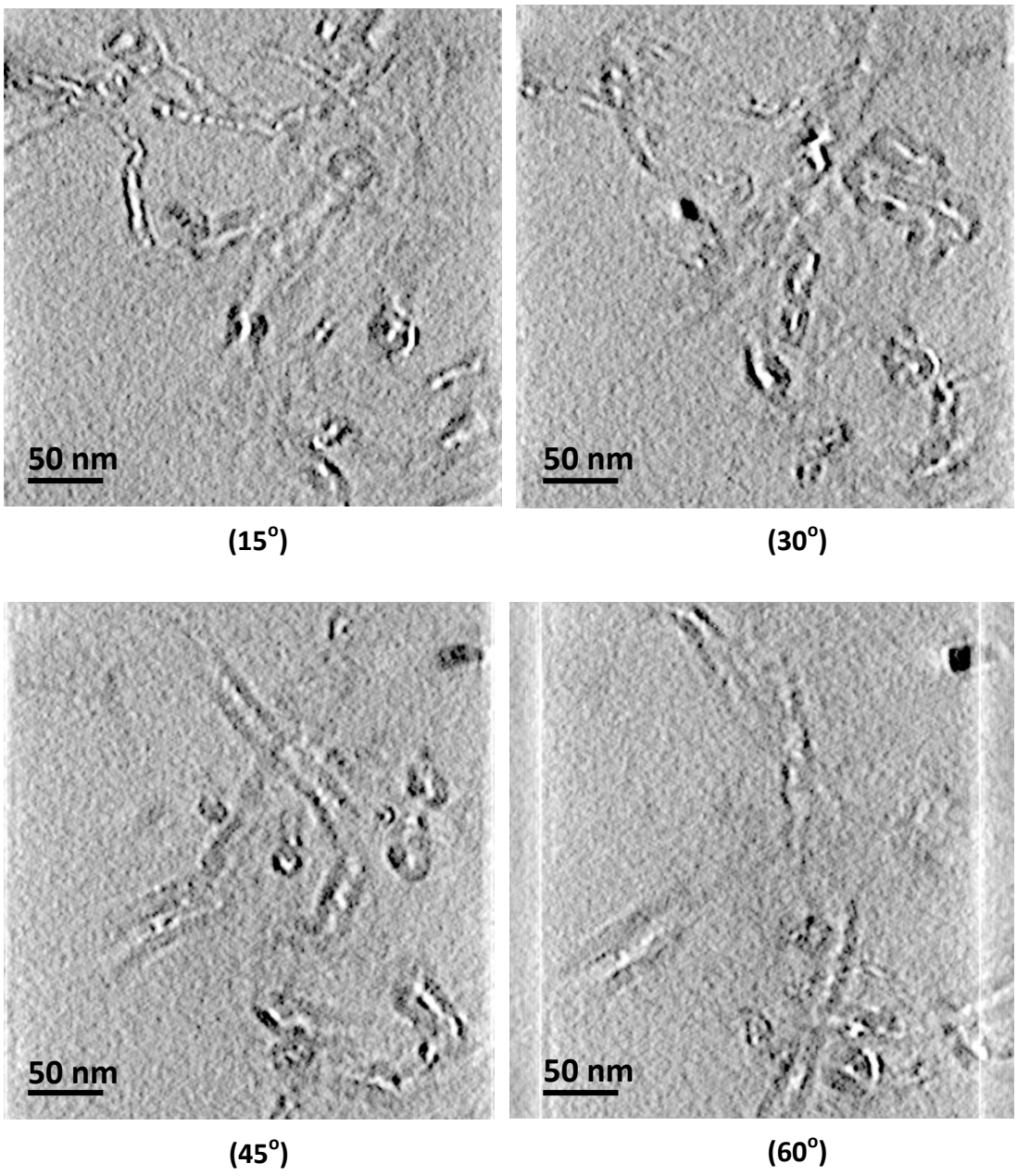

Figure 6-21b: 2D TEM images of a PA12-CNT laser sintered part at various tilt angles.

By combining all of the 2D TEM images of the PA12-CNT laser sintered specimen from -60^{o} to 60^{o}, 3D TEM images were reconstructed, as shown in Figure 6-22a and b. Each colour strand represents a single CNT. With the increase in tilt angle, the 3D nano-size structure of the CNTs distributed in the PA12 matrix was revealed gradually.

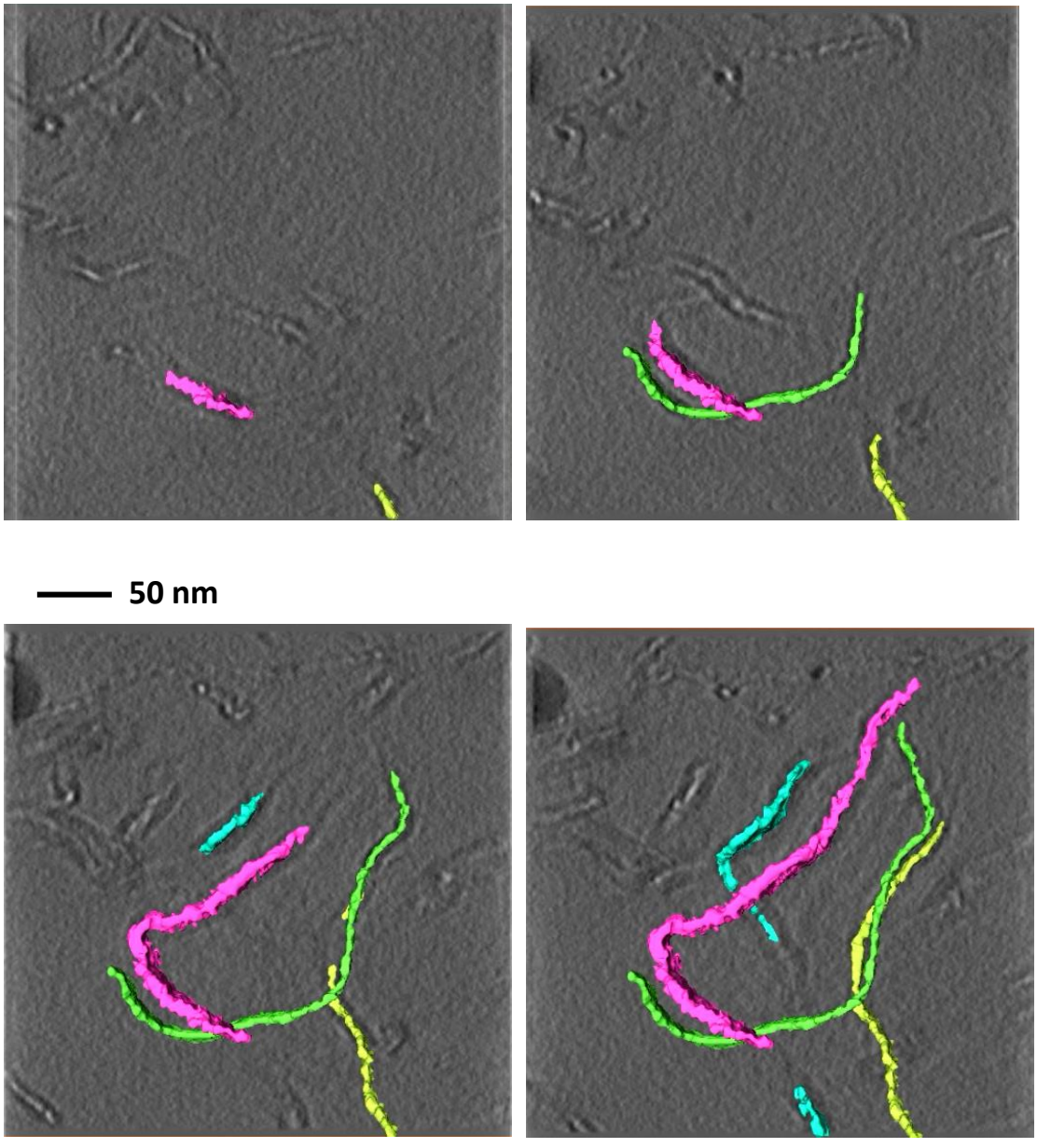

Figure 6-22a: 3D TEM reconstruction process for a PA12-CNT laser sintered specimen. Each colour represents a single CNT

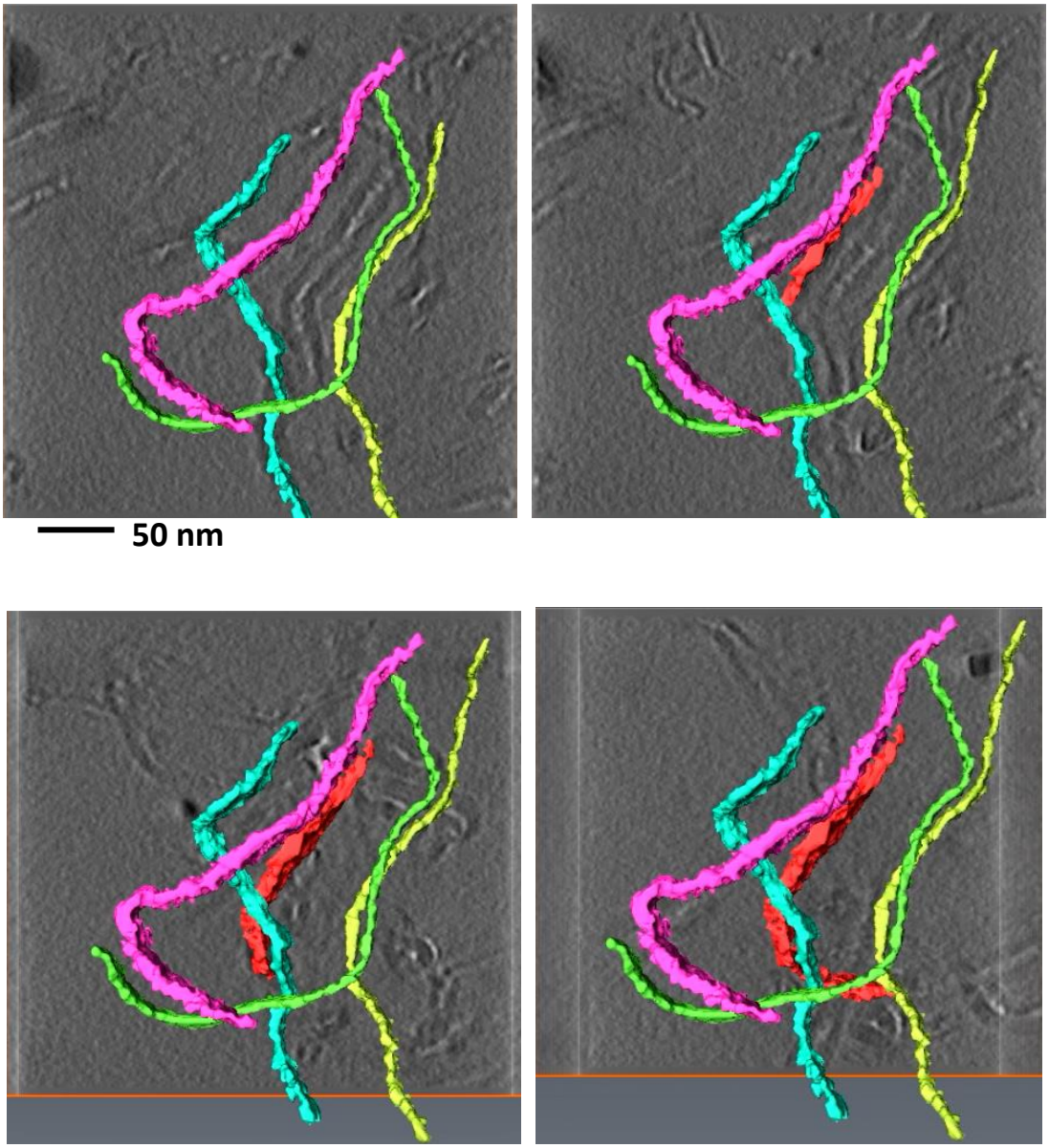

Figure 6-22b: 3D TEM reconstruction process for a PA12-CNT laser sintered specimen. Each colour represents a single CNT.

Following computer reconstruction, the 3D representations of the CNTs in a PA12-CNT laser sintered part are shown in Figure 6-23, where each colour strand denotes a single CNT. These 3D images clearly show that CNTs remained agglomerate-free in the PA12 matrix after laser sintering, which is very important in order to achieve an enhancement in the mechanical properties of

laser sintered nanocomposite parts. It has previously been shown that the method to prepare the PA12-CNT powder allows the CNTs to be dispersed agglomerate-free on the surface of the powder (section 5.1.3). 3D TEM results demonstrates that this remains the case within the sintered nanocomposite parts, indicating that the laser sintering process does not vary the dispersibility of the CNTs in the PA12 matrix.

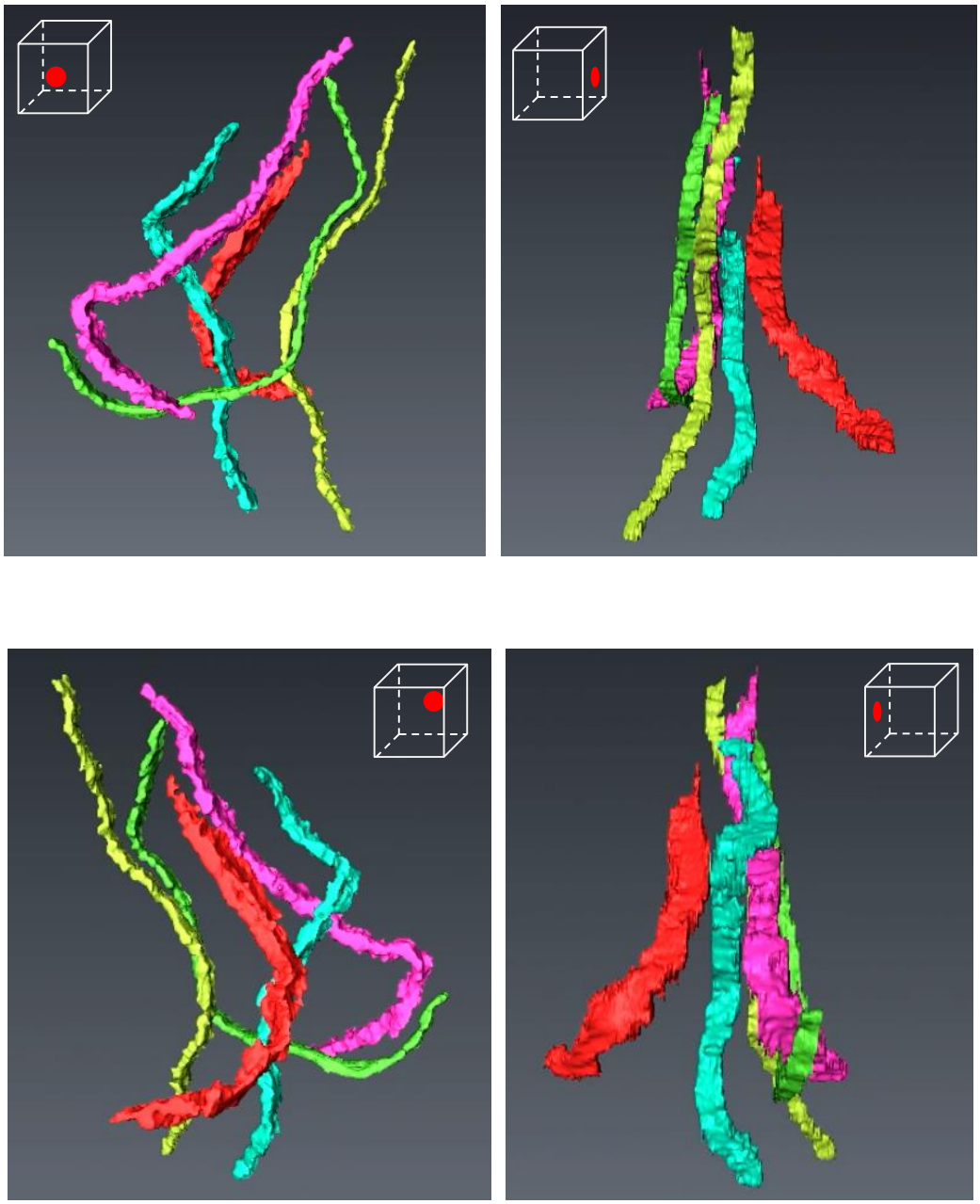

Figure 6-23: 3D representations of CNTs in the PA12-CNT laser sintered parts; each colour represents a single CNT

6.4. Discussion

The laser sintered PA12-CNT parts, along with PA12 laser sintered parts, were characterised by mechanical, thermal and microscopy experiments. Results showed that PA12-CNT laser sintered parts had improved mechanical properties compared to PA12.

According to the rule of mixtures for discontinuous and randomly oriented fibre composites[185]:

$$E_c = K E_f V_f + E_m V_m \qquad \text{Equation 11}$$

Where E_c, E_f, E_m are the modulus for composites, fibre (here nanotube: 0.95 TPa[186]) and matrix (here PA12: 1.5 GPa), V_f and V_m are the volume percentage for fibre and matrix, and K is a fibre efficiency parameter (here assume K = 0.6[185]). By using bulk density for PA12: 0.9 g/cm³ (from manufacturer MSDS) and bulk modulus 1.5 GPa, the expected modulus improvement should be 16.2%. This is different from the results got from the work (for instance 54.0% improvement for Young's modulus), which might be because of the porosity in the laser sintered parts. Therefore, the greatest contribution for the observed increase in mechanical properties might be related to the increased density of the PA12-CNT composite parts (section 6.1.4).

Mechanical test results showed that compared to the best PA12 laser sintered parts, PA12-CNT laser sintered parts had 13.0% greater flexural modulus, 10.9% greater flexural strength, 123.9% increased impact strength, 54.0% greater Young's modulus and 6.2% higher UTS without sacrificing elongation. This enhancement may be attributed mostly to the good dispersion of the CNT in the

PA12 matrix and denser laser sintered parts.

In order to understand the statistical significance of the observed differences between the laser sintered PA12 and PA12-CNT parts, statistical analysis was carried out for mechanical properties test results (impact, flexural, tensile, density). T-test is a common statistic testing method to determine if two sets of data are significantly different from each other. The *p*-value, the probability under the assumption of no statistical significant difference between these two sets of data, can be obtained from the t-test. Commonly, if $p \leq 0.05$, the difference between these two sets of data are considered to be statistically significant. From example, if p = 0.01, which means that there is only 1% chance there is no real difference between these two data sets[187].

Microsoft Excel® was applied in this study to perform the t-test analysis, and the 'T.TEST' function was used. The p values from the analysis are shown in Table 6-6. It can be seen that all the mechanical tests results had much lower p value than 0.05, which indicates that the observed mechanical properties enhancement of PA12-CNT was statistically significant.

	Impact strength	Flexural modulus	Flexural strength	Tensile modulus	Tensile strength	Density
p-value	0.0022	0.000044	0.0022	0.0071	0.000070	0.0000088

Table 6-6: P values from statistical t-test for mechanical testing results between PA12 and PA12-CNT laser sintered parts

In order to get an overall view of polymer materials, Table 6-7 shows a comparison of the mechanical properties of laser sintered polymers and the

most common polymers processed by conventional processing techniques (such as injection moulding and extrusion) from both industry and researchers. The laser sintered PA12 parts showed similar tensile modulus (2373 MPa) and strength (51 MPa) to that of injection moulded parts (tensile modulus: 2300; strength: 55 – 83 MPa). However the elongation at break of laser sintered PA12 was obvious lower than injection moulded parts.

It can be seen that various reinforcing nanofillers combined with base PA12 have been investigated for laser sintering. Compared to these studied, the laser sintered PA12-CNT parts in the current study showed overall improved mechanical properties. Compared to most laser sintering materials, the PA12-CNT also had better performance. PEEK was reported to have higher modulus and strength than PA12 based materials. However, the elongation at break of PEEK was much less than the PA12 based material. Furthermore, the PEEK is nearly non-recyclable during the laser sintering process, which makes it uneconomic and expensive compared to PA12. Compared to polymer parts made using conventional processing techniques, the PA12-CNT laser sintered parts in the current work showed competitive mechanical properties. The modulus (3524 MPa) and strength (54 MPa) was slightly lower than PA-CNT parts produced by injection moulding, which had a tensile modulus of 4400 MPa and strength of 60 MPa. However, the elongation at break for laser sintered parts was obviously lower than parts produced by traditional processes. Apart from that, the cost of laser sintering materials is still much higher than that of conventional polymer materials, which to a certain extent reduces the commercial viability of laser sintering for many applications.

Manufacturing method	Materials	Tensile modulus (MPa)	Ultimate tensile strength (Mpa)	Elongation at break (%)	Reference (Note)
Laser sintering	PA12 base materials				
	PA12	1700	50	24	[74]
		1586	43	14	[75]
		2373	**50**	**20**	**Current work**
	PA12-Glass	3200	51	9	[74]
	PA12-Carbon fibre	2896	66	3.6	[76]
	PA12-CNT	**3524**	**54**	**22**	**Current work**
	PA12-Carbon black	1042	-	-	[133]
	PA12-Nanosilica	1980	46.3	20	[126]
	PA12-Nanoclay	802	47	14	[131]
	Other polymers				
	PS	1600	5.5	0.4	[74]
		1604	2.8	-	[75]
	PP	1165	21	48	[75]
	PEEK	4250	90	2.8	[74]
Injection moulding/ extrusion	PA12	2300	55 – 83	60 – 200	[37]
	PA-CNT	4400	60	81	[188]
	PS	3300	53	3	[185]
	PEEK	3600	95	50	[189]

	PVC	2775	47	120	[190]
	PE	900	23	600	[191]

Table 6-7: Comparison of mechanical properties of laser sintered polymers (from industry and researchers) and polymers processed by conventional processing techniques

The average density of PA12-CNT laser sintered parts was 4.1% higher than that of PA12. The density of CNTs used in this study was 2100 kg/m^3, and addition of CNT's to PA12 would increase the density of material by 0.1%. Therefore the 4% density increase for PA12-CNT, which also would suggest removal of 4% porosity, was due to the improved sintering efficiency as a result of the presence of the CNTs during the laser sintering process. Thermal analysis (Figure 6-11) and SEM of the fracture surface (Figure 6-15a) indicated the presence of unmelted powder and voids remaining in the PA12 sintered parts, which were not observed in the PA12-CNT parts (Figure 6-15b).

DSC results suggested the CNTs nucleating effect on the laser sintered PA12 matrix. With a tubular structure, the nucleating ability of CNTs for polymers has been reported widely in the literature[192-195]. There are two steps in the polymer crystallisation process, the nuclei formation and crystal growth. The formation of nuclei, which is defined as nucleation, can be divided into homogeneous and heterogeneous nucleation. When the formation of nuclei takes places only due to supercooling without existing nuclei, the nucleation is homogeneous. If there are existing nuclei in the polymer solution or melts, this nucleation is referred to as heterogeneous nucleation. In this work, CNTs were regarded as the heterogeneous component in the PA12 matrix, which has shown their nucleating ability for semi-crystalline PA12. The crystalline coating around CNTs

could engineer the CNT-PA12 interface, which can contribute to the stress transfer from CNTs to the polymer matrix to enhance the mechanical properties[193,196].

Phonon scattering phenomenon, which happens when phonons travel through a material, can limit the thermal conductivity improvement of CNTs in polymer nanocomposites[197,198]. The crystallised PA12-CNT interface could reduce the interfacial phonon scattering phenomenon, and then enhance thermal conductivity of the PA12-CNT[199].

When comparing nanofillers with conventional macro-fillers, one of the most important differences is the surface-to-volume ratio. Nanofillers have an exceptionally high surface-to-volume ratio and the area at the interface between the matrix and reinforcement phase is much greater than conventional composite materials. This large reinforcement surface area means that a relatively small amount of nanoscale reinforcement fillers can have an observable effect on the macroscale properties of the composite[106]. However, this advantage has not previously been fully observed when processing polymer nanocomposites by laser sintering.

Previous researchers have either found an increase in Young's modulus and UTS, but a decrease in other properties, such as elongation at break[130,200] or even a reduction in all properties[134]. Some researchers who have observed an increase in properties have reported that increase against a control PA12 with lower mechanical properties normally achievable by laser sintered PA12[200]. Goodridge *et al* [57] have previously highlighted this ability to increase mechanical properties through incorporation of nanoparticles, but reduced properties from the commercial standard as a result of the method used to produce the powders.

Yan *et al* [85] prepared PA12/carbon fibre composite by dissolution-precipitation method. The laser sintered composite parts exhibited significant enhancement in flexural strength and modulus only after a high volume of carbon fibre, from 30 wt% to 50 wt%, was used. No other mechanical properties, including elongation at break, were reported. In the present work, the weight percentage of CNT used to prepare the PA12-CNT was small. Just 0.1 wt% CNT saw a significant improvement in all mechanical properties tested in Section 6.1.1. – 6.1.5. With such a small amount of CNTs, beside good dispersion and interfacial bonding of the CNT in the PA12 matrix, the increased part density was believed to be the main reason for the evident mechanical properties improvement.

With outstanding mechanical, thermal and electrical properties, the potential application of Polymer/CNTs nanocomposites is promising. Compared to the polymer matrix, the cost of CNTs is very expensive, which blocks the application of Polymer/CNTs nanocomposites to some extent. Laser sintering polymer powders also cost much more than commercial bulk polymers. As the cost of materials has a direct influence on the costs of laser sintered parts, the method used in this research of coating the PA12 powder surface with small weight percentage of CNTs provides a more cost-efficient and effective way to produce polymer nanocomposite powder for laser sintering.

Another noticeable result is the elongation at break of the PA12-CNT composite parts compared to PA12 parts (Figure 6-5). It has been previously reported that when using nanofillers to make polymer composite parts via laser sintering, an obvious decrease in elongation at break has been observed for the nanocomposite parts compared to the polymer parts, even though other mechanical properties such as Young's modulus, UTS, flexural strength, flexural modulus or impact strength were improved[80,128,126]. One reason for the decrease

in elongation at break could be the poor dispersion of filler in the polymer matrix, where filler agglomerates act as defects when a force is loaded[131]. Even when the filler is well dispersed, the large amount of filler existing in the matrix could become a force defect[128]. In this work, the elongation at break of PA12-CNT composites parts remained the same as that of PA12 parts due to good CNT dispersion and the small amount of CNT existing in the polymer matrix.

In the laser sintering process, polymers melt and flow. Understanding the motion of the polymer composites liquid is very important for the analysis of the processing operation and optimisation, as well as investigating the structure-property relationship of the nanocomposites. From studies carried out on the conventional polymer nanocomposites, rheological properties have been shown to influence the fabrication and processing (residual stress, void content, etc.) of such materials[201,202]. Jin and co-workers[203] found that the amount of nanoclay loading had a significant influence on the rheology of a polyol/nanoclay mixture when processing Polyurethane nanocomposites. It was found that to achieve good dispersion of the nanoclay with critical viscosity, 3 wt% was the optimum nanoclay loading. This finding provided useful information for the preparation of PU/nanoclay composites in their study, which could also be a helpful guideline for polymer nanocomposite preparation for laser sintering. Several studies have shown that the composite phase morphology and the interfacial interactions between polymer chains and nanofiller also have a direct correlation to the rheological properties of nanocomposites[123,204,205]. Lim and Park[204] reported these effects on the rheological behaviour of different polymer/nanoclay composite by oscillatory frequency and shearing rheological tests. The results indicated the existence of strong interactions between polymer matrix and nanoclay, and the formation of some particle network

structure and randomly oriented silicate layers. These rheological studies with conventional polymer nanocomposites could also be carried out on polymer nanocomposites for laser sintering to offer a fundamental understanding of the processability of these materials, as well as the structure-properties relationship in the nanocomposites. However, the rheological behaviour of polymers and polymer nanocomposites for laser sintering has rarely been investigated in the past.

In this work, for the first time, a rheological investigation of polymer nanocomposites for laser sintering was carried out to examine the influence of the nanofiller on the rheology properties of the polymer matrix. Parallel oscillatory test results demonstrated that CNTs have a substantial effect on the melt rheological properties of the PA12-CNT nanocomposites, as the storage modulus G', loss modulus G'' and viscosity η of the PA12-CNT nanocomposites increased compared to PA12. A strong shear thinning effect is noticed for PA12-CNT nanocomposites, which may suggest good dispersion of CNT.

A notable observation is the viscosity increase with the increase of temperature for both PA12 and its composites, which is a converse result compared to common polymeric materials. For conventional polymers, polymer molecular chains are dispersed and entangled homogeneously, where free volumes exist between these chains. When the temperature is raised, the free volumes expand and the space between polymer chains increase, as shown in Figure 6-24a and b. This thermal expansion strengthens the polymer chains flow, which results in the decrease in viscosity. For the PA12 and PA12-CNT composites specimens in this study, which were made from powders, there may be voids and unmelted PA12 particles/particle cores left inside the specimens. Polymer chains did not disperse and entangle well between those unmelted

particles/cores, shown as Figure 6-24c. When the temperature was increased, the unmelted particles/cores were fused further, which led to the decrease in the number and size of voids and more entanglement of the polymer chains between particles (Figure 6-24d). Even the free volumes inside of the particles expanded; the major influence on the viscosity might count as void decrease and entanglement increase between particles, which caused the increase in viscosity as the temperature increased. As voids and unmelted particles/cores were reported for the laser sintered parts in the literature[26,35], similar viscosity phenomenon could happen for laser sintered parts.

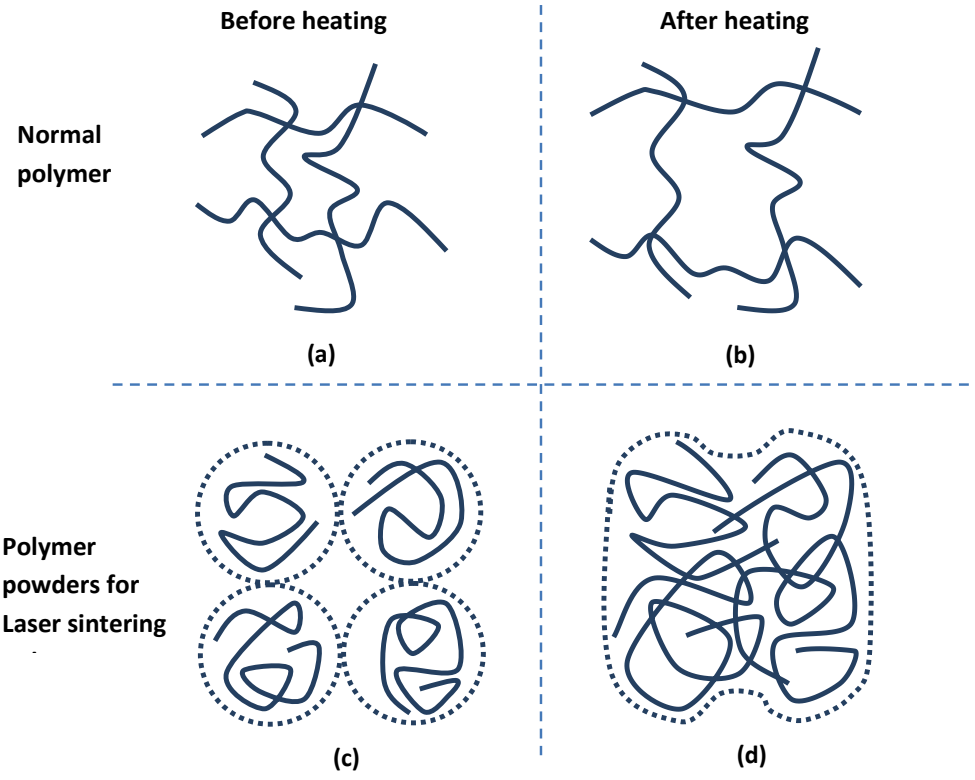

Figure 6-24: Schematic explanation of: (a) normal polymer structure before heating, (b) normal polymer structure after heating, (c) polymer for laser sintering before heating, (d) polymer for laser sintering after heating.

It is well known that the dispersion and distribution of nanofillers in the polymer matrix is one of the most important factors affecting the properties of the nanocomposites[136,137]. Particulate nanofillers tend to form agglomerates very easily, which can weaken the properties of the final nanocomposites parts. Therefore, to achieve desirable properties of nanocomposites parts, the nanofillers should be well dispersed in the polymer matrix. In the research of polymer nanocomposites for laser sintering, the dispersion of nanofillers is mainly examined by scanning electron microscopy (SEM) and transmission electron microscopy (TEM).

SEM can only provide information about the sample's surface topography and composition. The information inside of the sample is lost. Also, it is very difficult to observe the nanofillers on the surface of laser sintered parts with SEM as the nanofillers are embedded in the polymer matrix. Yan et al[200] used a dissolution-precipitation process to incorporate montmorillonite (3 wt%) with PA12 to prepare montmorillonite/PA12 nanocomposite for laser sintering. The dispersion of montmorillonite in the PA12 matrix was examined at fractured surface by SEM. Very rare and unclear montmorillonite was observed. The information underneath the surface of the sample was not reported. In the study carried out by Salmoria et al[135], PA12/Carbon nanotube (0.5 wt%) nanocomposites for laser sintering were produced by mechanical mixing. SEM was unable to detect the CNTs from the fracture surface of laser sintered PA12/CNT parts.

Traditional TEM can provide high-resolution information of an ultra-thin specimen by projecting 3D body onto 2D plane. However the information along the thickness direction of the sample is lost. Recent advanced 3D-TEM is a useful method to provide a 3D characterisation of both the surface and the bulk of a

material.

In this work, 3D TEM tomography was applied to provide a 3D nano-structural observation of the CNTs in the laser sintered polymer nanocomposites parts for the first time. The author carried out this experiment at National Institute for Materials Science (NIMS), Japan.

For TEM observation, preparing high quality specimens is of great importance. Focused ion beam milling is a powerful method for preparing TEM specimens. The biggest advantage of using FIB is that site-specific TEM specimens can be prepared. FIB is also independent of the nature of the materials, which is particularly suitable for composites materials. Furthermore, FIB technique is generally faster and more accurate than manual preparation methods[206]. In this work, FIB was used to prepare the TEM samples at a desired location successfully (Figure 6-18).

High density CNT areas were found in the PA12-CNT laser sintered parts. The different CNT densities between Figure 6-19 and 6-20 could be explained by the method used to produce the PA12-CNT powders and also the mechanism by which the particles are consolidated in laser sintering. In this work, the PA12-CNT powders were prepared by coating the CNTs on the surface of the PA12 particle. When processed by laser sintering, most of the PA12-CNT powder particles were only partially melted. Therefore, most of the CNTs were distributed at the sintering borders rather than dispersed all over the nanocomposites matrix evenly. This is illustrated schematically in Figure 6-25. Therefore, in most regions of the laser sintered PA12-CNT part, there were only a few CNTs, as was seen in Figure 6-19. On the other hand, in the sintering border region between PA12-CNT particles, intensive CNTs were expected, as

was imaged in Figure 6-20.

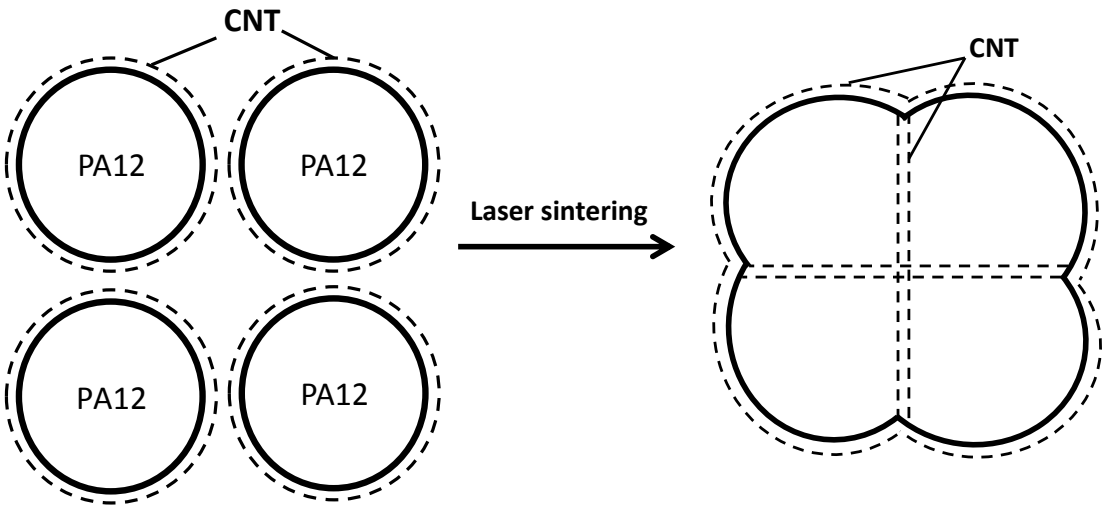

Figure 6-25: Schematic explanation of laser sintering of CNTs coated PA12 nanocomposites, dash lines represent the CNTs

The three dimensional tomography of the CNTs dispersed in the laser sintered PA12-CNT matrix was obtained successfully by 3D-TEM. Results revealed that the CNTs were agglomerate-free in the laser sinter PA12-CNT parts, which is very important for the mechanical enhancement of the nanocomposites. This work demonstrated that 3D TEM tomography could be a feasible way to assess the nano-size structure of laser sintered polymer nanocomposites.

Chapter 7

Conclusions and future work

7.1. Conclusions

In this work, a novel method has been used to prepare PA12-CNT nanocomposites for laser sintering. Powder size, powder morphology, CNT dispersion, thermal and rheological analysis were carried out to evaluate the suitability of the PA12-CNT powders for laser sintering. The PA12-CNT powders, along with neat PA12, were laser sintered to produce test specimens using various laser powers. The effect of addition of CNTs on the laser sintering processing and mechanical/thermal properties of the laser sintered PA12 parts was examined. A three dimensional characterisation of the dispersion of CNTs in the laser sintered PA12-CNT parts was studied by 3D-TEM tomography. The following conclusions can be drawn from this work:

- Well-dispersed PA12-CNT powder with spherical morphology was successfully produced by a novel method of coating the PA12 powders with CNTs. The particle size, size distribution and morphology of the PA12 powder did not change during the process of producing the PA12-CNT nanocomposite powder.

- DSC results showed that the crystallisation temperature of the PA12-CNT powder was higher than that of PA12, which suggests that the CNTs acted as nucleating agents on the PA12. By adding the CNTs into the PA12 powder, the thermal conductivity was increased by 14.2%. With increased thermal conductivity, the heat from laser beam could be conducted more efficiently by the powder. Melt flow index showed that the viscosity of the PA12-CNT powder was higher than the PA12, which may be due to the interfacial force between the CNTs and the PA12 hindering the movement of PA12 chains.

- Flexural, impact and tensile tests specimens for both PA12 and PA12-CNT were laser sintered with good definition and no distortion. Results showed that compared to the best PA12 laser sintered parts, PA12-CNT laser sintered parts had 13.0% greater flexural modulus, 10.9% greater flexural strength, 123.9% increased impact strength, 54.0% greater Young's modulus and 6.2% higher UTS without sacrificing elongation. This enhancement may be attributed mostly to the good dispersion of the CNT in the PA12 matrix and denser laser sintered parts.

- Dynamic mechanical analysis showed that the incorporation of CNTs provided a considerable improvement in the elastic modulus for laser sintered parts. Higher loss modulus for PA12-CNT was due to the interaction between the CNT and the polymer matrix, which caused restricted segmental motions. This also led to a decrease in the thermal expansion coefficient for PA12-CNT.

- Parallel oscillatory test results demonstrated that CNTs had a substantial effect on the melt rheological properties of the PA12-CNT, as the storage modulus G', loss modulus G'' and viscosity η of the PA12-CNT increased compared to PA12. Strong shear thinning effect was noticed for PA12-CNT, which could suggest a good dispersion of CNT in the polymer matrix.

- The density of the PA12–CNT laser-sintered parts was 4.1% higher than that of PA12, which might be due to the increased heat conduction with CNTs during the laser sintering process.

- 3D TEM tomography was used to provide a nano-structural observation of the CNTs in the laser sintered polymer nanocomposites parts for the first time. Results revealed that the CNTs were agglomerate-free in the laser sintered PA12-CNT, which is very important for the mechanical enhancement by nanofillers. This work demonstrated that the 3D TEM tomography could be a feasible way to assess the nano-size structure of laser sintered polymer nanocomposites

7.2. Future work

The current study has identified a novel feasible route to prepare well-dispersed PA12-CNT nanocomposite powders, which result in improved mechanical properties of laser sintered parts. Outcomes of this work have led to a better understanding of preparing, processing and characterisation of polymer nanocomposites for laser sintering. Further research is encouraged in order to expand the understanding and utilisation of the current work. Several recommendations for future work include:

- A more comprehensive study of the sintering parameters, such as laser scanning speed and scan spacing to establish what effects they would have on the properties of laser sintered PA12-CNT.

- A mechanical analytical computer model could be developed to analysis the mechanical reinforcement effect of the CNT on the laser sintered parts under a force.

- With regards to mechanical properties reinforcement, the mechanical behaviour of the laser sintered parts under various tensile strain rates could be investigated. This could indicate the applications of the laser sintered PA12-CNT for various areas, such as military body armour which experiences high strain rates.

- Besides the superior mechanical properties, the electrical conductivity of the CNT is also very good compared to neat polymer materials. The effect of the CNTs on the electrical properties of laser sintered polymer/CNT nanocomposites can be studied.

- Alternative suitable nanofillers, such as graphite or nanoclay, can be used to prepare polymer nanocomposite powders for laser sintering by this novel method, and the properties (mechanical, thermal, electrical) can be investigated.

- The CNTs have shown nucleating ability for crystalline PA12. In the presence of the CNTs, the crystalline morphology of the laser sintered PA12 could be

changed. Polarised optical microscopy could be carried out to characterise the crystalline morphology of the laser sintered PA12-CNT.

- The molecular weight of polymers has a direct effect on the mechanical properties. It would be useful to employ the gel permeation chromatography (GPC) technique to characterise the molecular weight of the laser sintered PA12 and PA12-CNT.

- To observe the temperature distribution during the laser sintering process, a built-in thermal infrared imaging camera, which would produce a visual representation of the infrared energy emitted and reflected by materials, could be used in future research.

List of publications

Journal papers:

BAI, J., GOODRIDGE, R.D., HAGUE, R.J.M., SONG, M., 2013, Improving the mechanical properties of laser-sintered polyamide 12 through incorporation of carbon nanotubes, Polymer Engineering & Science, 53(9), 1937-1946.

BAI, J., GOODRIDGE, R.D., HAGUE, R.J.M., SONG, M., OKAMOTO, M., Influence of carbon nanotubes on the rheology and dynamic mechanical properties of polyamide-12 for laser sintering, submitted to 'Composites Part A: Applied Science and Manufacturing'.

BAI, J., GOODRIDGE, R.D., HAGUE, R.J.M., SONG, M., MURAKAMI, H., Nano-structural characterisation of carbon nanotubes in laser sintered polyamide 12 by 3D-TEM, In Progress.

Conferences contribution:

BAI J, GOODRIDGE RD, HAGUE RJM and SONG M, 2012, Processing and Characterisation of a Polyamide 12-Carbon Nanotube Composite by Laser Sintering, In: 23rd Annual International Solid Freeform Fabrication Symposium, Texas, US.

BAI J, GOODRIDGE RD, HAGUE RJM and SONG M, 2011. Processing and Characterisation of a Polyamide 12-Carbon Nanotube Composite by Laser Sintering In: Proceedings of the 19th Annual International Conference on Composites and Nano Engineering, 79, Shanghai, China.

References

1 Fischer, H., Polymer nanocomposites: from fundamental research to specific applications. Materials Science and Engineering C 23: 763–772, 2003

2 Gebhardt, A., Understanding Additive Manufacturing: Rapid Prototyping, Rapid Tooling, Rapid Manufacturing, Hanser Gardner Publications, 2012

3 Hopkinson, N., Hague, R.J.M., Dickens, P.M., Rapid Manufacturing: An industrial revolution for the digital age. England: John Wiley & Sons Ltd. ISBN 0470016132, 2005

4 Gibson, I., Rosen, D.W., Stucker, B., Additive Manufacturing Technologies: Rapid Prototyping to Direct Digital Manufacturing, Springer, 2009

5 Gideon, N., Levy, I., Schindel, R., Kruth, J.P., Rapid manufacturing and rapid tooling with layer manufacturing (lm) technologies, state of the art and future perspectives, CIRP Annals - Manufacturing Technology, 52, 2, 589-609, 2003

6 ASTM F2792, Standard Terminology for Additive Manufacturing Technologies, 2010

7 Wohlers, T., Recent trends in additive manufacturing, Proceeding of AEPR'12, 17th European Forum on Rapid Prototyping and Manufacturing, Paris, France, June, 2012

8 Cooper, D.E., Stanford, M., Kibble, K.A., Gibbons, G.J., Additive Manufacturing for product improvement at Red Bull Technology, Materials & Design, 41, 226 – 230, 2012

9 Wohlers, T., Wholers Report, Rapid Prototyping, Tooling & Manufacturing. State of the Industry, Annual Worldwide Progress Report. Colorado: Wholers Associate Inc. USA, 2003

10 Hague, R., Campbell, I., Dickens, P., Implications on Design of Rapid Manufacturing.

Proceedings of the Institution of Mechanical Engineers Part C, Journal of Mechanical Engineering Science, 217 (C1), 25 – 30, 2003

11 Hague, R., Mansour, S., Saleh, N., Design Opportunities with Rapid Manufacturing. Assembly Automation, 23(4), 346 – 356, 2002

12 Piller, F.T., and Muller, M., A new marketing approach to mass customization. International Journal of Computer Integrated Manufacturing, 17 (7), 583 – 593, 2004

13 Shaping our national competency in additive manufacturing, Technology Strategy Board, UK, September, 2012

14 Stocker, M., From Rapid Prototyping to Rapid Manufacturing, Auto Technology, 2, 28 – 40, 2002

15 Hopkinson, N., Dickens, P., Rapid Prototyping for Direct Manufacture, Rapid Prototyping Journal, 7, 4, 197 – 202, 2001

16 Ruffo, M., Tuck, C., Hague, R., Cost Estimation for rapid manufacturing – laser sintering production for low-medium volumes, Proceedings of the institute of Mechanical Engineers Part B – Journal of Engineering Manufacture, 220, B9, 1417 – 1428, 2006

17 Shen, J., Steinberger, J., Gopfert, J., Gerner, J., Daiber, F., Manetsberger, S., Ferstel, S., Inhomogeneous shrinkage of polymer materials in selective laser sintering, In Proceedings of the Solid Free Form Fabrications Symposium, University of Texas at Austin, USA., 298 – 305, 2002

18 Griffiths, A., Rapid manufacturing; The Next Industrial Revolution. Journal of Materials World, 10(12), 34 – 35, 2002

19 Caloud, H., Pietrafitta, M., Masters, M., Use of SLS technology in direct manufacture of hearing aids, In SLS users' group conference, San Francisco, USA, 2002

20 Beerens, M., Patient specific implants using additive manufacturing, Proceeding of the International conference on additive manufacturing, Nottingham, UK, 2012

21 http://www.xilloc.com/, accessed on 04/2013

22 Kumar, S., Selective laser Sintering: A qualitative and objective Approach, JOM, 55, 10, 43 – 47, 2003

23 Goodridge, R.D., Tuck C.J., Hague R.J.M., Laser sintering of polyamides and other polymers, Progress in Materials Science, 57(2), 229 – 267, 2011

24 Moeskops, E., Kamperman, N., Van de Vorst, B., Knoppers, R., Creep behaviour of polyamide in selective laser sintering. In: Proceedings of the 15th solid freeform fabrication symposium, Austin, Texas;. p 60–7, 2004

25 Kruth, J.P, Levy, G., Klocke, F., Childs, T.. Consolidation phenomena in laser and powder-bed based layer manufacturing. Ann CIRP, 56(2), 730-59, 2007

26 Zarringhalam, H., Majewski, C., Hopkinson, N., Degree of particle melt in Nylon-12 selective laser-sintered parts, Rapid Prototyping Journal, 15, 2, 126 – 132, 2009

27 Kruth, J.P., Levy, G., Schindel, R., Craeghs, T., Yasa, E., Consolidation of polymer powders by selective laser sintering, PMI2008, Ghent, Belgium; September 2008.

28 Gibson, I., Shi, D.P., Material properties and fabrication parameters in selective laser sintering process, Rapid Prototyping Journal, 3, 4, 129 – 136, 1997

29 Williams, J.D., Deckard, C.R., Advances in modelling the effects of selected parameters on the SLS process. Rapid Prototyping Journal, 4(2), 90–100, 1998

30 Cheah, C.M., Leong, K.F., Chua, C.K., Low, K.H., Quek, H.S., Characterisation of microfeatures in selective laser sintered drug delivery devices. Proceedings of the Institution of Mechanical Engineers Part H: Journal of Engineering in Medicine, 216, 2002

31 Dickens, E.D., Lee, B.L., Taylor, G.A., Magistro, A.J., Ng, H., Sinterable semi-crystalline powder and near-fully dense article formed therewith, U.S. Pat, 5, 990, 268, 1999

32 Mcalea, K.P., Forderhasse, P.F., Booth, R.B., Selective laser sintering of polymer powder of controlled particle size distribution, US Patent 5817206, 1998,

33 Goodridge, R.D., Hague, R.J.M., In search of new materials for laser sintering, Solid Freeform Fabrication Symposium, Austin, Texas, USA, 2010

34 Gibson, I., Rosen, D.W., Stucker, B., Additive Manufacturing Technologies: Rapid Prototyping to Direct Digital Manufacturing, Springer, 2009

35 Zarringhalam, H., Investigation into crystallinity and degree of particle melt in selective laser sintering, Loughborough University, Wolfson School of Mechanical and Manufacturing Engineering, LU thesis, 2007

36 Nelson, J.C., Selective laser sintering: a definition of the process and an empirical sintering model. PhD dissertation, University of Texas, Austin, TX; 1993

37 Kalpakjian, S., Schmid, S., Manufacturing Engineering and Technology, 4th edition, Prentice-Hall, Englewood Cliffs, New Jersey, 2001

38 Zarringhalam, H., Hopkinson, N., Post-processing of DuraForm parts for rapid manufacture, in Proceedings of the 14th Solid Freeform Fabrication (SFF) Symposium, Austin, Texas, 596 – 606, 2003

39 Polyamide PA2200 Material Data Sheet, EOS, Germany, 2013

40 Tontowi, A.E., Childs, T.H C., Density prediction of crystalline polymer sintered parts at various powder bed temperatures. Rapid Prototyping Journal, 7(3), 180 – 184, 2001

41 Ho, H.C.H., Cheung, W.L., Gibson, I., Morphology and properties of Selective Laser Sintered bisphenol a polycarbonate. Industrial and Engineering Chemistry Research, 42 (9), 1850 – 1862, 2003

42 Ho, H.C.H., Gibson, I., Cheung, W.L., Effects of energy density on morphology and properties of Selective Laser Sintered polycarbonate. Journal of Material Processing Technology, 89 – 90, 204 – 210, 1999

43 Caulfield, B., McHugh, P.E., Lohfeld, S., Dependence of mechanical properties of polyamide components on build parameters in the SLS process. Journal of Material Processing Technology, 182(1-3), 477 – 488, 2007

44 Tontowi, A.E., Childs, T.H.C., Density prediction of crystalline polymer sintered parts at various powder bed temperatures, Rapid Prototyping Journal, 7, 180–184, 2001

45 Saleh, N., Internal report on the design for rapid manufacture research project. Wolfson School of Mechanical and Manufacturing Engineering, Loughborough University, Loughborough, 2003

46 Grimm, T., User's guide to rapid prototyping, Society of Manufacturing Engineers, 2004

47 Moeskops, E., Kamperman, N., Vorst, B.V.D., Knoppers, R., Creep behaviour of polyamide in selective laser sintering, In Solid Freeform Fabrication Symposium, The University of Austin, Texas, 60 – 67, 2004

48 ASTM F2921-11, Standard Terminology for Additive Manufacturing—Coordinate Systems and Test Methodologies, 2011

49 Shi, Y., Li, Z., Sun, H., Huang, S., Zeng, F., Effect of the properties of the polymer materials on the quality of selective laser sintering parts. Proceedings of the Institution of Mechanical Engineers, Part L: Journal of Materials: Design and Applications, 218: 247–52, 2004

50 Kruth, J.P., Mercelis, P., Vaerenbergh, J.V., Binding mechanisms in selective laser sintering and selective laser melting, Rapid Prototyping Journal, 11, 26-36, 2005

51 Monsheimer, S., Baumann, F.E., Polymer powder with polyamide, use in a shaping

process, and molding produced from this polymer powder, US Patent Application No. US2006/0202395 A1, 2006

52 Chung, H., Das, S., Functionally graded Nylon-11/silica nanocomposites produced by selective laser sintering, materials science and engineering A 487, 251 – 257, 2008

53 Forderhase, P., McAlea, K., Booth, R., Solid Freeform Fabrication Symposium, The university of Texas at Austin, 287 – 297, 1995

54 Goodridge, R.D., Dalgarno, K.W., Wood, D.J., Indirect selective laser sintering of an apatite–mullite glass–ceramic for potential use in bone replacement applications, Proceedings of the Institution of Mechanical Engineers Part H: J. Engineering in Medicine, 220, 57–68, 2006

55 Karapatis, N.P., Egger, G., Gygax, P. E., Glardon, R., Optimisation of powder layer density in selective laser sintering. Proceedings of Solid Freeform Fabrication, 9 – 11 August 1999, pp. 255 – 264, The University of Texas at Austin, Austin, Texas, 1999

56 McGeary, R.K., Mechanical Packing of spherical particles, Journal of the American Ceramic Society, 44(10), 513 – 522, 1961

57 Goodridge, R.D., Shofner, M.L., Hague, R.J.M., McClelland, M., Schlea, M.R., Johnson, R.B., Tuck, C.J., Processing of a Polyamide-12/carbon nanofibre composite by laser sintering, Polymer Testing, 30(1), 94-100, 2011

58 German, R.M., Liquid Phase Sintering, Springer, ISBN 0306422158, 1985

59 Callister, W.D. Jr., Fundamentals of Materials Science and Engineering, John Wiley & Sons, Inc., Texas, 2001.

60 Childs, T.H.C., Tontowi, A.E., Selective laser sintering of a crystalline and glass-filled crystalline polymer: experiments and simulations, Proc. IMechE Part B, J. Engineering Manufacture, 215/11: 1481-1495, 2001

61 Dotchev, K., Yusoff, W., Recycling of polyamide 12 based powders in the laser sintering process, Rapid Prototyping Journal, 15/3, 192 – 203, 2009

62 Advanced Laser Materials, http://alm-llc.com/products/unfilled_Nylon12.shtml, accessed on 08/2013

63 Gornet, T.J., Davis, K.R., Starr, T.L., Mulloy, K.M., Proceedings of the solid freeform fabrication symposium characterization of selective laser sintering materials to determine process stability, University of Texas at Austin, USA, 2002

64 Kollross, P., Owen, A.J., The influence of hydrogen bonding on mechanical anisotropy in oriented nylon-12, Polymer, 1982;23:829 – 33, 1982

65 Pham, D.T., Dotchev, K.D., Yusoff, W.A.Y., Deterioration of polyamide powder properties in the laser sintering process, Proceedings of the Institution of Mechanical Engineers, Part C: Journal of Mechanical Engineering Science, 222:2163–76, 2008

66 Gornet, T.J., Davis KR, Starr TL, Mulloy KM. Characterization of selective laser sintering materials to determine process stability. In: Solid freeform fabrication symposium proceedings, 546 - 53, 2002

67 Beaman, J.J., Barlow, J.W., Bourell, D.L., Crawford, R.H., Marcus, H.L., McAlea, K.P., SFF: A new direction in manufacturing, Kluwer Academic Publishers, USA, 1997

68 Pham, D.T, Dimov, S., Lacan, F., Selective laser sintering: applications and technological capabilities. Proceedings of the Institution of Mechanical Engineers, Part B: Journal of Engineering Manufacture, 213(5):435 – 49, 1999

69 Kruth, J., Leu, M., Nakagawa, T., Progress in additive manufacturing and rapid prototyping. CIRP Annals - Manufacturing Technology, 47(2):525 – 40, 1998

70 Wohlers, T.T., Wohlers report 2009: state of the industry, annual worldwide progress report, Fort Collins: Wohlers Associates; 2009

71 Kruth, J.P., Levy, G., Klocke, F., Childs, T., Consolidation phenomena in laser and powder-bed based layer manufacturing. Ann CIRP, 56(2), 730-59, 2007

72 http://www.3dsystems.com/products/materials/sls/index.asp, accessed on 12/2012

73 http://www.eos.info/en/products/materials/materials-for-plastic-systems.html, accessed on 06/2013

74 Electro Optical Systems (EOS). EOS official website: http://www.eos.info, accessed on 07/2013

75 3D Systems. 3D Systems official website: http://www.3dsystems.com, accessed on 07/2013

76 Advanced Laser Materials (ALM). ALM official website: http://www.alm.com, accessed on 07/2013

77 Kumar, S., Kruth, J.P., Composites by rapid prototyping technology, Materials & Design, 31, 2, 2010

78 Gert, R., Strobl., The Physics of Polymers Concepts for Understanding Their Structures and Behavior. Springer-Verlag, 1996

79 Childs, T.H.C., Berzins, M., Ryder, G.R., Tontowi, A., Selective laser sintering of an amorphous polymer-simulations and experiments, Proceedings of the Institution of Mechanical Engineers, Part B: Journal of Engineering Manufacture, 213, 333 – 349, 1999

80 Salmoria, G.V., Leite, J.L., Ahrens, C.H., Lago, A., Pires, A.T.N., Rapid manufacturing of PA/HDPE blend specimens by selective laser sintering: Microstructural characterization, Polymer Testing, 26: 361 – 368, 2007

81 Chung, H., Das, S., Processing and Properties of Glass Bead Particulate-Filled Functionally Graded Nylon-11 Composites Produced by Selective Laser Sintering,

Materials Science and Engineering: A, 437, 226–234, 2006

82 Chung, H., Processing and Properties of Functionally Graded Polymer Composites Produced by Selective Laser Sintering. The University of Michigan, Ann Arbor, 2005

83 Gill, T.J., Hon, K.K.B., Experimental Investigation into the Selective Laser Sintering of Silicon Carbide Polyamide Composites, Proceedings of the institution of mechanical engineers part b-journal of engineering manufacture, 218, 1249–1256, 2004

84 Tan, K.H., Chua, C.K., Leong, K.F., Cheah, C.M., Cheang, P., Abu Bakar M.S., Scaffold development using selective laser sintering of polyetheretherketone–hydroxyapatite biocomposite blends, Biomaterials 24, 3115–3123, 2003

85 Yan, C., Hao, L., Xu, L., Shi, Y., Preparation, characterisation and processing of carbon fibre/polyamide-12 composites for selective laser sintering, Composites science and technology, 71, 1834 – 1841, 2011

86 Savalani, M.M., Hao, L., Harris, R.A., Evaluation of CO2 and Nd:YAG lasers for the selective laser sintering of HAPEX, Proceedings of the Institution of Mechanical Engineers, Part B: Journal of Engineering Manufacture, 220(2), 171 – 182, 2006

87 Kruth, J.P., Wang, X., Laoui, T., Froyen, L., Lasers and Materials in selective laser sintering, Assembly Automation, 23, 4, 357–371, 2003

88 Electro Optical Systems (EOS). EOS official website: http://www.eos.info

89 Drexler, K. Eric, Engines of Creation: The Coming Era of Nanotechnology. Doubleday, 1986

90 Drexler, K. Eric, Nanosystems: Molecular Machinery, Manufacturing, and Computation. New York: John Wiley & Sons, 1992

91 Prasad, S. K., Modern Concepts in Nanotechnology. Discovery Publishing House, 31–32, 2008

92 Allhoff, F., Lin, P., Moore, D., What is nanotechnology and why does it matter?: from science to ethics, John Wiley and Sons, 2010

93 Kahn, J., "Nanotechnology". National Geographic, 98–119, June 2006

94 Koo, H.J., Polymer Nanocomposites: Processing, Characterization, and Application, McGraw-Hill, 2006

95 Schaefer, H.E., Nanoscience: The Science of the Small in Physics, Engineering, Chemistry, Biology and Medicine, Springer, 2010

96 Carter, L.W., Hendricks, J.G., Bolley, D.S., US Patent, 2,531,396, 1950

97 Usuki, A., Koiwai, A., Kojima, Y., Kawasumi, M., Okada, A., Kurauchi, T., Kamigaito, O. Interaction of nylon 6-clay surface and mechanical properties of nylon 6-clay hybrid. Journal of Applied Polymer Science 55 1, 119, 1995

98 Ajayan, P.M., Schadler, L.S., Braun, P.V., Nanocomposite science and technology. Wiley, 2003

99 Twardowski, T.E., Twardowski, T.A., Introduction to Nanocomposite Materials: Properties, Processing, Characterization, DEStech Publications, Inc, 2007

100 Chou, T.W., Sun, C.T., Nanocomposites, DEStech Publications, Inc, 2012

101 Gupta, R.K., Kennel, E., Kim, K.J., Polymer nanocomposites handbook, CRC Press, 2010

102 Bhattacharya, S.N., Kamal, M.R., Gupta, R.K., Polymeric nanocomposites: Theory and Practice, Hanser Verlag, 2008

103 Luo, J.J., Daniel, I.M., Characterization and Modeling of Mechanical Behavior of Polymer/Clay Nanocomposites, Composites Science & Technology, 63(11), 1607–1616, 2003

104 Thostenson, E.T., Li, C., Chou, T.W., Nanocomposites in Context, Journal of Composites Science & Technology, 65, 491-516, 2005

105 Schmidt, D., Shah, D., Giannelis, E.P., New Advances in Polymer/Layered Silicate Nanocomposites, Current Opinion in Solid State and Materials Science, 6(3), 205–212, 2002

106 Mittal, V., Optimization of Polymer Nanocomposite Properties, Wiley-Vch, Weinheim, Germany, 2010

107 Thostenson, E., Li, C. and Chou, T., Review Nanocomposites in Context, Journal of

Composites Science & Technology, 65: 491–516, 2006

108 Hussain, F., Hojjati, M., Okamoto, M., Gorge, R.E., Review article: Polymer-matrix Nanocomposites, Processing, Manufacturing, and Application: An Overview, Journal of Composite Materials, 40(17), 1511-1575, 2006

109 Schmidt, D., Shah, D. and Giannelis, E.P., New Advances in Polymer/Layered Silicate Nanocomposites, Current Opinion in Solid State and Materials Science, 6(3): 205–212, 2002

110 Haggenmueller, R., Gommans, H.H., Rinzler, A.G., Fischer, J.E. and Winey, K.I., Aligned Single-wall Carbon Nanotubes in Composites by Melt Processing Methods, Chemical Physics Letters, 330(3 - 4): 219 – 225, 2000

111 Thostenson, E.T., Ren, Z. and Chou, T.W., Advances in the Science and Technology of Carbon Nanotubes and their Composites: a Review, Composites Science and Technology, 61(13): 1899–1912, 2001

112 Gorga, R.E. and Cohen, R.E., Toughness Enhancements in Poly(methyl methacrylate) by Addition of Oriented Multiwall Carbon Nanotube, J. Polym. Sci., Part B: Polym. Phys., 42(14): 2690–2702, 2004

113 Alexandre, M., Dubois, P., Polymer-layered silicate nanocomposites: preparation, properties and uses of a new class of materials, 28 (1-2), 1 – 63, 2000

114 Han, J., Anantram, M.P., Jaffe, R.L., Kong, J. and Dai, H., Physical Review B, 57: 14983, 1998

115 C. Oriakhi, Nano sandwiches, Chem. Br. 34, 59-62, 1998

116 Yano, K., Usuki, A., Synthesis and Properties of Polyimide-Clay Hybrid, Journal of Polymer Science Part A: Polymer Chemistry, 31: 2493 – 2498, 1993

117 Chen, B., Polymer-Clay nanocomposites: an overview with emphasis on interaction mechanisms. British Ceramic Transactions: Vol. 103, No. 6, pg 241, 2004

118 Okada, A. and Usuki, A., The Chemistry of Polymer-Clay Hybrids, Mater. Sci. Eng., C3: 109–115, 1995

119 Kearns, J.C., Shambaugh, R.L., Polypropylene Fibers Reinforced with Carbon Nanotubes, Journal of Applied Polymer Science, 86(8): 2079–2084, 2002

120 Winey, K.I., Vaia, R.A., Polymer nanocomposites, MRS Bull; 32:314–9, 2007

121 Ray, S.S., Okamoto, M., Polymer/layered silicate nanocomposites: a review from preparation to processing. Progress in Polymer Science, 28, 1539–642, 2003

122 Chen, C., Cloos, L., Rice, B.P., Carbon Fiber Composites: Part I, SAMPE Journal, 37(5), 2001

123 Xia, H., Song, M., Preparation and characterisation of polyurethane grafted single-walled carbon nanotubes and derived polyurethane nanocomposites, Journal of Materials Chemistry, 16, 1843 – 1851, 2006

124 Fukushima, H., Drazal, L.T., Graphite Nanocomposites: Structural & Electrical, Properties, In: Proceedings of the 14th International Conference on Composite

Materials (ICCM-14), San Diego, CA, 2003

125 Kim, J., Creasy, T.S., Selective laser sintering characteristics of nylon 6/clay-reinforced nanocomposite, Polymer Testing, 23, 629–636, 2004

126 Yan, C., Shi, Y., Yang, J., Liu, J., A Nanosilica/Nylon-12 Composite powder for selective laser sintering, Journal of Reinforced Plastics and Composites, 28, 2889, 2009

127 Koo, J.H., Pilato, L., Wissler, G., Cheng, J., Ho, W., Nguyen, K., Lao, S., Cummings, A., Ervin, M., Innovative selective laser sintering: rapid manufacturing using nanotechnology, Proceedings of the solid freeform fabrication symposium, The University of Texas at Austin, Texas, 2005.

128 Lao, S.C., Kan, M.F., Lam, C.K., Chen, D.Z., Koo, J.H., Moon, T., Londa, M., Takatsuka, T., Kuramoto, E., Wissler, G., Pilato, L., Luo, Z.P., Polyamide 11-Carbon Nanotubes Nanocomposites: Processing, Morphological, and Property Characterisation, Proc. SAMPE, Seattle, WA, May 17-20, 2010.

129 Kim, J., Creasy, T.S., Selective Laser Sintering Characteristics of Nylon 6/Clay-Reinforced Nanocomposite, Polymer Testing, 23, 629 – 636, 2004

130 Wang, Y., Shi, Y., Huang, S., Selective laser sintering of polyamide–rectorite composite, Proceedings of the Institution of Mechanical Engineers, Part L: Journal of Materials: Design and Applications, 219 (L1), 11–15, 2005

131 Jain, P.K., Pandey, P.M., Rao, P.V.M., Selective laser sintering of clay-reinforced polyamide, Polymer Composites, 31(4), 732–743, 2009

132 Zheng, H.Z., Zhang, J., Lu, S.Q., Wang, G.C., Xu, Z.F., Effect of Core-Shell Composite Particles on the Sintering Behavior and Properties of Nano-Al2O3/polystyrene Composite Prepared by SLS, Materials Letters, 60, 1219–1223, 2006

133 Athreya, S.R., Kalaitzidou, D., Das, S., Mechanical and microstructural properties of Nylon-12/carbon black composites: Selective laser sintering versus melt compounding

and injection molding, Composites science and technology, 71, 506 – 510, 2011

134 Athreya, S.R., Kalaitzidou, D., Das, S., Processing and characterization of a carbon black-filled electrically conductive nylon-12 nanocomposite produced by selective laser sintering, Materials Science and Engineering A, 527, 2637 – 2642, 2010

135 Salmoria, G.V., Paggi, R.A., Lago, A., Beal, V.E., Microstructural and mechanical characterization of PA12/MWCNTs nanocomposite manufactured by selective laser sintering, Polymer Testing, 30, 611 – 615, 2011

136 Ajayan, P.M., Schadler, L.S., Giannaris, C., Rubio, A., Single-Walled Carbon Nanotube-Polymer Composites: Strength and Weakness, Advanced Materials, 12, 750, 2000

137 Xie, X.L., Mai, Y.W., Zhou, X.P., Dispersion and alignment of carbon nanotubes in polymer matrix: A review, Materials Science and Engineering: R: Reports, 49(4), 89-112, 2005

138 Salvetat, J.P., Briggs, A.D., Bonard, J.M., Bacsa, R.R., Kulik, A.J., Stockli, T., Burnham, N.A., Forro, L., Elastic and shear moduli of single-walled carbon nanotube ropes, Physical Review Letters, 82, 944, 1999

139 Wahab, M.S., Dalgarno, K.W., Cochrane, R.F., Hassan, S., Development of Polymer Nanocomposites for Rapid Prototyping Process, Proceeding of the World Congress on Engineering Vol II, London, 2009

140 Cai, D., Jin, J., Song, M., Pub.No.: WO/2009/034361, International Application No.: PCT/GB2008/003130, 2009

141 Iijima, S., Carbon nanotubes: past, present, and future, Physica B, 323, 1 – 5, 2002

142 Belluci, S., Carbon nanotubes: Physics and applications, Physica Status Solidi C 2 (1): 34–47, 2005

143 Sinnott, S.B., Andrews, R., Carbon Nanotubes: Synthesis, Properties, and Applications, Critical Reviews in Solid State and Materials Sciences 26 (3), 145–249, 2001

144 Charlier, J.C., Blase, X., Roche, S., Electronic and transport properties of nanotubes, Reviews of Modern Physics, 79, 677-732, 2007

145 Demczyk, B.G.; Wang, Y.M; Cumings, J; Hetman, M; Han, W; Zettl, A; Ritchie, R.O., Direct mechanical measurement of the tensile strength and elastic modulus of multiwalled carbon nanotubes, Materials Science and Engineering A 334 (1–2), 173–178, 2002

146 Mohamed, M., Sayed, A., Madiha, M., Hatem, A., E, Khairy, E., Thermal conductivity of silicate and borate glasses, Journal of the American Ceramic Society, 66 (5), 76-C-77, 1983

147 Han, Z., Fina, A., Thermal conductivity of carbon nanotubes and their polymer nanocomposites: A review, Progress in Polymer Science, 36 (7), 914 – 944, 2011

148 Martel, R., Derycke, V., Lavoie, C., Appenzeller, J., Chan, K., Tersoff, J., Avouris, Ph., Ambipolar Electrical Transport in Semiconducting Single-Wall Carbon Nanotubes, Physical Review Letters, 87 (25): 256805, 2001

149 Iijima, S., Helical microtubules of graphitic carbon, Nature, 354, 56-58, 1991

150 FORMIGA P100 user manual, EOS GmbH, 2009

151 Skoog, Douglas A., F. James Holler and Timothy Nieman, Principles of Instrumental Analysis (5 ed.). New York., 805–808, 1998

152 Wunderlich, B., Thermal Analysis. New York: Academic Press., 1990

153 Hohne, G., Hemminger, W., Flammersheim, H.J., Differential scanning calorimetry, Springer, Berlin, 2003.

154 ASTM D1238, Standard Test Method for Melt Flow Rates of Thermoplastics by Extrusion Plastometer, 2004

155 Menard, H.P., Dynamic mechanical analysis, A practical introduction, CRC Press, Boca Ratonk, Fla, 2008

156 P5687 Thermal conductivity apparatus instruction manual, Cussons technology, 2003.

157 ISO 180:2000, Plastics -- Determination of Izod impact strength, 2000

158 http://www.eos.info/en/products/materials/materials-for-plastic-systems/pa-22002201.html, accessed on 12/2012

159 Yan, C.Z., Shi, Y.S., Yang, J.S., Xu, L., Preparation and Selective Laser Sintering of Nylon-12-Coated Aluminum Powders, Journal of Composite Materials, 43, 1835, 2009.

160 Liu, L., Qi, Z., Zhu, X., Studies on nylon 6/clay nanocomposites by melt-intercalation process, Journal of Applied Polymer Science, 77, 7, 1133-1138, 1999

161 ASTM D790-10, Standard Test Methods for Flexural Properties of Unreinforced and Reinforced Plastics and Electrical Insulating Materials, 2010

162 ASTM D638-99, Standard Test Method for Tensile Properties of Plastics, 1999

163 ASTM D5279, Standard Test Method for Plastics: Dynamic Mechanical Properties: In Torsion, 2008

164 Biswas, M., Sinha, R.S., Recent progress in synthesis and evaluation of polymer–montmorillonite nanocomposites, Advances in Polymer Science, 155, 167–221, 2001

165 Fischer, H., Polymer nanocomposites: from fundamental research to specific applications. Materials Science and Engineering C 23: 763–772, 2003

166 Ash, B. J.; Eitan, A.; Schadler, L. S., Polymer Nanocomposites with Particle and Carbon Nanotube Fillers, Dekker Encyclopedia of Nanoscience and nanotechnology, 2004

167 Ruoff, R.S., Lorents, D.C., Mechanical and thermal properties of carbon nanotubes, Carbon, 33, 7, 925-930, 1995

168 Kim, P., Shi, L., Majumdar, A., McEuen, P.L., Physical Review Letters., 87, 215502, 2001

169 Usuki, A., Koiwai, A., Kojima, Y., Kawasumi, M., Okada, A., Kurauchi, T., Kamigaito, O. Interaction of nylon 6-clay surface and mechanical properties of nylon 6-clay hybrid. Journal of Applied Polymer Science 55 1, 119, 1995

170 Yan, C., Shi, Y., Yang, J., Liu, J., A Nanosilica/Nylon-12 Composite powder for selective laser sintering, Journal of Reinforced Plastics and Composites, 28, 2889, 2009

171 Hopkinson, N., Hague, R.J.M., Dickens, P.M., Rapid Manufacturing: An Industrial Revolution for the Digital Age, John Wiley, England, 2006.

172 Mittal, V., Optimization of Polymer Nanocomposite Properties. Weinheim: John Wiley & Sons; 2010.

173 Karamipour, S., Ebadi-Dehaghani, H., Ashouri, D., Mousavian, S., Effect of nano-CaCO3 on rheological and dynamic mechanical properties of polypropylene: Experiments and models, Polymer Testing; 30(1), 110-7, 2011

174 Abu-Zurayk, R., Harkin-Jones, E., McNally, T., Menary, G., Martin, P., Armstrong, C., McAfee, M., Structure–property relationships in biaxially deformed polypropylene nanocomposites. Composites Science and Technology, 70(9), 1353-9, 2010

175 Woodward, A.E., Crissman, J.M., Sauer, J.A., Investigations of the dynamic mechanical properties of some polyamides, Journal of Polymer Science; 44(143), 23-34, 1960

176 Sinha, Ray. S., Okamoto M. Polymer/layered silicate nanocomposites: a review from preparation to processing, Progress in Polymer Science; 28(11), 1539-641, 2003

177 Tipler, P.A., Mosca G. Physics for Scientists and Engineers: W. H. Freeman; 2007

178 Zarringhalam, H., Hopkinson, N., Kamperman, N.F., Vlieger, J.J., Effects of processing on microstructure and properties of SLS Nylon 12, Materials Science and Engineering: A, 435, 172, 2006

179 Macosko, C.W., Rheology: Principles, Measurements, and Applications: John Wiley & Sons; 1994

180 Mizuno, C., John, B., Okamoto, M., Percolated Network Structure Formation and Rheological Properties in Nylon 6/Clay Nanocomposites. Macromolecular Materials and Engineering, 10.1002/mame.201200065, 2012

181 Krishnamoorti, R., Giannelis, E.P., Rheology of End-Tethered Polymer Layered Silicate Nanocomposites. Macromolecules, 30(14), 4097-102, 1997

182 Wang, M., Wang, W., Liu, T., Zhang, W.D., Melt rheological properties of nylon 6/multi-walled carbon nanotube composites, Composites Science and Technology; 68(12), 2498-502, 2008

183 Zhang, W.D., Shen, L., Phang, I.Y., Liu, T.. Carbon Nanotubes Reinforced Nylon-6 Composite Prepared by Simple Melt-Compounding, Macromolecules, 37(2), 256-9, 2003

184 Xia HS, Song M. Preparation and characterization of polyurethane-carbon nanotube composites, Soft Matter;1(5):386-394, 2005

185 W.D. Callister, Material Science and Engineering: An Introduction, John Wiley & Sons Incorporated, Texas, 1999

186 Yu, M.F., Lourie, O., Dyer, M.J., Moloni, K., Kelly, T.F., Ruoff, R.S., Strength and

breaking mechanism of multiwalled carbon nanotubes under tensile load, Science, 287, 637, 2000

187 O'Mahony, Michael, Sensory Evaluation of Food: Statistical Methods and Procedures. CRC Press, 1986

188 Kausar, A., Iqbal, A., Hussain, S., Preparation and properties of polyamide/epoxy/multi-walled carbon nanotube nanocomposite, Journal of plastic film and sheeting, published online 21 August 2013

189 Mark, James E., Polymer Data Handbook (2nd Edition). Oxford University Press, 2009

190 Wilkes, C.E., Summers, J.W., Daniels, C. A., Berard, M.T., PVC Handbook. Hanser Verlag. p. 414. ISBN 978-1-56990-379-7, 2005

191 Material properties of PE, akatherm, http://www.akatherm.com/, accessed on 11/2013

192 Xia, H., Song, M., Preparation and characterisation of polyurethane grafted single-walled carbon nanotubes and derived polyurethane nanocomposites, J. Mater. Chem. 16, 1843-1851, 2006

193 Cadek, M., Coleman, I.N., Barron, V., Hedicke, K., Blau, W.J., Morphological and mechanical properties of carbon nanotube reinforced semi-crystalline and amorphous polymer composites, Applied Physics Letters, 81, 5123-5125, 2002

194 Haggenmueller, R., Fischer, J.E., Winey, K.I., Single wall carbon nanotube/polyethylene nanocomposites: nucleating and templating polyethylene crystallites, Macromolecules. 39, 2964-2971, 2006

195 Vehara, H., Kato, K., Kakiage, M., Yamanobe, T., Komoto, T., Single-walled carbon nanotube nucleated solution-crystallization of polyethylene, The Journal of Physical Chemistry C, 111, 18950-18957, 2007

196 Cai, D., Song, M., Latex technology as a simple route to improve the thermal conductivity of a carbon nanotube/polymer composite, Carbon, 46, 15, 2008

197 Gojny, F.H., Wichmann, M.H.G., Fiedler, B., Kinloch, I.A., Bauhofer, W., Windle, A.H., Schulte, K., Evaluation and identification of electrical and thermal conduction mechanisms in carbon nanotube/epoxy composites, Polymer, 47, 6, 2036 – 2045, 2006

198 Kim, W., Wang, R., Majumdar, A., Nanostructuring expands thermal limits, Nanotoday, 2 (1), 40–47, 2007

199 Haggemnueller, R., Guthy, C., Lukes, J.R., Fischer, J.E., Winey, K.I., Single wall carbon nanotube/polyethylene nanocomposites: thermal and electrical conductivity, Macromolecules. 40, 2417-2421, 2007

200 Yan, C.Z., Shi, Y.S., Yang, J.S., Liu, J.H., An organically modified montmorillonite/nylon-12 composite powder for selective laser sintering, Rapid Prototyping Journal, 17, 28-36, 2011

201 Gupta, R.K., Polymer and Composite Rheology, Second Edition: Taylor & Francis; 2000.

202 Sinha, Ray. S., Okamoto, M., Polymer/layered silicate nanocomposites: a review from preparation to processing. Progress in Polymer Science, 28(11):1539-1641, 2003

203 Jin, J., Chen, L., Song, M., Yao, K., An Analysis on Enhancement of Fatigue Durability of Polyurethane by Incorporating Organoclay Nanofillers. Macromolecular Materials and Engineering, 291(11):1414-1421, 2006

204 Lim, Y.T., Park, O.O., Phase morphology and rheological behavior of polymer/layered silicate nanocomposites, Rheologica Acta, 40(3):220-229, 2001

205 Hyun, Y.H., Lim, S.T., Choi, H.J., Jhon, M.S., Rheology of Poly(ethylene oxide)/Organoclay Nanocomposites, Macromolecules, 34(23):8084-8093, 2001

206 Mayer, J., Giannuzzi, L.A., Kamino, T., Michael, J., TEM sample preparation and FIB-induced damage, Mrs Bulletin, 32(5):400-407, 2007